

# Doctoral Dissertation

Ameer Nassrah

Budapest

2024



DOCTORAL DISSERTATION

# Photoalignment at Liquid Crystal–Polymer Interface

**Ameer R. K. Nassrah**

Doctoral School of Physics

Material Science and Solid State Physics Programme

Head of Doctoral School: Prof. Gergely Palla, DSc

Head of Program: Prof. István Groma, DSc



Supervisor: Tibor Tóth-Katona

Institute for Solid State Physics and Optics, Wigner RCP

Complex Fluid Research Department

Head of Department: László Péter

Partially Ordered Systems Research Group

Group leader: Tamás Börzsönyi

Eötvös Loránd University

Budapest

2024





---

# CONTENTS

<b>Preface</b>	<b>1</b>
<b>Acknowledgment</b>	<b>4</b>
<b>1 Introduction</b>	<b>7</b>
1.1 Types of liquid crystals . . . . .	9
1.1.1 Lyotropic LCs . . . . .	9
1.1.2 Thermotropic LCs . . . . .	10
1.2 Properties of nematic liquid crystals . . . . .	12
1.2.1 Elastic properties . . . . .	14
1.2.2 Electric and dielectric properties . . . . .	16
1.2.3 Magnetic properties . . . . .	17
1.2.4 Viscosity . . . . .	18
1.2.5 Optical properties . . . . .	19
1.3 An overview on photoalignment of nematic liquid crystals . . . . .	21
1.4 Motivations and research objectives . . . . .	24
<b>2 Methodology and materials</b>	<b>27</b>
2.1 Substrate preparation . . . . .	27

## CONTENTS

---

2.2	LC sandwich cell assembly . . . . .	28
2.3	Materials . . . . .	29
2.3.1	Liquid crystals . . . . .	29
2.3.2	Polymers with photochromic units for the command surface . . . . .	30
2.4	Pump–probe beam optical setup . . . . .	32
2.5	Polarized optical microscope . . . . .	34
2.6	Atomic force microscope . . . . .	36
<b>3</b>	<b>Role of the liquid crystalline molecular structure in photoalignment</b>	<b>39</b>
3.1	Azimuthal (in-plane) photoalignment . . . . .	40
3.2	Zenithal (out-of-plane) photoalignment . . . . .	43
3.3	Back-relaxation from the azimuthal photoalignment . . . . .	45
3.4	Discussion . . . . .	47
<b>4</b>	<b>Role of the liquid crystalline phase in photoalignment</b>	<b>63</b>
4.1	Azimuthal (in-plane) photoalignment . . . . .	63
4.2	Zenithal (out-of-plane) photoalignment . . . . .	64
4.3	Discussion . . . . .	66
<b>5</b>	<b>Role of the polymer composition in photoalignment</b>	<b>69</b>
5.1	Photoalignment at different polymer layers . . . . .	71
5.2	Photoinduced mass transfer . . . . .	74
5.3	Discussion . . . . .	80
<b>6</b>	<b>Summary</b>	<b>83</b>
	<b>Appendix A Photoalignment in ferroelectric nematic phase</b>	<b>87</b>
	<b>Bibliography</b>	<b>94</b>
	<b>List of publications</b>	<b>116</b>
	<b>Theses</b>	<b>118</b>



---

# PREFACE

Liquid crystal displays have revolutionized the field of visual technology and are widely used in modern society. However, to optimize the performance of these displays, the orientation of the liquid crystal molecules must be precisely controlled. The photoalignment technique is a unique method for aligning liquid crystal molecules in a specific direction, and it involves the use of light and photosensitive layer to align the liquid crystal. The control of surface orientation of nematic liquid crystals with the help of polarized light is not only an alternative, contactless method to ensure proper alignment at the cell boundaries, but – because of its reversible character – also opens up new possibilities of applications (rewritable displays and dynamic holography).

The dissertation is structured as follows. Chapter 1 gives an introduction to liquid crystals. Here the properties of nematic liquid crystals will be discussed, as well as the motivations and the objectives will be highlighted. Chapter 2 describes the methodology and the materials that have been used in this work. Chapters 3 and 4 present the results on photoalignment at the nematic liquid crystal interfacing a photosensitive polymer, where we discuss the influence of the liquid crystalline molecular structure and that of the phase sequence on the photoalignment process. Chapter 5 discusses the role of the composition of the polymeric command layer in photoalignment, as well as the photoinduced mass transfer at the polymer–air interface. Chapter 6 provides a sum-

mary. Additionally, in the Appendix, we briefly discuss preliminary measurements on ferroelectric nematics, which have not yet been published.

The scientific outcome of this work are published in three papers [N1], [N2] and [N3] and presented at three conferences.



---

# ACKNOWLEDGMENT

Sometimes, words of thanks seem to be not enough to express the depth of gratitude one feels. It is with utmost sincerity that I express my profound appreciation to the individuals who have played an important role in my academic journey.

Foremost, I am profoundly grateful to my supervisor, Dr. Tibor Toth-Katona, for his continued support and kindness. His guidance has been invaluable in shaping my path and enriching my understanding. I extend my sincere appreciation to the partially ordered system group leader Dr. Tamás Börzsönyi, for taking the time to discuss and answer the questions raised during the study courses. Also, I would like to thank my colleagues for their support and for creating a conducive scientific environment.

I am thankful to the Stipendium Hungaricum scholarship programme for the financial support during my unique study experience. Additionally, I am thankful to the ERASMUS+ scholarship and the head of Complex Fluid Research Department Dr. László Péter for their financial support during my stay in Košice, Slovakia.

I would like to thank our colleagues from the Institute of Experimental Physics, Slovak Academy of Sciences, namely, Dr. Natália Tomašovičová and Veronika Lacková, for organizing my stay during the ERASMUS+ mobility. I would also like to express my deep gratitude to Dr. Marianna Baťková for her invaluable teaching on using the atomic force microscope. I truly appreciate it.

Last but not least, I am profoundly thankful to my parents for supporting my decision to complete my PhD. For your patience, understanding and unconditional love during all these years I spent to study abroad, I am deeply grateful for everything you've done for me. I do not know how to repay you. To Katharina Schaidt, brothers, sisters, friends, whether near or far, for their support and for being a part of my study journey. Thank you all.





---

---

# CHAPTER 1

---

## INTRODUCTION

Liquid crystals (LCs) caused some confusion when they were first observed [1]. How is it possible for a material to exhibit both crystalline characteristics and the ability to flow? However, it becomes much easier to understand when we introduce these substances as a "new state of matter" that possesses characteristics lying between those of crystals and liquids. LCs can flow and form drops like typical isotropic liquids but exhibit anisotropic properties due to the partial order.

This new state of matter revolutionized our life and became essential element in our daily use devices (e.g., smartphones, TVs, monitors, etc. [2]). The story of LCs began in the late 19th century when the botanist Friedrich Reinitzer [3] published his observations on the behavior of cholesterol benzoate crystals (extracted from carrot's root). He noticed that these crystals have "two melting points". The crystals melted first at  $145.5^{\circ}\text{C}$  and turned into a milky liquid which with further heating became transparent at  $178.5^{\circ}\text{C}$  (which is called clearing point), and remained unchanged with further temperature increase. He wrote a letter describing this new phenomenon to Otto Lehmann who was specialist in crystallography. Physicist Lehmann examined Reinitzer's substance using a polarizing microscope and found that the studied substance in the cloudy state exhibited optical anisotropy like crystals and it was flowing like liquid and, therefore called them

”flowing crystals” and then ”liquid crystals” [4]. Reinitzer and Lehmann understood that they were experiencing a brand-new, intermediate phase of matter—a phase that has both crystalline and liquid characteristics. Thus, LCs are known as ”mesomorphic states”, where ”meso” means between and ”morphic” means shape or form in Greek [5].

At the beginning of the 20th century, the chemist Daniel Vorländer started to synthesize many liquid crystal substances [6]. He found that LCs are mainly organic molecules of elongated shape. Meanwhile, Georges Friedel was working on the classification of LCs. Friedel found that LC compounds might have different phases where the molecular order sorts between the crystalline state and the isotropic liquid state. Friedel was the first who named the LC phases as [7]: nematic (N), smectic (Sm), and cholesteric (Ch), see Figure 1.1.

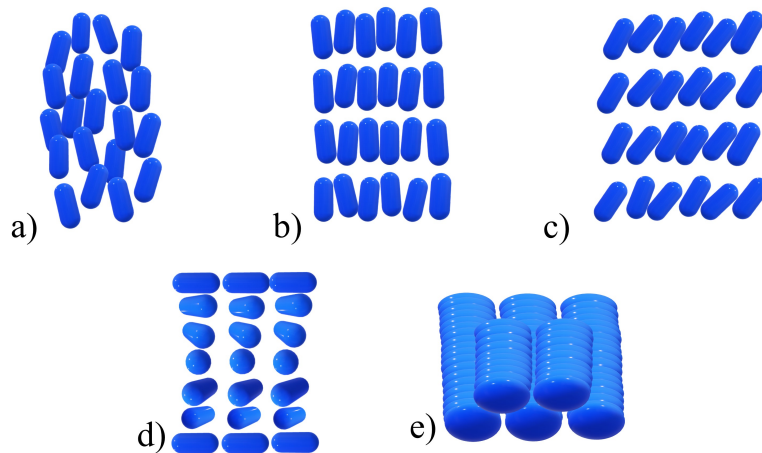


Figure 1.1: Some thermotropic LCs phases: a) nematic, b) smectic A, c) smectic C, d) cholesteric, and e) columnar.

In 1927, Vsevolod Fréedericksz used magnetic field to induce deformation in LCs. Fréedericksz showed that the molecular orientation of LC can be deformed when the applied magnetic field exceeds a threshold value [8, 9]. This deformation called ”Fréedericksz transition”. Similarly, electric field can also induce deformation in LCs. The effect of the electric Fréedericksz transition is a significant factor in the optical device industry. Many years after the experimental and theoretical studies to understand the nature of

LCs [8, 10, 11, 12], the first liquid crystal display (LCD) came to light in 1968 [5].

The twisted nematic (TN) display is the implementation of electric Fréedericksz transition effect. TN display is invented in 1971 by Schadt and Helfrich [13]. In these devices, nematic liquid crystals (NLCs) are confined between two glass substrates as a sandwich cell. LC materials lose the arbitrary orientation when they touch a substrate, so it is important to treat the substrate in specific way to get a desired alignment of LC [14, 15].

Mainly alignment layers fabricated by rubbing method have been used in LCD industries. The interaction of liquid crystals with the bounding substrates, however, remained a particularly significant academic research area. Namely, there is a continuous search for alternative methods for aligning LCs that are applicable in diverse novel fields of LC research, such as micro-, nano- and biotechnology, medicine, polymer and colloid science, photonics, etc. [16, 17]. One of the most stimulating alternative method is the so called photoalignment of nematic liquid crystals. Photoalignment can be used not only to ensure the desired orientation in LC devices, but opens up the possibility to reorient (control) LC through light irradiation in a contactless manner [18].

This dissertation concerns the experimental study of photoalignment. An overview on photoalignment is provided at the end of this chapter.

## 1.1 Types of liquid crystals

### 1.1.1 Lyotropic LCs

LCs that experience phase transitions as a result of changing the solvent concentration are called lyotropic LCs. Besides the concentration, the temperature also induces phase transitions in these solutions. Name lyotropic originates from the Greek words "lúō" which means "to dissolve" and "tropikós," which means "way" [5]. This kind of LCs is important for biological research, living organism understanding, and for biological sensors. The most known examples of lyotropic LCs are the "soap–water" mixture, DNA, and RNA [19]. Lyotropic liquid crystals are outside the scope of our research, and

therefore, for more information see Refs. [20, 21].

### 1.1.2 Thermotropic LCs

The other class of LCs is called thermotropic, where "thermós" means "hot" in Greek. Thermotropic LCs are important for the fundamental research, electro-optic devices, displays, pressure and thermal sensors, etc. [19]. These LCs experience phase transitions as a result of temperature change. By increasing the temperature, the molecular order decreases, and finally, it will be completely disordered when the isotropic phase is reached, see Figure 1.2.

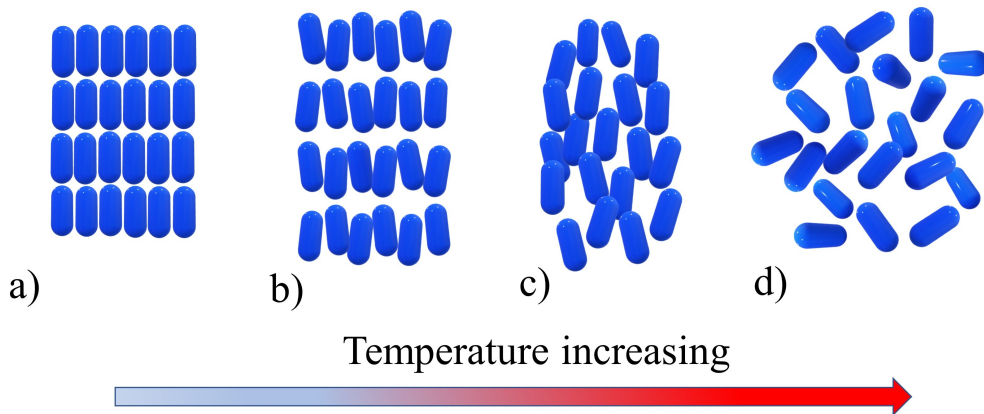


Figure 1.2: Examples of thermotropic phase transitions: crystalline (a) to smectic A (b), to nematic (c) to isotropic (d) phase. The order parameter of the molecules decreases with increasing the temperature.

Material is isotropic when it exhibits the same physical properties when measured from different directions at a given temperature, so it has a single value of refractive index, dielectric constant, etc. The anisotropic material exhibits different physical properties when measured from different directions due to the partial order of the anisometric molecules [22].

Molecules of various anisometric shape may create LC phases, e.g., rod-like (calamitic), disk-like, bowl-shape, bent-core (banana-like) – see Figure 1.3 [19]. In general, rod-like molecules contain at least two rings connected with each other via rigid bridging group,

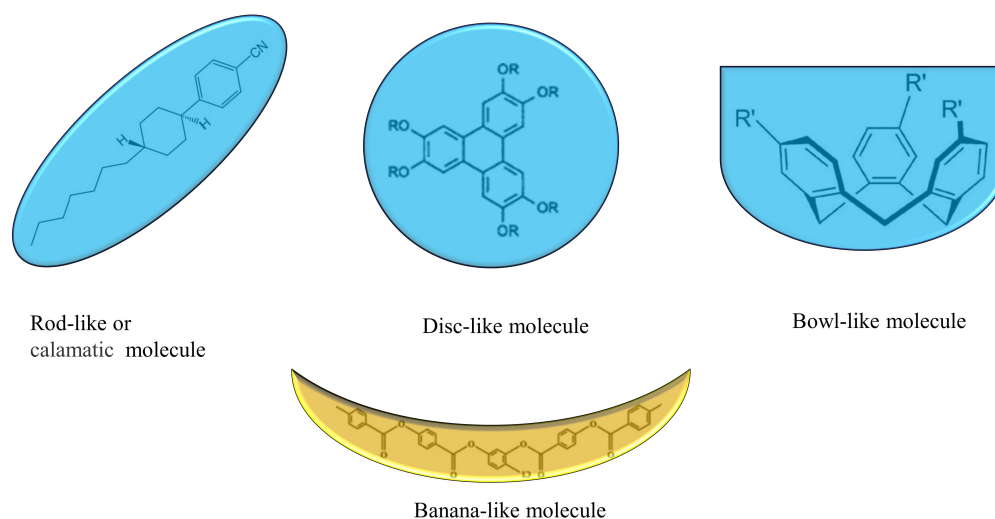


Figure 1.3: Examples of the molecular shape of some mesogenic compounds. Rod-like (calamatic) molecule of the PCH7 LC compound, disc-like molecule of a triphenylene [23]. Bowl-like molecule is a cyclotrimeratrylene (CTV) [24]. Bent-core (banana-like) molecule of ClPbis10BB [25].

and one of the rings linked with a hydrocarbon chain, while the other ring is linked for example to a unit with permanent dipole. Rod-like molecules can form various phases such as, smectic (SmA, SmB, SmC, etc.), nematic (N) and cholesteric (Ch) – see Figure 1.1. Disc-like molecules may exhibit discotic nematic, hexagonal columnar, tilted columnar (see an example in Figure 1.1(e)). Bent-core molecules may exhibit nematic and various other ( $B_1 - B_8$ ) phases [26].

The dissertation work concerns mainly nematic phase (and in small part smectic A phase – see Figure 1.1(b)) composed of rod-like molecules. In the nematic phase the long axes of the molecules statistically align along a specific direction, called the director  $\mathbf{n}$ . The mass centers of the molecules, however, remain disordered – see Figures 1.1(a) and 1.2(c). In the smectic A phase, besides of the orientational order, the mass centers of the molecules form layers perpendicular to  $\mathbf{n}$ , however, they remain disordered within the layers and the mass centers do not correlate between the layers – see Figures 1.1(b) and 1.2(b). In the followings, the basic properties of the nematic liquid crystal (NLC) phase will be shortly discussed. Peculiarities of the SmA phase will be introduced in Chapter 4, which deals with the role of liquid crystal phase in photoalignment. For more information

regarding other LC phases, see e.g., Refs. [19, 27, 28, 29, 30].

## 1.2 Properties of nematic liquid crystals

Among all thermotropic LC phases, NLC is the most widely used in electro-optic devices like LCDs. The nomenclature of nematic came from the Greek word "nêmatos" which means thread-like [31]. Under polarizing optical microscope (POM) with crossed polarizer and analyzer, one can see disclination lines (see Figure 1.4). These disclinations look like threads, and therefore, Friedel named the phase nematic [5, 7, 8, 26]

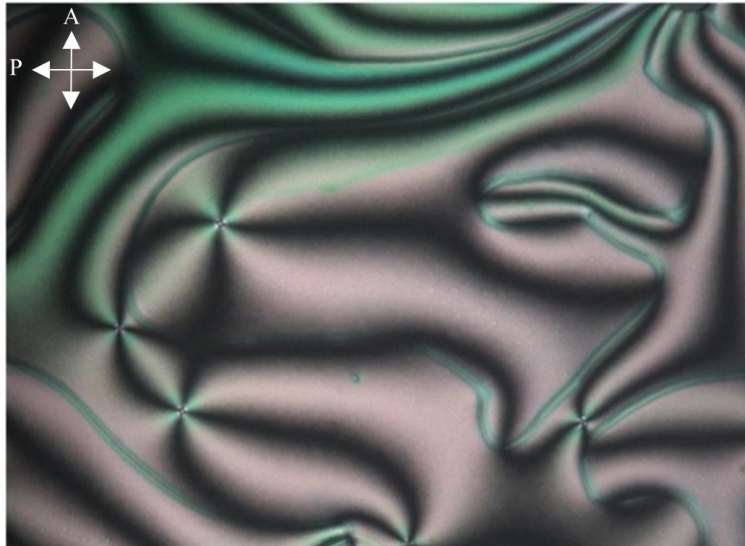


Figure 1.4: Typical NLC between crossed polarizers ( $P \times A$ ).  $P$  is the polarizer and  $A$  is the analyzer.

The bright and dark regions in Figure 1.4 represent different orientations of the director. When the director is oriented parallel with the polarizer, or perpendicular to it, no change in the state of light polarization occurs. Therefore, the transmitted light through the NLC layer will be blocked by the analyzer, and dark regions appear. When the director makes an angle with the polarizer, then the light splits into two components propagating through LC material with different velocities (details in Sec. 1.2.5). Passing through the NLC layer, the two components combine into an elliptically polarized light. Part of the light passes through the analyzer, resulting in bright colored regions. The

## 1.2. PROPERTIES OF NEMATIC LIQUID CRYSTALS

---

texture of NLC is called Schlieren texture which shows brushes pinned with singularities (point defects). The description of POM will be provided in Chapter 2, while variety of LC textures are illustrated in Ref. [32].

NLC rod-like molecules align themselves statistically parallel to each in a specific direction, called the director ( $\mathbf{n}$ ), which is a unit vector. NLCs have no positional order where the centers of mass for the molecules are randomly distributed just like in isotropic liquid. To describe the relative orientation of the molecule to the director, one can introduce a scalar component, the so called the order parameter  $S$  [26, 33].

$$S = \langle P_2 \cos(\theta) \rangle = \frac{1}{2} \langle 3 \cos^2 \theta - 1 \rangle, \quad (1.1)$$

where  $P_2$  is the second Legendre polynomial, the angle brackets denote the average orientation of the molecules, and  $\theta$  is the angle between the molecular axis and  $\mathbf{n}$ , see Figure 1.5.

The order parameter can take values between 0 and 1, where 1 corresponds to the perfect ordered crystalline state, and 0 to the disordered liquid state. NLC order parameter typically takes values between 0.3 and 0.8 [26]. As the temperature increases, the order of the molecules and with that the order parameter, continuously decreases, see Figure 1.2. At a certain temperature, the nematic phase undergoes a phase transition to the isotropic (I) phase. During this transition, the order parameter drops discontinuously to zero, indicating a first-order phase transition [33].

This phase transition temperature is also known as "clearing point" and is denoted by  $T_{NI}$ . The nematic phase is uniaxial, which means that a physical parameter has "extraordinary" value along the director, while it has another, "ordinary" value perpendicular to it [5, 26, 33]. Therefore, the physical properties in the nematic phase are anisotropic and will be discussed in the following subsections.

The N phase has additional notable characteristics [5, 33]. It exhibits a rotational



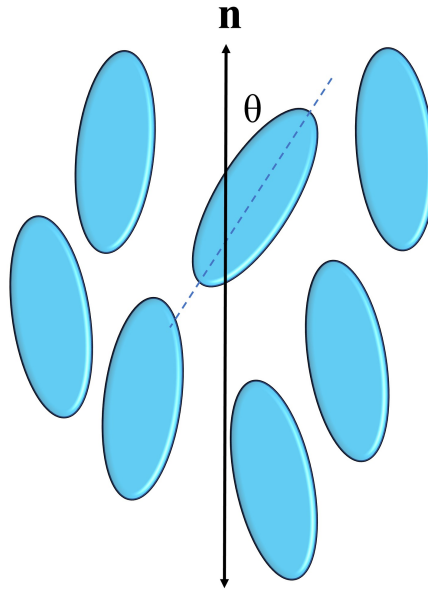


Figure 1.5: Molecular order in the nematic with the director  $\mathbf{n}$ .

symmetry around the nematic director, and therefore, the states " $+\hat{n}$ " and " $-\hat{n}$ " are physically equivalent. The direction of the nematic director can be rotated or reoriented in any direction without affecting the properties of the nematic phase as a whole. This is a consequence of the rotational symmetry of the nematic phase. The anisotropic properties of NLCs make them suitable for various technological applications, including displays, sensors, and optical communication devices [34, 35, 36]. One of the essential characteristics of NLCs is their ability to align under the influence of external stimuli, such as electric or magnetic fields, surface treatment, and light [37, 38].

### 1.2.1 Elastic properties

The "elastic constants" are among the properties that depend on order parameter. These constants are referred as Frank-Oseen elastic constants, after Oseen [10], the first who established the basis of the continuum model and based on his work, Frank [11] introduced the theory of elasticity. Frank-Oseen elastic free energy per unit volume is given by:

$$F = \frac{1}{2}K_{11}(\nabla \cdot \mathbf{n})^2 + \frac{1}{2}K_{22}(\mathbf{n} \cdot \nabla \times \mathbf{n})^2 + \frac{1}{2}K_{33}(\mathbf{n} \times \nabla \times \mathbf{n})^2 \quad (1.2)$$

where  $K_{11}$ ,  $K_{22}$  and  $K_{33}$  are the elastic constants that describe the splay, twist and bend deformations, respectively – see Figure 1.6. In most NLCs  $K_{22} < K_{11} < K_{33}$ .

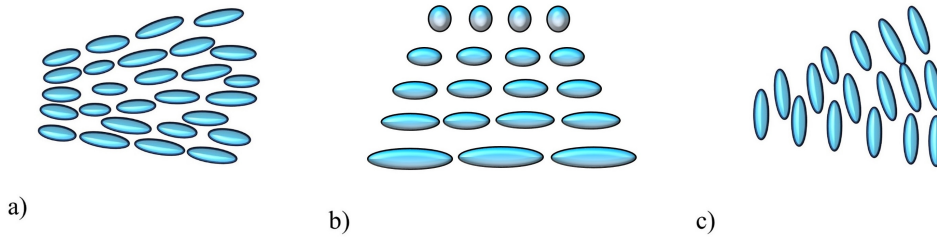


Figure 1.6: Basic deformations of NLC: a) splay, b) twist, and c) bend deformation.

Usually, NLC is confined between two solid substrates forming a sandwich cell, or just lie on a solid substrate forming a sessile droplet. In both cases the nematic director will take a specific orientation depending on the alignment layer at the interface. In most cases,  $\mathbf{n}$  is either parallel with the substrate (planar alignment), or it is perpendicular to the substrate (homeotropic alignment) – see Figure 1.7. The anchoring strength can be used to describe how the alignment layer interacts with the liquid crystal. Planar alignment is typically regarded as a strong anchoring condition. Since  $\mathbf{n}$  is a unit vector which describes the average molecular orientation, it is related to the azimuthal  $\varphi$  and zenithal  $\theta$  angles as [38]:

$$\mathbf{n} = \begin{pmatrix} \cos \varphi \cos \theta \\ \cos \varphi \sin \theta \\ \sin \varphi \end{pmatrix} \quad (1.3)$$

The direction of  $\mathbf{n}$  is established by minimizing the total free energy, where the elastic

energy is crucial.

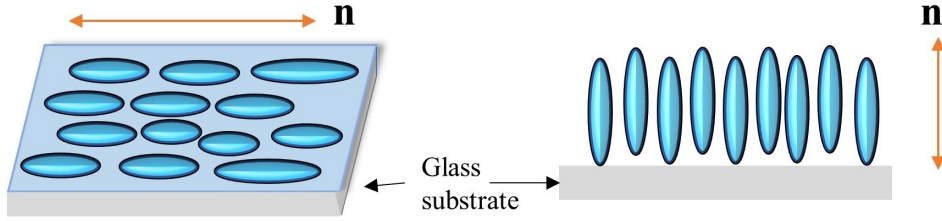


Figure 1.7: Typical nematic liquid crystal alignments on glass substrate. The left side drawing illustrates planar alignment. The right side drawing illustrates homeotropic alignment.

## 1.2.2 Electric and dielectric properties

Nematic liquid crystals are in principle insulators, however, in reality they have a finite electric conductivity. This finite conductivity comes from ions remaining from the synthesis, or from the interfaces in contact with liquid crystals. In general, the electric conductivity of nematics is of the order of  $10^{-10} - 10^{-7}$  S/m. Because of the small conductivity, nematics can be often regarded with good approximation as ohmic materials, in which the relation between  $\mathbf{J}$  current density and the  $\mathbf{E}$  electric field is defined by the  $\sigma$  symmetric electric conductivity tensor:  $\mathbf{J} = \sigma \mathbf{E}$ . The two independent elements of the  $\sigma$  tensor, namely,  $\sigma_{\parallel}$  and  $\sigma_{\perp}$ , – which are the electric conductivities parallel with the director and perpendicular to it, respectively – define the anisotropy of the electric conductivity,  $\sigma_a$ :

$$\sigma_a = \sigma_{\parallel} - \sigma_{\perp}. \quad (1.4)$$

Similarly to the anisotropy of the electric conductivity, the  $\varepsilon_a$  dielectric permittivity anisotropy of the nematics can be also written as:

$$\varepsilon_a = \varepsilon_{\parallel} - \varepsilon_{\perp}, \quad (1.5)$$

where  $\varepsilon_{\parallel}$  and  $\varepsilon_{\perp}$  are the dielectric permittivities parallel with, and perpendicular to the director, respectively. The anisotropy of the dielectric permittivity depends on the

molecular structure of the liquid crystal. More precisely, it depends on the magnitude and direction of the molecular dipole moments, and may vary in a wide range of  $\epsilon_a \sim \pm(1 - 10)$ .

The dielectric free energy density,  $\rho f_e$  of liquid crystal placed in an  $\mathbf{E}$  external electric field is defined as (see, e.g., [33]):

$$\rho f_e = -\frac{1}{2}\epsilon_0\epsilon_{\perp}E^2 - \frac{1}{2}\epsilon_0\epsilon_a(\mathbf{n}\mathbf{E})^2, \quad (1.6)$$

where  $\epsilon_0$  is the permittivity of vacuum. The minimum of the Eq. (1.6) determines the orientation of the director in the external electric field. In case of  $\epsilon_a > 0$ , the director is parallel with the electric field ( $\mathbf{n} \parallel \mathbf{E}$ ), while, in case of  $\epsilon_a < 0$  perpendicular to it ( $\mathbf{n} \perp \mathbf{E}$ ). With minimization of the free energy, one can obtain the threshold voltage required for the reorientation of the liquid crystal layer (electric *Fréedericksz* [9] threshold):

$$U_F = \pi \sqrt{\frac{K_i}{\epsilon_0|\epsilon_a|}}, \quad (1.7)$$

where  $K_i$  is the relevant elastic constant of the deformation.

### 1.2.3 Magnetic properties

Similarly to the dielectric permittivity, the magnetic susceptibility of nematic liquid crystals is also anisotropic [33]:

$$\chi_a = \chi_{\parallel} - \chi_{\perp}, \quad (1.8)$$

where  $\chi_{\parallel}$  and  $\chi_{\perp}$  are the magnetic susceptibilities parallel with, and perpendicular to the director, respectively. The vast majority of liquid crystals are diamagnetic. Therefore, the magnetic susceptibilities having magnitude of the order of  $10^{-7} - 10^{-6}$  are negative in both directions, i.e.,  $\chi_{\parallel} < 0$  and  $\chi_{\perp} < 0$ . The sign of the magnetic susceptibility anisotropy (of typical magnitude of  $\chi_a \sim 10^{-7}$ ) depends on the structure of the rigid core of the liquid crystal molecules: the anisotropy of nematics containing aromatic rings is positive ( $\chi_a > 0$ ), while those with aliphatic structure, or with cyclohexane rings are

negative ( $\chi_a < 0$ ).

The  $\rho f_m$  magnetic free energy density of liquid crystal placed in a  $\mathbf{H}$  external magnetic field is:

$$\rho f_m = -\frac{1}{2}\mu_0\chi_\perp H^2 - \frac{1}{2}\mu_0\chi_a(\mathbf{n}\mathbf{H})^2, \quad (1.9)$$

where  $\mu_0$  is the magnetic susceptibility of vacuum. Analogously to the case of electric field, the minimum of the Eq. (1.9) determines the orientation of the director in external magnetic field. In the case of  $\chi_a > 0$  the director orientation is parallel with the magnetic field ( $\mathbf{n} \parallel \mathbf{H}$ ), while for  $\chi_a < 0$  perpendicular to it ( $\mathbf{n} \perp \mathbf{H}$ ). One has to note, however, that because of the small values of  $\chi_a$ , relatively high magnetic fields are required for the reorientation of liquid crystals. Minimization of the free energy gives the threshold magnetic field, required for reorientation of liquid crystal layer having a thickness of  $d$  (magnetic Fréedericksz threshold):

$$H_F = \frac{\pi}{d} \sqrt{\frac{K_i}{\mu_0|\chi_a|}}, \quad (1.10)$$

For more information about electric and magnetic properties see the references [8, 26, 27, 33, 39, 40].

## 1.2.4 Viscosity

In 1960s Ericksen and Leslie have developed the continuum theory of nematic liquid crystals [41, 42, 43], in which the anisotropic flow properties are described by six viscosity coefficients  $\alpha_1, \dots, \alpha_6$ . In fact, only five of the coefficients are independent due to the relation  $\alpha_6 - \alpha_5 = \alpha_2 + \alpha_3$ , which is introduced by Parodi [44]. The Leslie viscosity coefficients for E7 nematic liquid crystal at  $25^\circ\text{C}$  are [45]:  $\alpha_1 = -0.018$ ,  $\alpha_2 = -0.1746$ ,  $\alpha_3 = -0.0214$ ,  $\alpha_4 = 0.1736$ ,  $\alpha_5 = 0.1716$ ,  $\alpha_6 = 0.0244$  Pa.s.

The apparent viscosity  $\eta$  of a nematic liquid crystal depends on the shear rate  $dv_x/dy$ . Miesowicz has found that nematics aligned in different geometries have different apparent viscosity coefficients [46]. Upon application of shear rate  $dv_x/dy$  in three different alignments of NLC with  $\mathbf{n}$  a magnetic field along  $z$ ,  $x$  and  $y$  axis, three different viscosity

coefficients will be obtained, also known as "the Miesowicz coefficients",  $\eta_a$ ,  $\eta_b$  and  $\eta_c$ , respectively:

$$\begin{aligned}\eta_a &= \alpha_4/2 \\ \eta_b &= 1/2(\alpha_3 + \alpha_4 + \alpha_6) \\ \eta_c &= 1/2(-\alpha_2 + \alpha_4 + \alpha_5)\end{aligned}\tag{1.11}$$

For more information about viscosity, see [8, 27, 33, 39, 42, 46].

### 1.2.5 Optical properties

The optical properties of nematic liquid crystals are uniaxial. The director  $\mathbf{n}$  is the only optical axis, and the optical indicatrix (index ellipsoid) is an ellipsoid of revolution about the principal symmetry axis (i.e., invariant for the rotation around  $\mathbf{n}$ ). When the light propagates in a direction different from the optical axis  $\mathbf{n}$ , it splits into two rays with a polarization perpendicular to each other that travel with different velocities in the liquid crystal. Thus, the refractive index  $n$ , is polarization dependent and the material (liquid crystal) is birefringent. Let  $\mathbf{k}$  be the propagation direction of the light and  $\mathbf{e}$  its polarization vector, and let the unpolarized light propagate from a direction enclosing an angle  $\vartheta$  with  $\mathbf{n}$ . In that case, the light can be decomposed into two rays. One is independent from the angle  $\vartheta$  of the propagation, having *ordinary* polarization ( $\mathbf{e} \perp \mathbf{n}$ ), and traveling with velocity  $c/n_o$  ( $n_o$  being the ordinary refractive index). The other ray propagates with velocity of  $c/n_e$ , has an *extraordinary* polarization, which depends on the propagation direction (i.e., from  $\vartheta$  angle of incidence) [45]:

$$n_e(\vartheta) = \frac{n_{\parallel}n_{\perp}}{\sqrt{n_{\parallel}^2 \cos^2 \vartheta + n_{\perp}^2 \sin^2 \vartheta}},\tag{1.12}$$

where  $n_{\parallel}$  and  $n_{\perp}$  are the refractive indices parallel with-, and perpendicular to  $\mathbf{n}$ , respectively. Note, that for  $\vartheta = 0$ ,  $n_e(\vartheta) \equiv n_{\perp}$ , and this orientation corresponds to the so called *homeotropic* liquid crystal alignment. In the case of  $\vartheta = \pi/2$ , then  $n_e(\vartheta) \equiv n_{\parallel}$ ,

that corresponds to the so called *planar* (or *homogeneous*) alignment. The values of  $n_{\parallel}$  and  $n_{\perp}$  typically fall in the range of 1.4 – 1.9, and in the nematics from rod-like molecules the relation  $n_{\parallel} > n_{\perp}$  holds, and the value of birefringence

$$\Delta n = n_{\parallel} - n_{\perp} \quad (1.13)$$

is in the range of 0.05 and 0.3, depending on the molecular structure. The birefringence  $\Delta n$  can be determined under crossed polarizers. When the director and the polarizers are in the same plane, the intensity of the transmitted light,  $I$  is [45]

$$I = A_0^2 \sin^2 2\varphi \cdot \sin^2(\delta/2), \quad (1.14)$$

where  $A_0$  is the amplitude of the polarized light,  $\varphi$  is the angle between  $\mathbf{n}$  and the polarization direction of the polarizer in front of the LC layer, and

$$\delta = \frac{2\pi\Delta nd}{\lambda} \quad (1.15)$$

is the retardation (phase difference between the ordinary and extraordinary ray),  $d$  is the thickness of the LC layer, and  $\lambda$  is the wavelength of the light. In case of  $\varphi = \pi/4$ , the transmitted light intensity has a maximum value:

$$I_{max} = A_0^2 \sin^2 \frac{\pi\Delta nd}{\lambda}. \quad (1.16)$$

One can see that the dependence of the transmitted light intensity on  $d$ ,  $\Delta n$  and on  $\lambda$  has an oscillatory character.

### 1.3 An overview on photoalignment of nematic liquid crystals

The proper alignment of the liquid crystal molecules at the boundaries is the key factor for correct operation of all devices based on LCs [47]. Consequently, proper surface treatment of the substrates interfacing the LC material has practical importance [15]. For a long time, it has been known that uniform orientation of LC can be achieved when it is placed between mechanically rubbed solid substrates [48, 49, 50]. This feature is crucial, e.g. in liquid crystal display (LCD) industries, where unidirectional alignment is needed [14]. Development of alignment layers, has led LCs to align either homogeneously in a unidirectional manner [51, 52], like in twisted nematic (TN) displays, or homeotropically, like in the vertically aligned nematic (VAN) LCDs [37, 53]. Rubbing a polymer layers unidirectionally with soft cloths helps in aligning LC molecules homogeneously [14, 54, 55]. Over the years, various methods were employed [54, 55, 56, 57, 58]. Initially, glass substrates were coated with long-chain polymers like polyvinyl alcohol (PVA) and other organic compounds like silanes [59], which were subsequently buffed. Later, polyimide layers replaced these materials and showing better alignment performances. However, mechanical rubbing has drawbacks, such as producing and accumulating dust particles and static charges on the polymer surface, and causing mechanical damages on it [60, 61]. Moreover, with rubbing method one can not align LCs in enclosed area, or in microfluidic channels.

To overcome the drawbacks of polymer rubbing, a new technique has been developed [37]. This alternative method, known as photoalignment [62, 63, 64]. The concept of photoalignment was reported more than three decades ago [64, 65, 66, 67]. Ichimura *et al.*, in 1988 showed that the azo-dye molecules attached to the substrate are working as "command surface" [68, 69, 70, 71, 72]. As the name indicates, an azo-dye unit is able to reorient approximately one million molecules of LC in the bulk [37]. Gibbons *et al.*, created a simple LC cell using polyimide alignment layers on both the bottom and top



substrates. The top substrate was doped with a chromophore dye. Both substrates were rubbed unidirectionally. The cell was then filled with NLC and irradiated with linearly polarized light, oriented parallel with the rubbing direction of the polyimide. It was discovered that LC molecules in the irradiated area oriented themselves perpendicular to the light polarization and maintained this orientation even after the light was switched off. Many other researchers began to use this concept by using UV/Vis light and azobenzene derivatives to photoalign LC molecules [62, 73, 74, 75, 76].

Various methods exist for achieving photoalignment of LC systems. LCs can be doped with photochromic guests, some LCs are photosensitive themselves (possess photosensitive moiety in the molecular structure), or LCs can be brought into contact with photosensitive substrates [36, 37, 77, 78]. These photoalignment methods are reversible, while some others are irreversible, like bond breakage in polyimides, or photochemical crosslinking of polymer precursors [79].

The dissertation work concerns only photoalignment at the LC–photosensitive substrate interface. For the fabrication of the photosensitive substrate, as photochromic units azobenzene dye derivatives exhibiting trans-cis (E/Z) isomerization [80] (see Figure 1.8) are the most widely used. The wide use is due to their remarkable photo- and chemical stability, relative ease of synthesis, good solubility in liquid crystals, and due to the reversibility of their polarization dependent photoisomerization [81]. Azobenzene derivatives can usually excited by green, blue, or UV light (depending on their absorption spectra) [80]. Photo-excitation causes a trans-cis isomerisation of azobenzene – see Figure 1.8. [68, 80, 82]. The trans isomer is a rod-like isomer, while the cis isomer has a bent-shape and the trans isomer is more stable than the cis from thermodynamic considerations [82]. The trans-cis photoisomerization happens with largest probability when the polarization of the light parallel with the long axis of the trans isomer [83], because the "dipole transition moments" of the trans isomer is in the same direction as the polarization of the light [82, 84, 85, 86]. In contrast, when the dipole transition moments encloses  $90^\circ$  with the polarization of the light light, the photoisomerization probability is the lowest [80]. Molecular reorientation occurs when the photons of polarized light are ab-

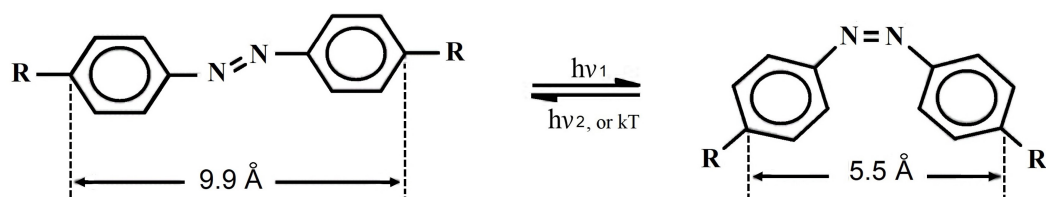


Figure 1.8: Trans-cis isomerisation of azobenzene derivatives.

sorbed by azobenzene molecules [37, 85]. Namely, polarized irradiation selectively excites the trans azo isomers depending on their orientation, and rapid successive trans-cis-trans isomerization cycles result in the orientation of the azobenzene long axis perpendicular to the light polarisation [37, 80], see Figure 1.9.

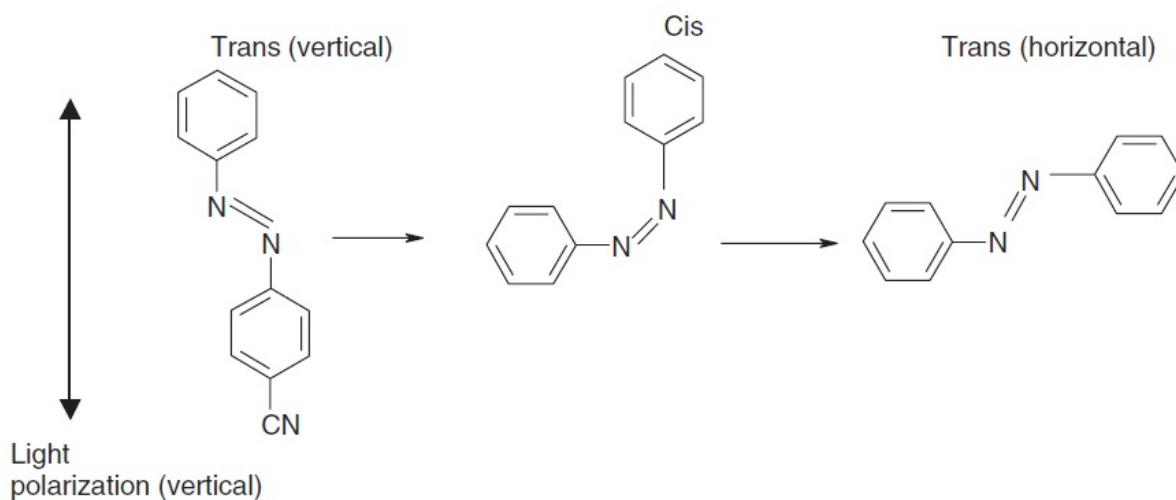


Figure 1.9: Irradiation of azo-dye with linearly polarized light causes a transformation of trans isomers resulting in their orientation perpendicular to the light polarization direction [37].

In Section 1.2.1, I have illustrated the two basic alignments of the liquid crystal at the solid substrate: the planar and the homeotropic – see Figure 1.7. Both alignments can be achieved at the photosensitive command surface by a proper surface treatment by which the trans isomers of the azobenzene moieties are aligned. When the long axis of the trans isomers are aligned perpendicular to the substrate, a homeotropic alignment

of the interfacing LC molecules is achieved initially. In that case, upon photo-excitation, the cis isomers trigger a homeotropic-to-planar orientational transition of the interfacing LC molecules, which is also called out-of-plane photocontrol, or zenithal photoalignment [37].

When the long axis of the trans isomers are aligned in one direction, and in the plane of the substrate, the interfacing LC is planarly (homogeneously) aligned, with  $\mathbf{n}$  parallel with the long axis of the azobenzene trans isomer. In that case the photo-excitation with polarized light, (having polarization direction parallel with the long axis of the trans isomers) triggers a series of trans-cis-trans isomerisations, ending up with the long axis of trans isomers oriented perpendicular to the initial orientation, but still in the plane of the substrate as illustrated in Fig. 1.9. Such a reorientation of the azobenzene moieties causes an "in-plane" reorientation of the liquid crystal director by  $90^\circ$ , i.e., causing an azimuthal twist deformation in the initially planar LC cell [47, 65, 67, 87, 88, 89]. This is the so called in-plane photocontrol, or azimuthal photoalignment.

## 1.4 Motivations and research objectives

The motivation for this doctoral work follows from an earlier experimental observation on the photoalignment at an LC–polymer interface [90]. Namely, when a polymer containing an azobenzene derivative was interfacing various nematic LCs having biphenyls in their molecular structure, the photoalignment mechanism turned out to be far more complex than the usually considered two-dimensional photo-reorientation described in the Section 1.3. First, depending on the temperature, both azimuthal and zenithal photo-reorientations have been observed. Second, at high temperatures, close to the nematic-to-isotropic phase transition temperature  $T_{NI}$ , a temperature induced reorientation (anchoring transition) has occurred, without any photo-excitation. Finally, when the photo-, or thermal-excitation has been switched off, the system has relaxed back to the initial orientation relatively fast. The authors have proposed different temperature dependence of the azimuthal and zenithal anchoring strengths as an explanation, and

#### 1.4. MOTIVATIONS AND RESEARCH OBJECTIVES

---

suggested that the LC–polymer interface should be regarded as a coupled system, where the two components mutually influence each other [90].

To shed light on the predicted interaction between the interfacing polymer and LC, the aim of my research was to answer the questions such as:

- Does the molecular structure of LCs influence the photoalignment? If yes, how?
- Does the type of the LC phase play a role in the photoalignment process?
- Does the photoalignment mechanism depend on how the azobenzene derivative is embedded in the polymer layer?
- What happens with the free polymer surface upon photo-excitation?



---

---

# CHAPTER 2

---

## METHODOLOGY AND MATERIALS

This chapter discusses the substrate preparation (including the cleaning procedure, the spin-coating, the thermal annihilation), the assembly of the LC sandwich cells, overviews the materials used, and describes the experimental methods that have been employed during the doctoral work.

### 2.1 Substrate preparation

First, microscope slides have been cut into  $25 \times 25$  mm pieces using a glass cutter having carbide or diamond tip (Figure 2.1(a)). The glass substrates were cleaned by sonication (Elmasonic S), following the recipe of Ref. [91]: for 10 min in each of the following solvents in the order of ethanol, trichloroethylene, methylene chloride, ethanol again, rinsed by Millipore water (obtained by ELGA Purelab Option), and dried with a nitrogen jet.

Spin-coating of the solution of the photosensitive polymer in toluene has been performed with Polos SPIN150i spin-coater (Figure 2.1(b)) at 800 rpm for 5 s, and then at 3000 rpm for 30 s (all with spin acceleration of  $\pm 1000$  rpm/s). The spin-coated substrates have been baked in an oven for at least 2 h at 140 °C. The thickness of the polymer layer has been estimated to be of the order of 0.1  $\mu\text{m}$ , based on the spin-coating experiments

on PMMA [91].

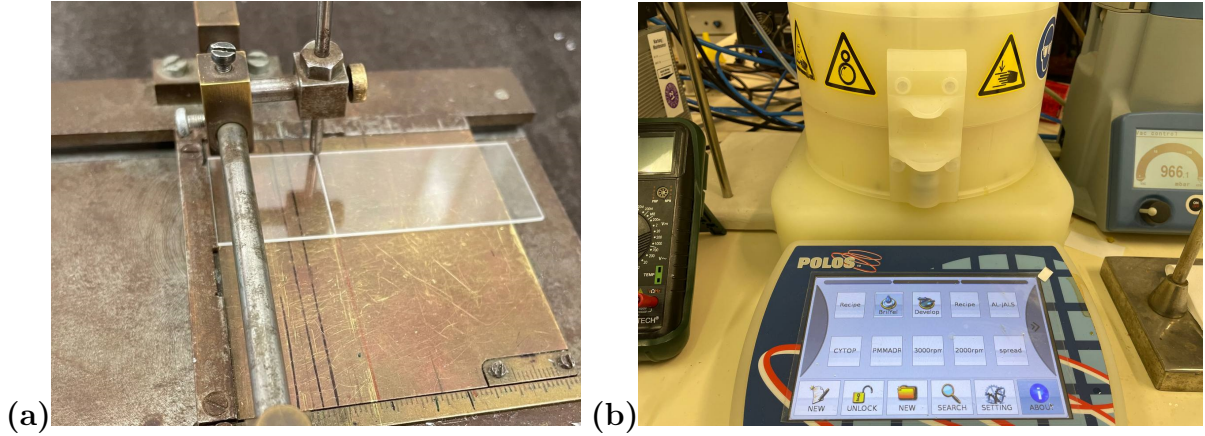


Figure 2.1: (a) The glass cutter tool. (b) Spin-coater device.

## 2.2 LC sandwich cell assembly

Sandwich LC cells (Figure 2.2) have been prepared from two glass plates separated by teflon, mylar, or nylon spacers. Two components epoxy glue has been used to fix the two plates together.

One of the glass plates is the so called reference plate coated with rubbed polyimide layer (RPI), which ensures planar orientation of the LC molecules at the surface. The other glass plate is coated with the photosensitive layer prepared as described in the previous section.

When the epoxy glue has hardened, the thickness  $d$  of the empty LC cell has been measured by interferometric method with Ocean Optics USB2000 spectrophotometer. The thickness  $d$  of the cells was of the order of  $10 \mu\text{m}$  in my experiments.

The given liquid crystal material has been introduced into the sandwich cell by capillary action at a temperature of few centigrade below the clearing (nematic-to-isotropic phase transition) temperature  $T_{NI}$ . Prior and during the NLC flowing in the cell, the whole cell was illuminated by polarized light with a polarization perpendicular to the rubbing direction on the RPI reference plate (see Fig. 2.2). Such a procedure usually results in a LC cell with good planar initial orientation. The initial alignment has been checked with polarizing optical microscope (POM).

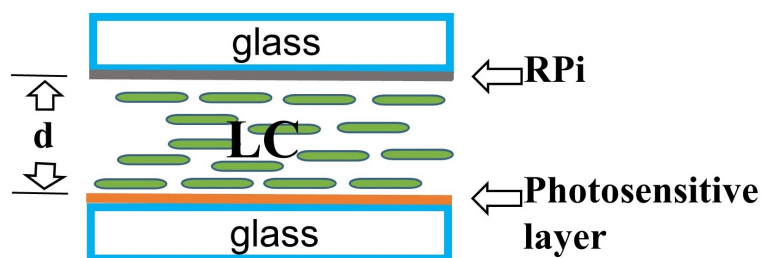


Figure 2.2: Schematic drawing of the cross-section of a LC sandwich cell. RPi denotes the rubbed polyimide layer.

## 2.3 Materials

### 2.3.1 Liquid crystals

Commercially available (from Merck KGaA, Sigma-Aldrich, and Synthon Chemicals) liquid crystal compounds and mixtures have been selected according to the research objectives to investigate the role of the LC molecular structure and that of the LC phase on photoalignment. The acronyms, molecular structures and phase transition temperatures of the selected (in the LC community well known) LCs are listed in Table 2.1.

For the NLC having only phenyl rings in the rigid core, the previously investigated [90] NLC mixture E7 has been selected, for which most of the physical parameters (and their temperature dependence) have been previously determined, which possesses a wide temperature range of the nematic phase, and which has shown rich photoalignment mechanisms [90]. For NLCs containing both phenyl and cyclohexane rings some members of the PCH homologous series (PCH3, PCH5 and PCH7), and the 6CHBT compound have been chosen. For the NLC having exclusively cyclohexane rings in the rigid core, the mixture ZLI1695 has been selected. Note that all of these compounds (except 6CHBT) have the same (CN) polar head, and somewhat different length of the flexible alkyl-chain.

The cyano-biphenyl compound 8CB has been chosen for studies on the influence of the LC phase on the photoalignment, since this compound beside the nematic (N) phase



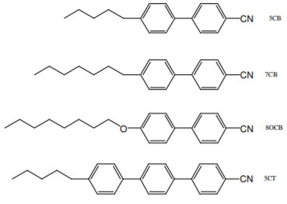
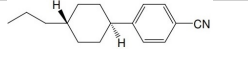
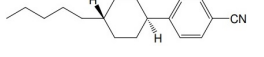
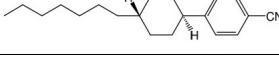
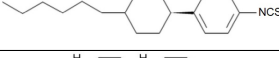
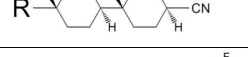
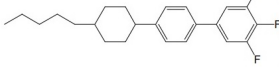
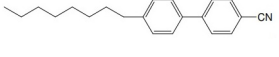
LC	Phase transition temperature	Chemical formula	Chemical structure
E7 mixture	N 60°C I	$C_xH_yO_zN$	
PCH3	N 47°C I	$C_{16}H_{21}N$	
PCH5	N 53.5°C I	$C_{18}H_{25}N$	
PCH7	N 58.5°C I	$C_{20}H_{29}N$	
6CHBT	N 43°C I	$C_{19}H_{27}NS$	
ZLI1695 mixture	N 72.5°C I	$C_{17}H_{28}N$	
5CPUF	Cr 31°C N 56.5°C I	$C_{23}H_{27}F_3$	
8CB	SmA 33°C N 41.5°C I	$C_{21}H_{25}N$	

Table 2.1: Acronyms, molecular structures and phase transition temperatures of liquid crystals compounds used in photoalignment experiments. Cr, SmA, N and I stand for crystal, smectic A, nematic and isotropic phase, respectively.

posses smectic A (SmA) phase too.

Nematic compound 5CPUF, having biphenyl in its rigid core, with three fluorine atoms attached to one of them has been investigated for a reason which will be detailed in Chapter 3.

All the above LC compounds and mixtures have been received from the manufacturer, and were used as received.

### 2.3.2 Polymers with photochromic units for the command surface

Molecular structures of the polymers with embedded (chemically attached, or physically mixed) photochromic units, which have been used for the preparation of the command surface, are shown in Figure 2.3. To our knowledge, for the first time I have compared directly the photoaligning efficiency of two polymeric command surfaces composed from

### 2.3. MATERIALS

---

the same constituents.

Polymethyl-methacrylate (PMMA) polymer functionalized with the azo-dye Disperse Red 1 (DR1) called as pDR1 – see Figure 2.3(a), has been obtained from Alphamicon Inc., Kent, OH, USA. The pDR1 polymer has been dissolved in toluene in concentration of 2 wt% prior spin-coating.

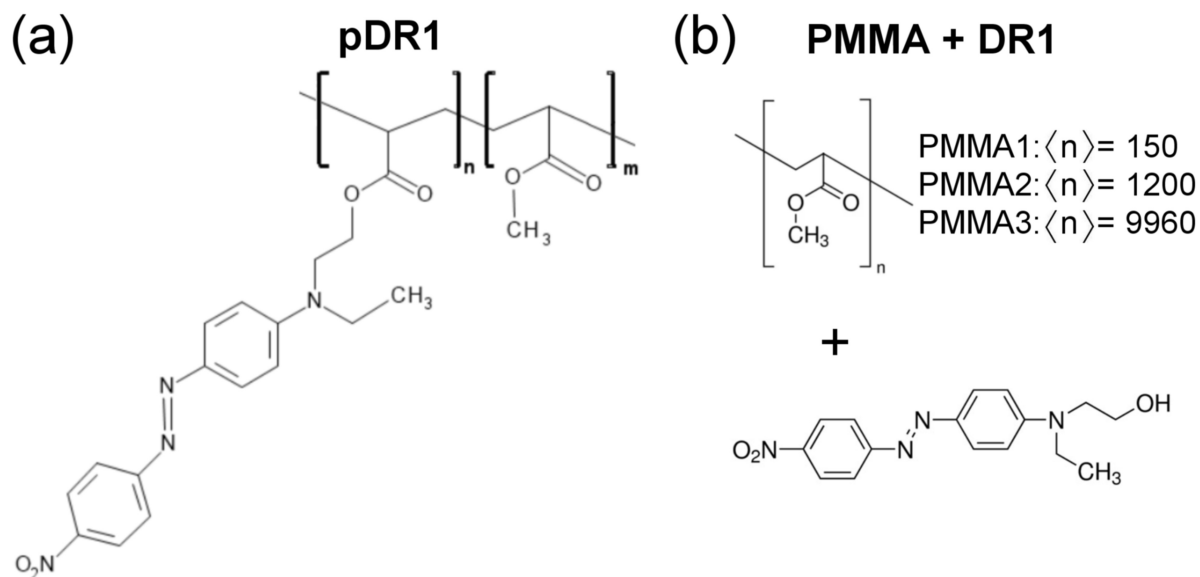


Figure 2.3: Molecular structures of (a) photosensitive polymer pDR1,  $n : m \approx 1 : 9$ , (b) polymethyl-methacrylates (PMMA) of different number-average degree of polymerization  $\langle n \rangle$  physically mixed the azo-dye Disperse Red 1 (DR1).

Physical mixtures PMMA+DR1 have been prepared with PMMA polymers having different number-average degree of polymerization from  $\langle n \rangle = 150$  to  $\langle n \rangle = 9960$ , as indicated in Figure 2.3(b). Namely, on one hand, the increase of the degree of polymerization increases the glass transition temperature,  $T_g$  of PMMA [92, 93]. On other hand,  $T_g$  in thin polymer films is known to influence the dynamic processes of other contacting materials, thus difference in  $T_g$  of the underlying polymer may substantially affect the photoalignment behavior of the layer [94]. For the midpoint of the glass transition temperature values of  $T_g = 105$  °C and  $T_g = 125$  °C have been given by the provider for PMMA1 and PMMA3, respectively [see Figure 2.3(b)], while for pDR1 [Figure 2.3(a)]  $T_g = 119$  °C has been measured [95]. The glass transition temperature of these polymers

are far above the clearing temperature  $T_{NI}$  of the liquid crystals (see Table 2.1). The content of DR1 in the mixture with PMMA has been varied in a wide range: from 6.2 wt% of DR1 (that corresponds to the DR1 content of pDR1), up to 42 wt% of DR1. PMMA polymers of different degree of polymerization, and the azo-dye DR1 have been purchased from Sigma-Aldrich, and used as received.

## 2.4 Pump–probe beam optical setup

A pump-probe optical setup combined with a lock-in amplifier has been used for photoalignment measurements. A schematic drawing, as well as a photograph of the setup is shown in Figure 2.4. The pump beam originating from a diode-pumped solid-state (DPSS) laser (MSLFN-457, 20 mW, 457 nm), or alternatively from a diode laser (Toptica iBeam-Smart 445-S, up to 100mW, 445nm) [(1) in Figure 2.4(b)] enters the NLC cell [placed in a hot-stage (4)] from the photosensitive side. A rotatable  $\lambda/2$  plate (2) has been used to control the pump beam’s polarization direction, and a biconcave lens (3) has been used to increase the diameter of the beam to a few millimeters (significantly greater than the probe beam’s diameter). The probe beam from a He-Ne laser (6) (5 mW, 633 nm) entered NLC cell at the reference plate. The polarization of the probe beam has been controlled by a rotatable polarizer (7). The probe beam transmitted through the LC cell passes through a fast rotating (60 – 70Hz) polarizer sheet (9) before it gets into the photodetector (11) (Thorlabs PDA 100A-EC). Simultaneously, a reference beam from a diode laser (8) also falls on the non-transparent part of the rotating polarizer having a single gap, thus providing a single light pulse per rotation to the photodetector (10) which serves as a reference signal for the lock-in amplifier (12) (Signal Recovery 7265).

Signal from probe beam, provided by the photodetector (11) goes to the input of the lock-in amplifier. The amplifier measures the phase and the amplitude of the signal, and transmits the data to the digital multimeter (13) (Keithley 199 System DMM/Scanner) which is connected to a personal computer (14) used for archivation.

## 2.4. PUMP-PROBE BEAM OPTICAL SETUP

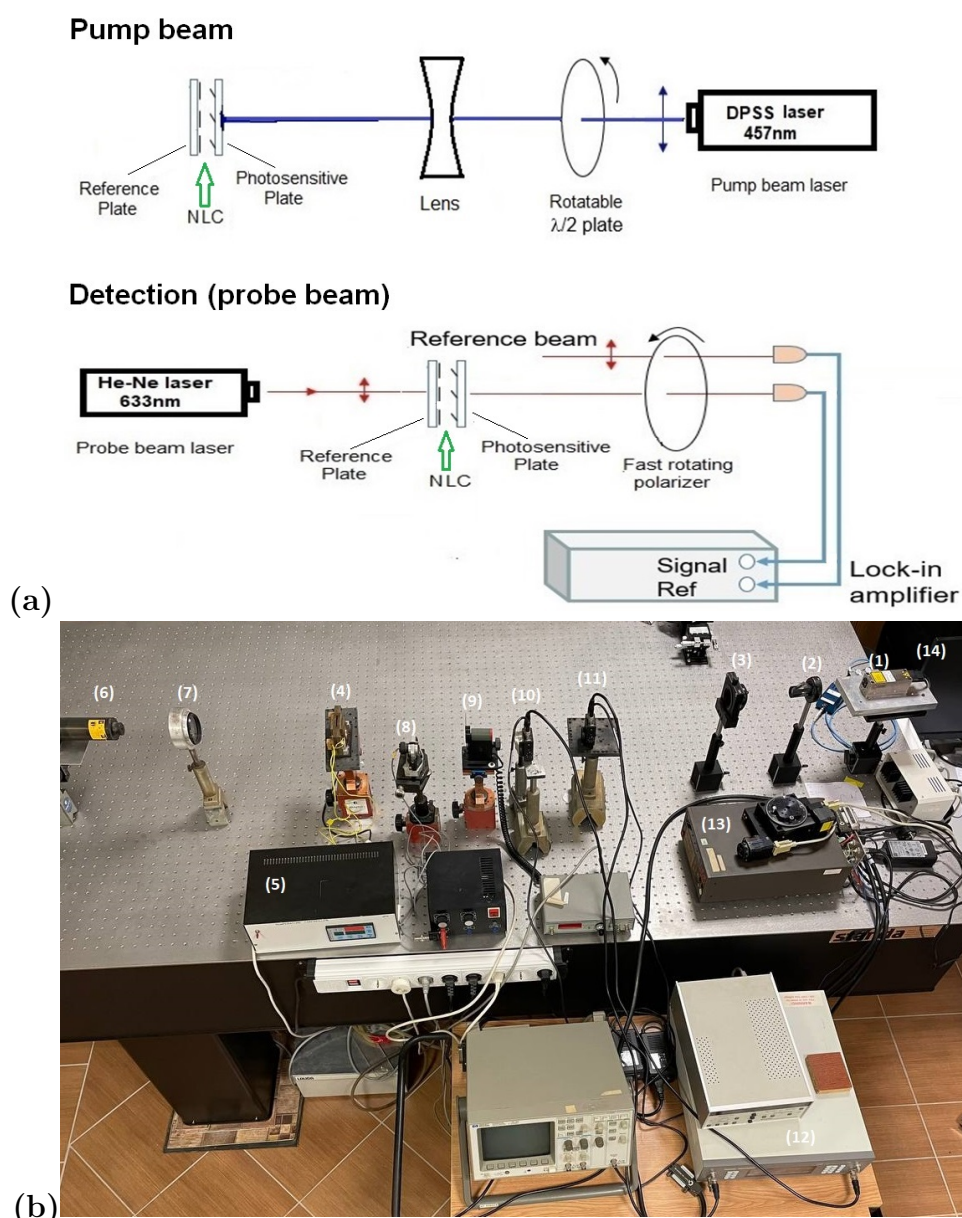


Figure 2.4: (a) Schematic drawing of the experimental setup. (b) Photograph on the optical setup: (1) pump laser; (2)  $\lambda/2$  plate, or  $\lambda/2$  Fresnel-rhomb; (3) biconcave lens; (4) hot-stage with the LC sample in it; (5) hot-stage temperature controller; (6) He-Ne probe laser; (7) rotatable polarizer; (8) reference diode laser; (9) fast rotating polarizer sheet; (10) photodetector for the reference beam; (11) photodetector for the probe beam; (12) lock-in amplifier; (13) digital multimeter; (14) personal computer.

For the determination of the "in-plane" (azimuthal) twist deformation angle  $\varphi$ , the polarization of the probe beam is parallel with the initial director (i.e., with the direction of rubbing on the reference plate), and  $\varphi$  at the command surface can be determined from the phase of the signal.

For the detection of the "out-of-plane" (zenithal) photo-orientation, the polarization of the pump beam is set perpendicular to the initial director (thus, no azimuthal photoalignment is expected), while, the polarization of the probe beam encloses  $45^\circ$  with the initial director, and the amplitude of the signal is measured.

When a significant out-of-plane photoalignment occurs, oscillations in the transmitted light intensity of the probe beam appear, similarly to the electric-, or magnetic-field induced Fréedericksz transition—see e.g., Ref. [96]. One has to note, that for a quantitative estimate of the zenithal photoalignment angle,  $\theta_{photo}$ , besides the sample thickness ( $d$ ), the temperature dependence of all relevant material parameters have to be known for the NLC [90].

## 2.5 Polarized optical microscope

Polarizing optical microscope (POM), is one of the basic devices to analyze mesogenic substances. It is frequently employed to determine phase transition temperatures, and to identify the LC phase type based on the LC textures. I have used Olympus BX50 polarizing optical microscope (shown in Figure 2.5) to determine the phase transition temperatures of LC compounds, and to test the quality of the prepared LC sandwich cells (see for example, the POM image made on an LC cell, shown in Figure 2.6). For details on the principles of polarizing optical microscopy see, e.g., Ref. [97].

I have designed an experimental setup based on the POM, by which some of the photoalignment processes could be visualized. The photograph of the setup is shown in Figure 2.7.

In the setup, the diode laser Toptica iBeam-Smart 445-S (at 445nm) serves as the source of the pump beam. The POM is equipped with a CCD camera (Flir BFS-U3-32S4C-C), and on the 5X objective of the microscope a 3D printed holder is mounted. The holder holds a beamsplitter cube and a band-pass filter preventing the laser light reflected from the sample to enter the objective, the ocular and the CCD camera. The LC sample is placed in a hot-stage (Instec HCS402) which temperature is regulated by

## 2.5. POLARIZED OPTICAL MICROSCOPE

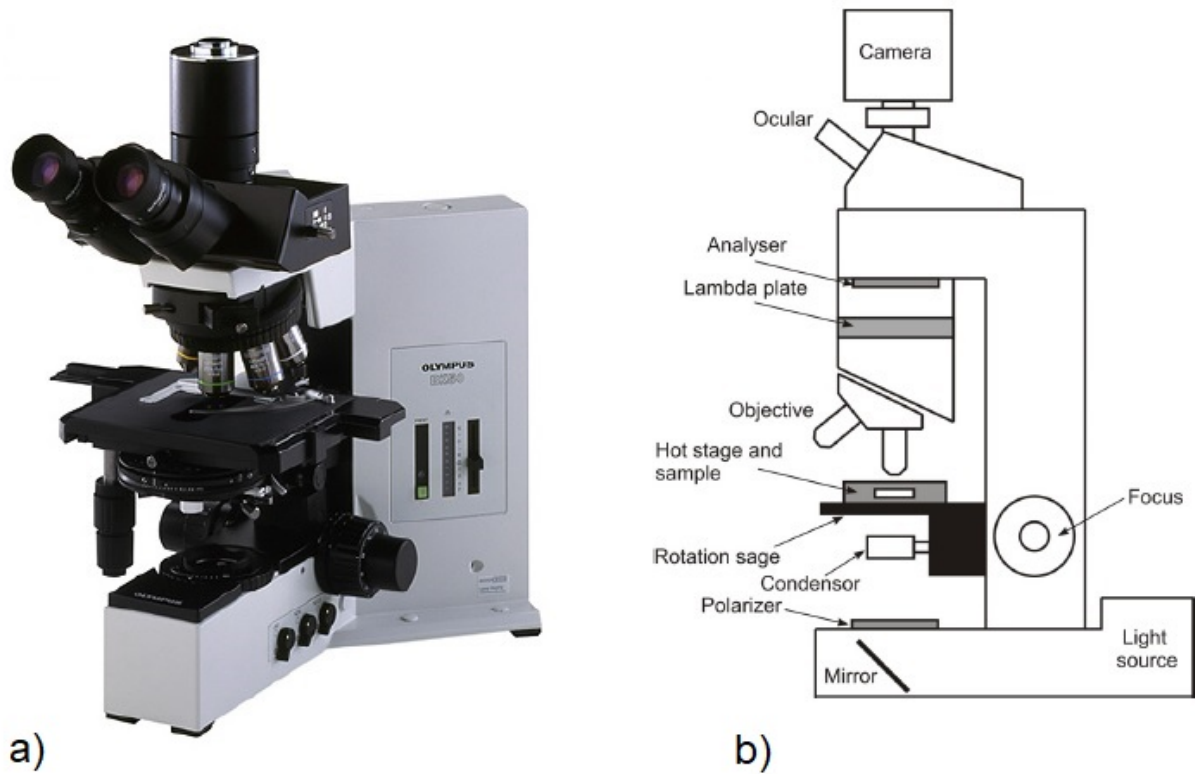


Figure 2.5: a) Olympus BX50 polarizing optical microscope. b) Schematic representation of the parts of a polarizing optical microscope equipped with a CCD camera. [98]

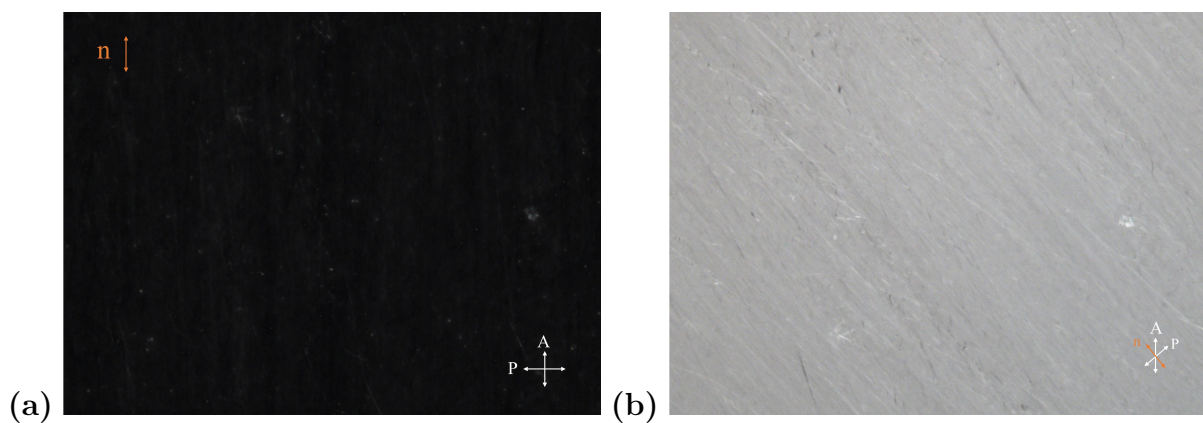


Figure 2.6: Photograph taken with the help of POM (equipped with a CCD camera) on a NLC layer in planarly oriented sandwich cell. The small white dots indicate some impurities or orientational imperfections in the sample. P and A denote the direction of the polarizer and analyzer, respectively, while  $\mathbf{n}$  denotes the nematic director.



the Instec mK2000 controller. POM works on transmission mode, i.e., the LC sample is illuminated from below with polarized white light. The polarization of the pump beam is regulated by the rotatable  $\lambda/2$  plate. The beam is focused by a biconvex lens, enters the beamsplitter cube from which 90% of it is reflected on the LC sample from above. This setup has allowed us to visualize some photoalignment processes, the results of which are still unpublished, and will shortly be discussed in the Appendix.

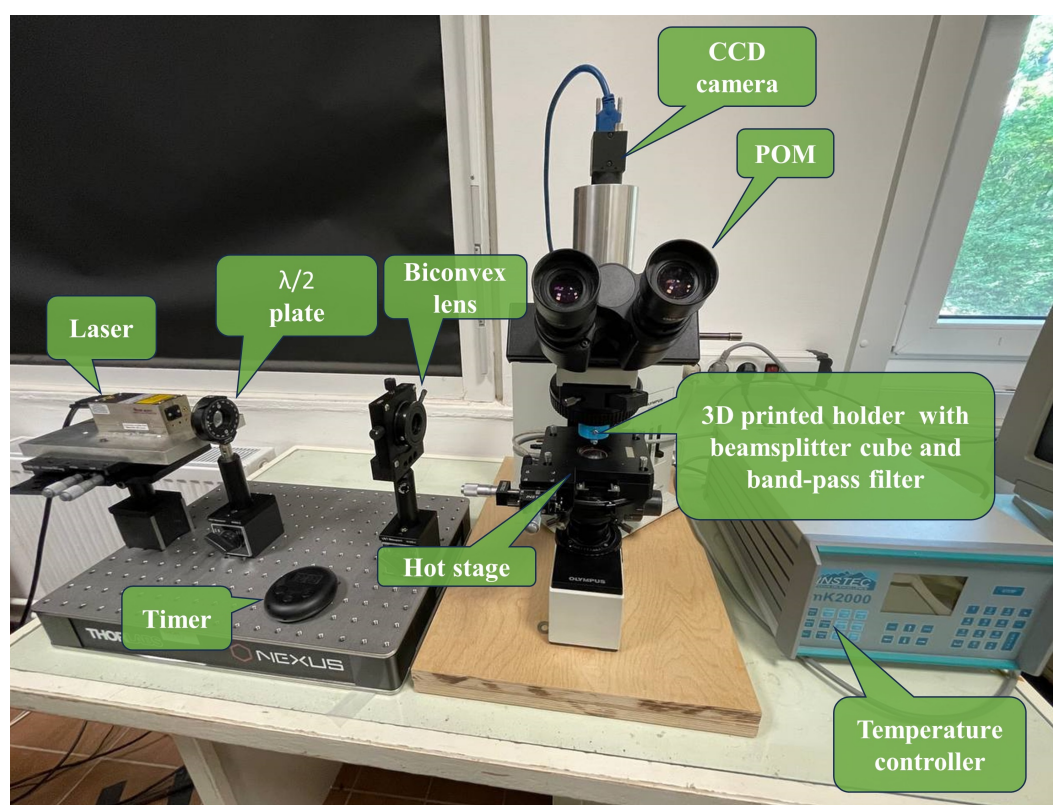


Figure 2.7: Optical setup combined with polarized optical microscope for visualization of the photoalignment processes.

## 2.6 Atomic force microscope

Atomic force microscope (AFM) measurements have been used to detect photo-induced changes (including photo-induced mass transfer) on the photosensitive polymer layers in contact with the air. I have performed these measurements at the Institute of Experimental Physics, Slovak Academy of Sciences, Košice in the framework of Erasmus+ Scholarship for Short-Term Doctoral Mobility.

## 2.6. ATOMIC FORCE MICROSCOPE

---

The preparation of the substrates, (cleaning and coating with the photosensitive polymer layer) is described in Section 2.1.

Atomic force microscopy (AFM) scans on the photosensitive substrates prior and after the polarized laser illumination were carried out with Agilent 5500 AFM system (Figure 2.8) equipped by PicoView 1.14.3 control software. The images were acquired in the semi-contact (tapping) mode using medium soft silicon cantilevers (Oxford Instruments, model AC240TS-R3) with the resonant frequency of 70 kHz (typ.), and spring constant of 2 N/m (typ.). The measurements were performed at ambient relative humidity of 30 – 40% at room temperature. The captured images were processed using freely available software from Gwyddion [99].

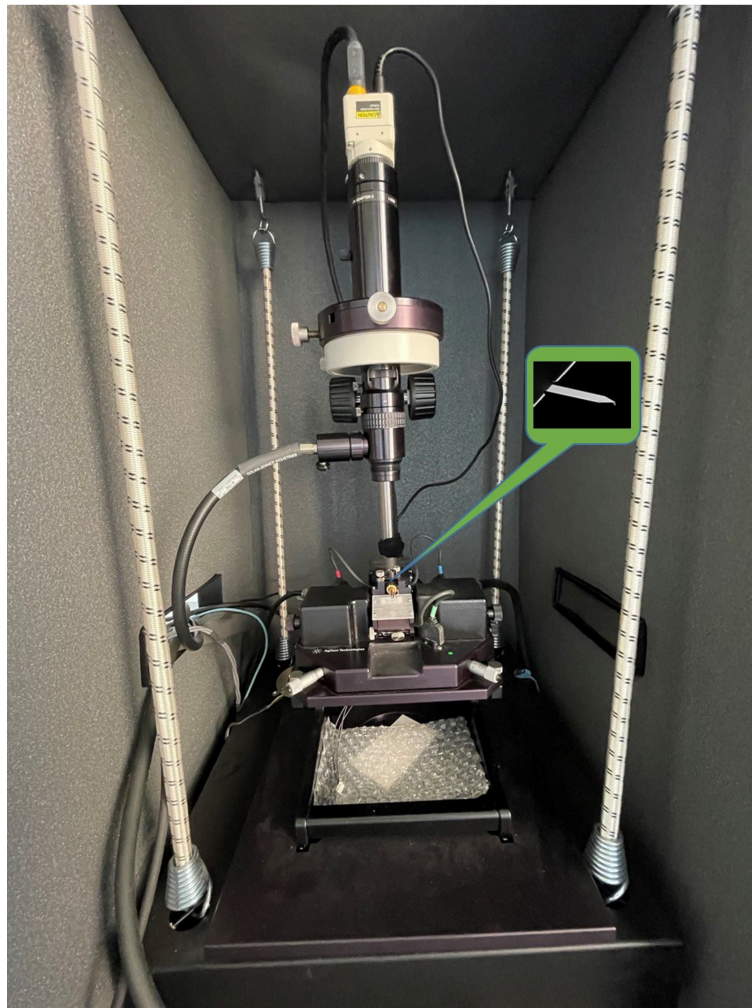


Figure 2.8: Agilent 5500 atomic force microscope. Inset: the tip of the AFM.





---

---

## CHAPTER 3

---

# ROLE OF THE LIQUID CRYSTALLINE MOLECULAR STRUCTURE IN PHOTOALIGNMENT

In order to clarify the role of the molecular structure of NLC in photoalignment process, we have systematically varied the rigid core of the liquid crystal molecules interfacing the pDR1 polymer. Besides the E7 LC mixture, in which the rigid core of the LC molecules contains biphenyl, LCs with phenylcyclohexane rigid core (PCH3, PCH5, PCH7 and 6CHBT, as well as, with bicyclohexane rigid core (ZLI1695) have been used in the experiments—see Table 2.1. Finally, for the experimental test of our interpretation regarding the interaction between the pDR1 polymer layer and the LC molecules, has been performed with 5CPUF LC containing biphenyl in the rigid core connected to three fluorine atoms (see Table 2.1).

Measurements have been focused on both azimuthal (in-plane) and zenithal (out-of-plane) photoalignment, as well as on the back-relaxation of the systems when the photo excitation is turned off.

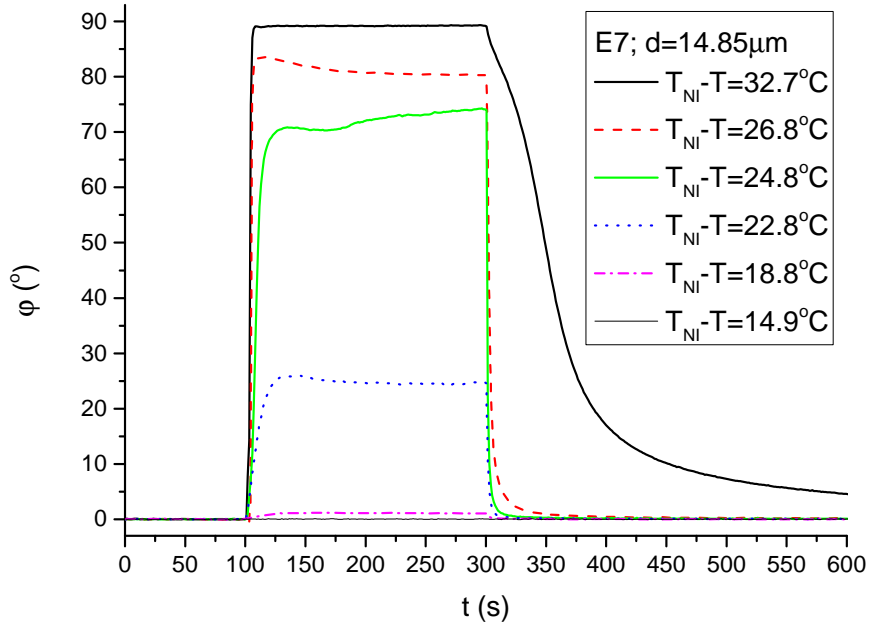
### 3.1 Azimuthal (in-plane) photoalignment

In the measurements of the azimuthal photoalignment the polarization of both the pump and the probe beam has been set parallel with the initial  $\mathbf{n}$ , and the phase of the probe beam has been measured, which is directly related to the azimuthal photoalignment angle  $\varphi$ . The temperature of the samples has been varied from room temperature up to  $T_{NI}$ . Under these conditions the pump beam is expected to induce a twist deformation at the photosensitive substrate resulting in a twisted LC cell from the initially planar one. In the case of complete photoalignment, the twist angle  $\varphi$  should saturate at  $90^\circ$ .

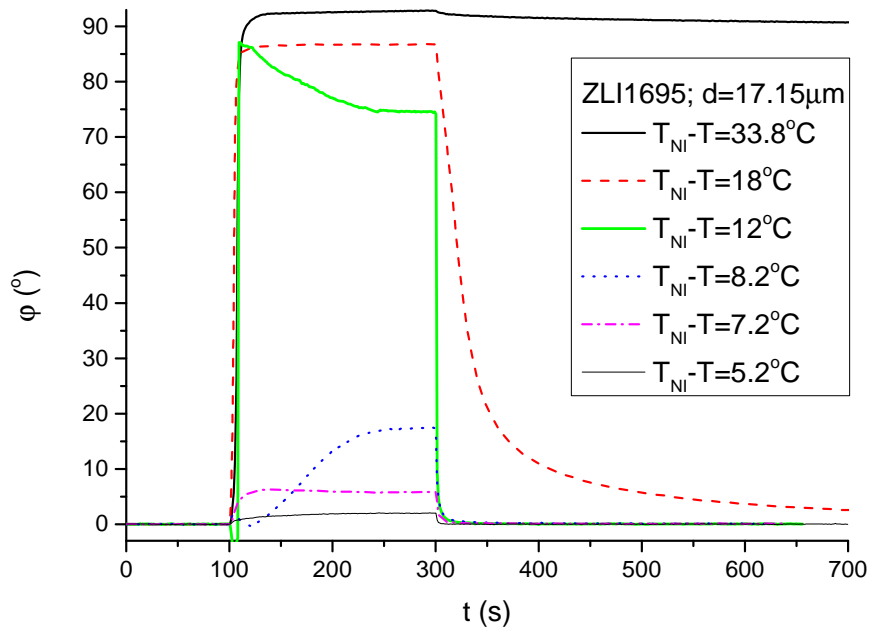
Figure 3.1(a) and 3.1(b) shows the temporal evolution of the photoinduced twist angle  $\varphi$  for LC cells containing E7 and ZLI1695, respectively, measured at different temperatures ( $\Delta T = T_{NI} - T$ ). The pump-beam has been switched on at  $t = 100$  s and switched off at  $t = 300$  s in all measurements. As one can see, at lower temperatures (e.g. at room temperature), the azimuthal twist deformation reaches the saturation value of approximately  $90^\circ$  for both E7 and ZLI1695, indicating a complete azimuthal photo-reorientation. With the increase of the temperature, the twist angle gradually decreases, and vanishes for E7 far below  $T_{NI}$ , while for ZLI1695 just below  $T_{NI}$  – see Figure 3.1 [N1].

Figure 3.2 shows the temporal evolution  $\varphi(t)$  for LC cells filled with NLCs from the PCH homologous series. The results on the azimuthal photoalignment angle for these cells are similar to those obtained for the cell filled with ZLI1695 [N1].

Figure 3.3 gives the temperature dependence (relative to the nematic-to-isotropic phase transition temperature,  $T_{NI}$ ) of the saturated value of the azimuthal photoalignment angle  $\varphi$ , measured for E7, ZLI1695 and PCH series. For all NLCs a sudden decrease of  $\varphi$  has been observed below  $T_{NI}$ . However, the decrease of  $\varphi$  for E7 occurred in a much lower temperature range of  $T_{NI} - T = 20 - 25$  °C, which is in full agreement with previous results [90]. For ZLI1695 and the PCH NLCs, the sudden decrease in  $\varphi$  occurs much closer to the nematic-to-isotropic phase transition temperature ( $T_{NI} - T \leq 10$  °C). Moreover, concentrating on PCH series in Figure 3.3, the decrease of  $\varphi$  occurs closer to

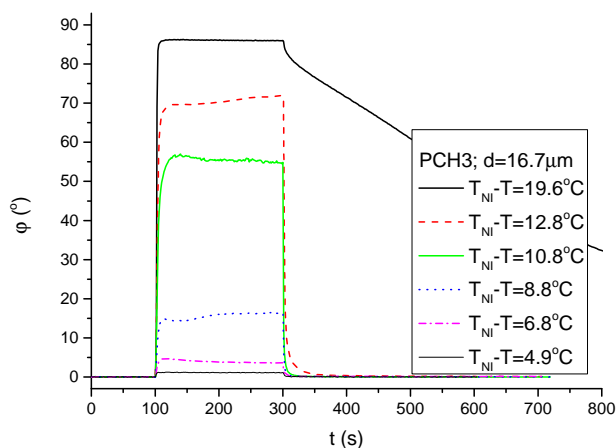


(a)

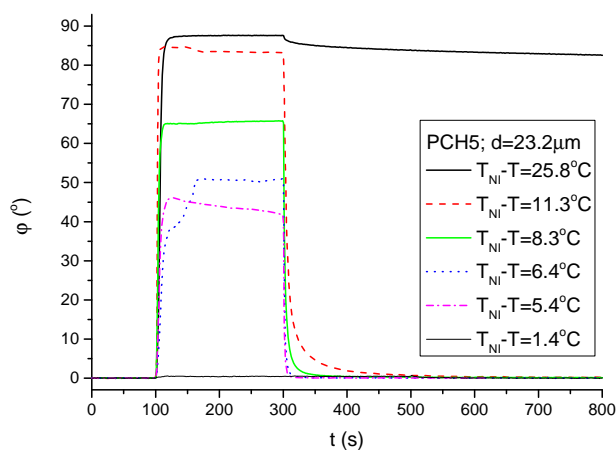


(b)

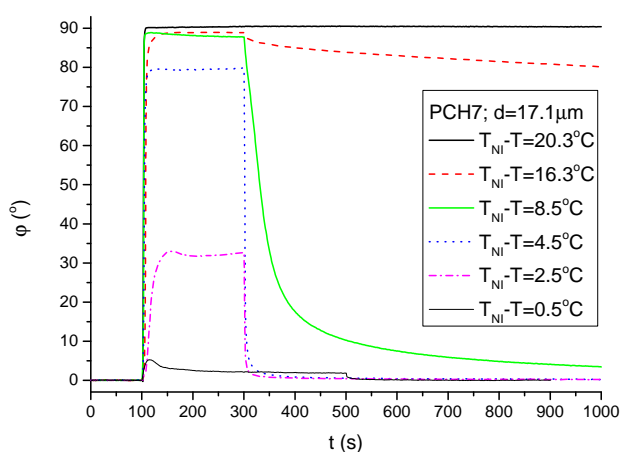
Figure 3.1: Azimuthal photo-reorientation angle  $\varphi$  in time, measured at different temperatures in cells filled with NLCs having: (a) phenyl rings in the rigid core (E7), and (b) cyclohexane groups in the rigid core (ZLI1695). The pump-beam was switched on at  $t = 100$  s, and switched off at  $t = 300$  s.



(a)



(b)



(c)

Figure 3.2: Azimuthal photo-reorientation angle  $\varphi$  in time, measured at different temperatures in cells filled with NLCs having a phenylcyclohexane rigid core: (a) PCH3, (b) PCH5, and (c) PCH7. The pump-beam was switched on at  $t = 100$  s, and switched off at  $t = 300$  s, or at  $t = 500$  s (for the highest temperature in case of PCH7).

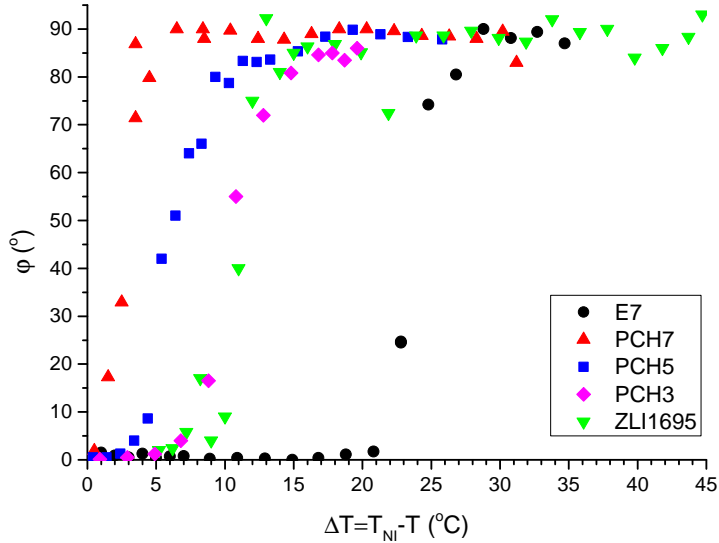


Figure 3.3: Temperature dependence of the saturated azimuthal photo-reorientation angle  $\varphi$ , measured in cells filled with various NLCs (E7, PCH5, PCH7 and ZLI1695) as indicated in the legend.

$T_{NI}$  as the length of the alkyl chain is increased, which may indicate a possible influence of the flexible alkyl chain on the photoalignment [N1].

## 3.2 Zenithal (out-of-plane) photoalignment

Previous measurements [90] have shown significant zenithal photoalignment in samples containing E7 with a biphenyl rigid core. Zenithal photoalignment occurred in the temperature range above which the azimuthal photo-reorientation angle  $\varphi$  suddenly drops (i.e., for  $\Delta T = T_{NI} - T \lesssim 20$  °C – see also in Figure 3.3).

To test whether a similar zenithal photoalignment occurs in samples with PCH compounds, or with ZLI1695, the experimental setup for zenithal reorientation was used (see Section 2.4 for pump-probe beam optical setup).

Measurements on the zenithal photoalignment have been performed from room temperature to the clearing temperature  $T_{NI}$  for PCH3, PCH5, PCH7, as well as for ZLI1695. None of these measurements resulted in oscillations of the transmitted light intensity, indicating the absence of a significant zenithal photo-reorientation. In all these samples,

only a slight change in transmitted light intensity has been observed at all temperatures [N1]. This change could be the result of a small misalignment of the director at the two confining surfaces (see Section 2.1), a small misalignment of the polarization direction of the pump beam and  $\mathbf{n}$ , or a small zenithal photoalignment as mentioned in Ref. [90].

Figure 3.4 illustrates the slight changes in the transmitted light intensity in a  $d = 17.1$   $\mu\text{m}$  thick cell filled with PCH7 [N1] at three different temperatures:  $\Delta T = T_{NI} - T = 24.3$   $^{\circ}\text{C}$ ,  $7.5$   $^{\circ}\text{C}$ , and  $1.5$   $^{\circ}\text{C}$ . The pump beam was activated at  $t = 100$  s and deactivated at  $t = 300$  s. Based on these measurements one can conclude that in samples with PCH NLCs and with the ZLI1695 mixture, the magnitude of the zenithal photoalignment is either zero, or it is much smaller than that detected in the NLC with biphenyl rigid core (E7) reported in Ref. [90].

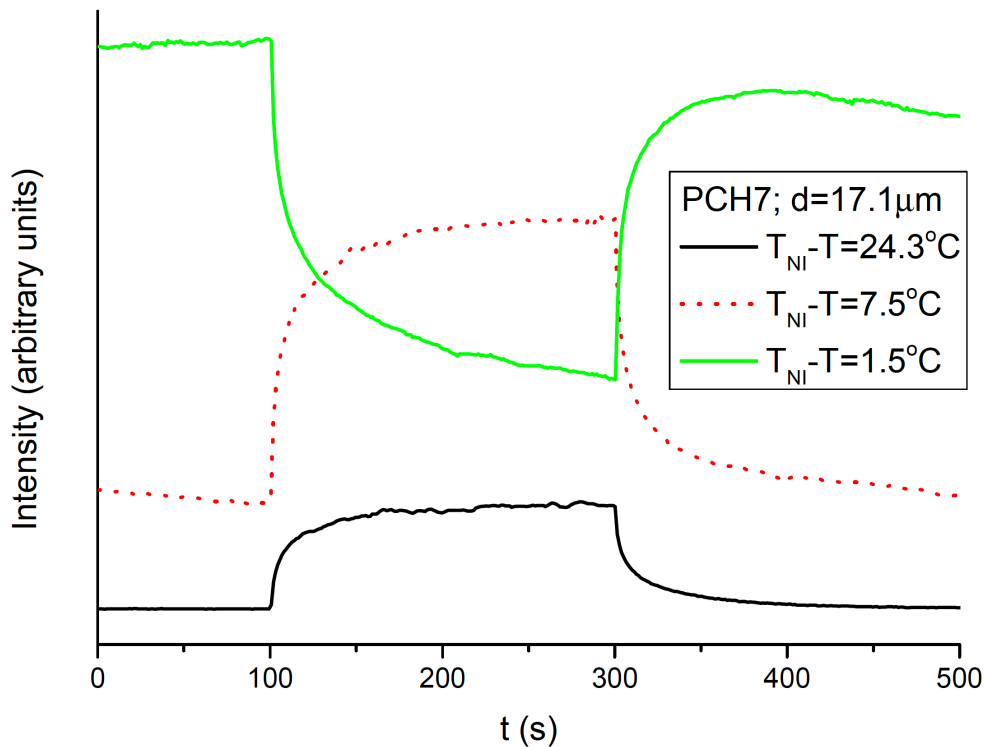


Figure 3.4: Temporal variation of the transmitted light intensity of the probe beam measured in a PCH7 cell at different temperatures in the setup for detection of zenithal photo-reorientation (pump beam polarization perpendicular to  $\mathbf{n}$ , probe beam polarization encloses  $45^{\circ}$  with  $\mathbf{n}$ ).

### 3.3 Back-relaxation from the azimuthal photoalignment

The relaxation process towards the initial (planar) alignment has been monitored as well, via the time evolution of the azimuthal photoalignment angle  $\varphi$  after switching off the pump beam.

One can deduce from Figures 3.1, 3.2 and 3.5 that with the increase of temperature, the back-relaxation becomes faster. Such temperature dependence of the back-relaxation dynamics has been attributed to the temperature dependence of the equilibrium concentration of the trans-cis isomers, and by that of the cis-to-trans isomerization kinetics [90]. The equilibrium concentration of the trans conformers at low temperature is much higher than the equilibrium concentration of the cis conformers, and upon the pump beam activation the trans-to-cis isomerization is faster than the cis-to-trans isomerization upon the deactivation of the pump beam. With the increase of the temperature, the equilibrium ratio of the two conformers undergoes a slight shift in favor of the cis isomer, and the trans-to-cis isomerization somewhat slows down, while the cis-to-trans isomerization speeds up. These processes ultimately lead to slower photoalignment and faster relaxation at higher temperatures, as observed [N1, N2].

Furthermore, it has been also observed that the speed of back-relaxation is influenced not only by the temperature dependence of the isomerization kinetics, but also depends on NLC material that is used in contact with the polymer. This can be seen in Figures 3.1, 3.2 and 3.5, which compare the behavior of E7, ZLI1695 and NLCs from PCH series [90]. The back-relaxation at a given temperature  $T_{NI} - T$  has been found much faster for E7 compared to other NLCs.

Figure 3.5 shows in details the temperature dependence of the back-relaxation kinetics for PCH7 at three different temperature ranges of the nematic phase: low temperature range (a), mid temperature range (b), and high temperature range (c). Obviously, the relaxation times differ by orders of magnitude at high and at low temperatures (from



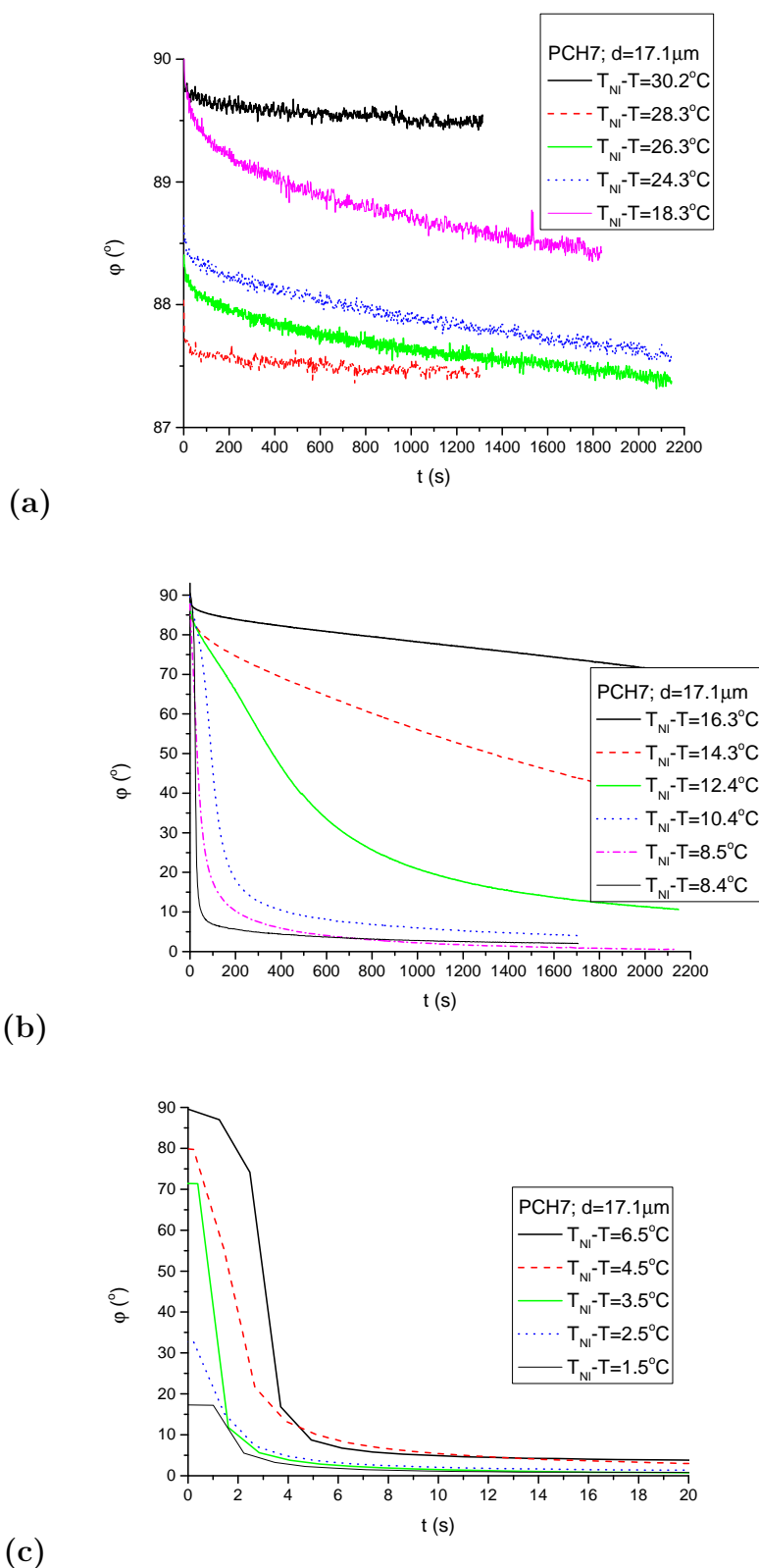


Figure 3.5: Back-relaxation of the azimuthal photo-reorientation angle  $\varphi$  (pump beam switched off at  $t = 0$  s) measured at different temperatures as indicated in the legend on a  $d = 17.1 \mu\text{m}$  thick cell filled with PCH7. (a) Low-temperature range; (b) mid-temperature range; (c) high-temperature range.

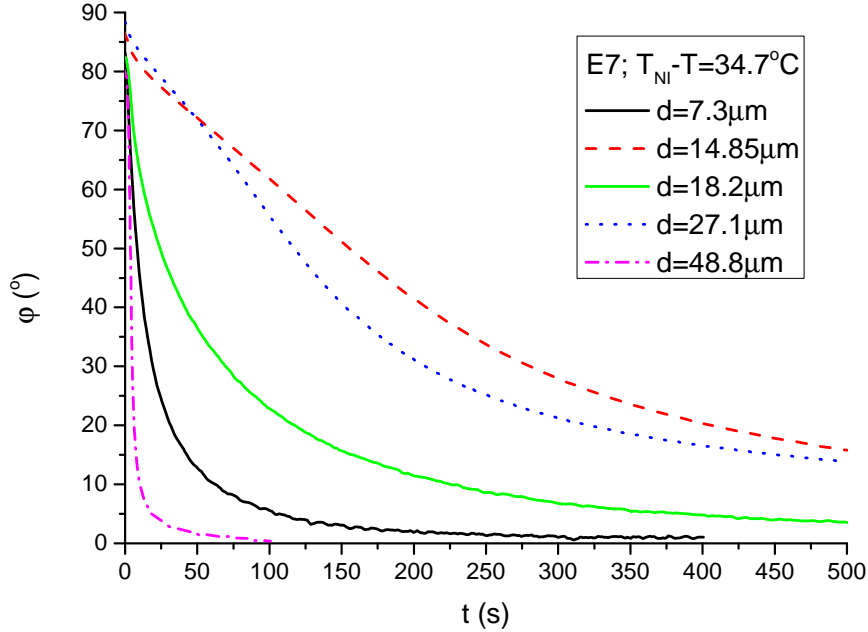


Figure 3.6: Back-relaxation of the azimuthal photo-reorientation angle  $\varphi$  (pump beam switched off at  $t = 0$  s) measured at a given temperature in cells of different thickness  $d$  filled with E7 as indicated in the legend.

seconds to days).

Figure 3.6 shows the temporal evolution of the back-relaxation of the photoinduced azimuthal (twist) angle  $\varphi$  in cells of different thickness ( $d$ ), filled with E7 and measured at the same temperature  $T_{NI} - T = 34.7$  °C. Surprisingly, no straightforward thickness dependence of the relaxation kinetics has been found: the thickest samples relaxed the fastest, followed by thinnest cell. This finding is reminiscent of non-trivial  $d$  dependence of the temperature range at which the sudden decrease of  $\varphi$  has been previously detected for E7 [90].

### 3.4 Discussion

The photoalignment experiments at the NLC-pDR1 polymer interface have led to an almost complete azimuthal photoalignment ( $\varphi \approx 90^\circ$ ) at room temperature (far below  $T_{NI}$ ) for all NLCs discussed in this dissertation [N1]. The only exception was the earlier

analyzed NLC, namely 5CB, for which  $T_{NI}$  is relatively close to room temperature [90]. As the temperature was increased, at some point  $\varphi$  started to decrease for all NLCs. Depending on the molecular structure of NLCs, considerable differences have been found in the temperature range at which the decrease of  $\varphi$  occurs. For NLCs with biphenyl rigid core, the sudden decrease of  $\varphi$  has been detected far below  $T_{NI}$ : for E63 in the temperature range  $T_{NI} - T = 30 - 35$  °C [90] and for E7 in the range of  $T_{NI} - T = 20 - 25$  °C (see Figure 3.3). In contrast, NLCs having a phenylcyclohexane or a bicyclohexane rigid core, the drop of  $\varphi$  has happened much closer to  $T_{NI}$ , at  $T_{NI} - T \lesssim 10$  °C, (see Figure 3.3). One has to note that in this high temperature range, a temperature induced change in the pretilt angle (anchoring transition towards the homeotropic alignment) has also been observed for E7 and 5CB NLCs [90].

According to the experimental results, NLCs with biphenyl rigid core exhibit significant zenithal photoalignment in the high temperature range, where the azimuthal photoalignment diminishes [90, N1]. In contrast, in NLCs with phenylcyclohexane or bicyclohexane rigid core only indications have been found for a possible slight zenithal photoalignment of negligible magnitude in the whole temperature range of the nematic phase.

At a given relative temperature,  $T_{NI} - T$ , the back-relaxation of the NLC having a biphenyl in the rigid core (E7) has been found faster by orders of magnitude compared to that of the NLCs having phenylcyclohexane (PCH3, PCH5, PCH7), or bicyclohexane (ZLI1695) in the rigid core—see Figures 3.1 and 3.2.

These findings, namely the diminishing azimuthal photoalignment far below  $T_{NI}$  and the appearance of the zenithal photoalignment instead, as well as the fast back-relaxation indicate that in NLCs with biphenyl rigid core something, presumably an interaction between the pDR1 polymer and the NLC, acts against the conventional azimuthal photoalignment and helps the relaxation towards the initial (planar) alignment. On the other hand, the persistence of the azimuthal photoalignment to temperatures much closer to  $T_{NI}$  (up to temperatures at which presumably the temperature induced orientational transition takes over [90]), the much smaller (if any) zenithal photoalignment, and the much slower back-relaxation, observed in NLCs with phenylcyclohexane or bicyclohex-

### 3.4. DISCUSSION

---

ane rigid core, indicate that in these systems no such interaction is present, or it is much smaller (compared to that in systems with NLCs having biphenyl rigid core).

To identify the potential source of such interaction, for simplicity, first we consider the size of the biphenyl core [100, 101] and that of the azobenzene trans-isomer [102] only, and we compare them in Figure 3.7(a). Phenyl rings are capable to exhibit aromatic interactions that have been proposed to consist of van der Waals, hydrophobic and electrostatic forces [103]. Several geometries have been proposed on the basis of the electrostatic component, arising from interactions of the quadrupole moments of the aromatic rings, based on the greater electron density on the face of the ring and reduced electron-density on the edge [104]. One of them is the so called offset stacked aromatic  $\pi - \pi$  interaction [105, 106], which is demonstrated by representation of the molecular electrostatic surface potential (MESP) for four benzene rings in Figure 3.7(b). We note here, that in the biphenyl structure, the two rings are somewhat twisted with respect to each other [100, 107], the CN polar head and the alkyl tail in the cyano-biphenyl NLCs [108], as well as the azo-coupling in the azobenzene derivative [109] introduce minor modifications in the simplified MESP shown in Figure 3.7(b). Despite these minor modifications, the dimensions of the NLCs with the biphenyl rigid core and the azobenzene moiety attached to the PMMA polymer suggest the presence of offset stacked aromatic  $\pi - \pi$  interactions between them [N1]. These interactions act against the trans-to-cis isomerization upon the excitation of the azobenzene moiety (i.e., against the photoalignment) by introducing additional restoring stresses. For further analysis, one has to take into account the temperature dependence of the azimuthal and zenithal anchoring strengths. Based on the experimental results [90] it has been proposed that the zenithal anchoring strength weakens with the increase of the temperature much faster than the azimuthal anchoring strength. This assumption has been supported by the experimental observations at high temperatures ( $T_{NI} - T < 10 \text{ }^\circ\text{C}$ ), at which a temperature induced orientational transition from planar towards the homeotropic has been observed without any pump beam illumination [90]. These phenomena have been originally attributed to the flexibility of the spacer consisting of two methylene units that connects the PMMA main chain with the

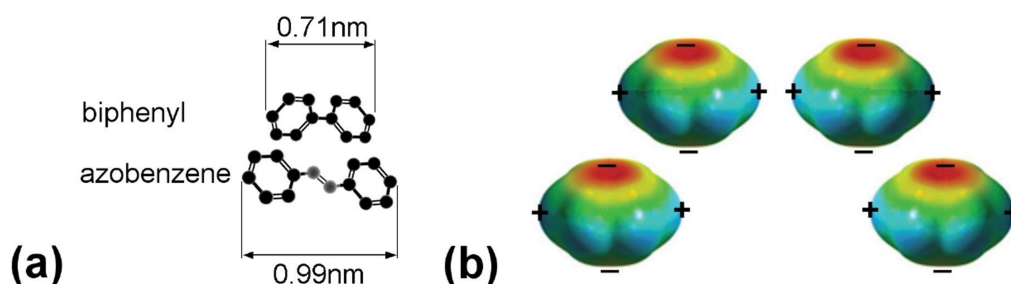


Figure 3.7: (a) Size of the biphenyl rigid core and that of the azobenzene trans-isomer. (b) Offset stacked aromatic interaction between benzene molecules enabled by the molecular electrostatic surface potential (MESP, blue is positive, red is negative).

azobenzene moiety (see between the oxygen and nitrogen atoms in Figure 2.3(a)) [90].

According to our interpretation, under the pump beam illumination, the additional restoring stresses originating from the offset stacked aromatic  $\pi - \pi$  interactions in case of the NLCs with biphenyl rigid core may cause the “crossover” between the zenithal and azimuthal anchoring strengths to occur at a considerably lower temperature. In other words, the orientational transition from planar towards homeotropic orientation under pump beam illumination occurs at much lower temperatures than it occurs without the photo-excitation. Naturally, when the photo-excitation is terminated, the driving force for trans-to-cis isomerization is also stopped, and the system relaxes back to the initial planar alignment [N1]. One has to note that in this scenario, it is not necessarily required to have a conventional trans-to-cis isomerization assisted photoalignment. The prerequisites are only the stresses induced by the isomerization and the offset stacked aromatic  $\pi - \pi$  interactions, along with the proper azimuthal and zenithal strengths.

On the other hand, one has also to note, that whenever the pump beam is switched off, the suggested  $\pi - \pi$  interaction helps the back-relaxation, by which it becomes faster. This can explain by orders of magnitude faster back-relaxation observed in NLCs with biphenyl rigid core compared to that in NLCs with phenylcyclohexane or bicyclohexane rigid core.

### 3.4. DISCUSSION

---

In case of NLCs with phenylcyclohexane or bicyclohexane rigid core, such  $\pi - \pi$  interaction between the NLC molecules and the azobenzene moiety of pDR1, acting against the trans-to-cis isomerization is not expected, see Figure 3.8 (for the MESP of cyclohexane see e.g. [110]). Therefore, the azimuthal photoalignment is maintained (almost) over the whole nematic temperature range, while the zenithal photoalignment is either insignificant or completely absent. Moreover, the back-relaxation of NLCs with a phenylcyclohexane or bicyclohexane rigid core is significantly slower when compared to NLCs containing a biphenyl rigid core. Therefore, the proposed  $\pi - \pi$  interaction together with the different temperature dependence of the azimuthal and zenithal anchoring strengths (proposed in Ref. [90]), can give a qualitative explanation for the experimental findings stated above.

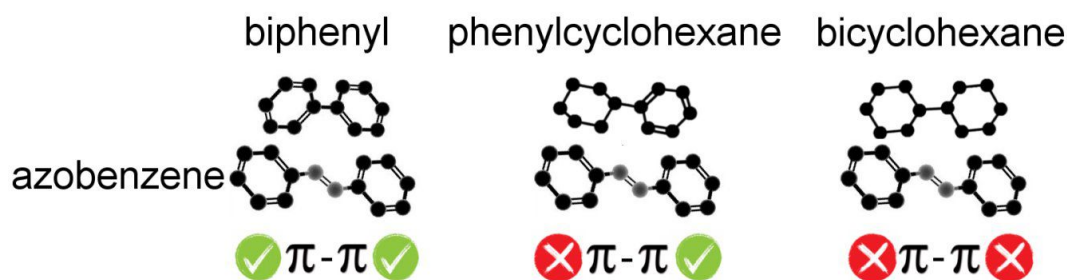


Figure 3.8: Scaled, schematic drawing of the trans isomer of the azobenzene and LC rigid cores of biphenyl, phenylcyclohexane and bicyclohexane, together with the aromatic interaction possibilities between them.

To validate the assumption about the role of the offset stacked  $\pi - \pi$  aromatic interaction, more NLC compounds have been chosen for further studies, namely, NLC compounds 6CHBT and 5CPUF—see Table 2.1. 6CHBT has similar molecular structure with phenylcyclohexane rigid core as PCH homologue series with the exception that the phenyl ring in 6CHBT is connected to a polar thiocyanate (SCN) group instead of a CN group in PCH LCs. Therefore, the photoalignment at the pDR1–6CHBT interface is expected to have similar characteristics as those at the interface pDR1–PCH homologue series, namely, efficient azimuthal photoalignment over a wide temperature range of the nematic phase without considerable zenithal photoalignment [N1].

The other NLC compound, 5CPUF, has biphenyl in the rigid core, with one of the phenyl rings connected to three fluorine atoms at 3,4,5 positions, which invert the MESP of the ring [111]. The three fluorine atoms change the MESP of the adjacent ring (and even that of the next phenyl ring) to a large extent (the details will be discussed later, at the end of this Chapter). These modifications in the MESP of the biphenyl part of the 5CPUF molecules prevent the offset stacked  $\pi - \pi$  aromatic interactions between the biphenyl part of the 5CPUF and the trans isomer of the azobenzene moiety of the interfacing polymer. Thus, if our assumption about the role of the aromatic  $\pi - \pi$  interaction is correct, it is expected that 5CPUF will exhibit the same photoalignment behavior as NLCs with phenylcyclohexane (6CHBT and PCH homologous series) or bicyclohexane (ZLI1695) rigid core. That means, a complete or near-complete azimuthal photoalignment throughout the temperature range of the nematic phase except extremely close to  $T_{NI}$ , where the thermal effect of the pump beam or the possible temperature induced anchoring transition may occur [90]. Furthermore, 5CPUF is not expected to show considerable zenithal photoalignment, and the back-relaxation is expected to be considerably slower than that in cyanobiphenyl NLCs (e.g. 5CB, E63 and E7) [90] due to the absence of the offset stacked  $\pi - \pi$  aromatic interactions between 5CPUF and the pDR1 polymer.

Figure 3.9 shows the temperature dependence of the saturated azimuthal photoalignment angle,  $\varphi_{sat}$  measured for 6CHBT and 5CPUF. A nearly complete azimuthal photoalignment has been detected in the whole temperature range of the nematic phase for both 6CHBT and 5CPUF, with  $\varphi_{sat}$  typically in the range between  $80^\circ$  to  $90^\circ$ . Close to the nematic-to-isotropic phase transition ( $T_{NI} - T \leq 2^\circ\text{C}$ ) a slight decrease of  $\varphi_{sat}$  has been observed, especially in the case of 6CHBT. Even closer to  $T_{NI}$ , at  $T_{NI} - T < 1^\circ\text{C}$  the measurements on the photoalignment angle have failed, because of the thermal effect of the pump beam. This is illustrated with temporal evolution of the signal in Figure 3.10 for both 6CHBT and 5CPUF: when the pump beam is switched on (at  $t = 100$  s), the photoalignment immediately takes place, however, before it ends, the absorbed light heats up the NLC layer at the photosensitive substrate and it undergoes the nematic-to-isotropic phase transition within seconds, and the photoalignment angle

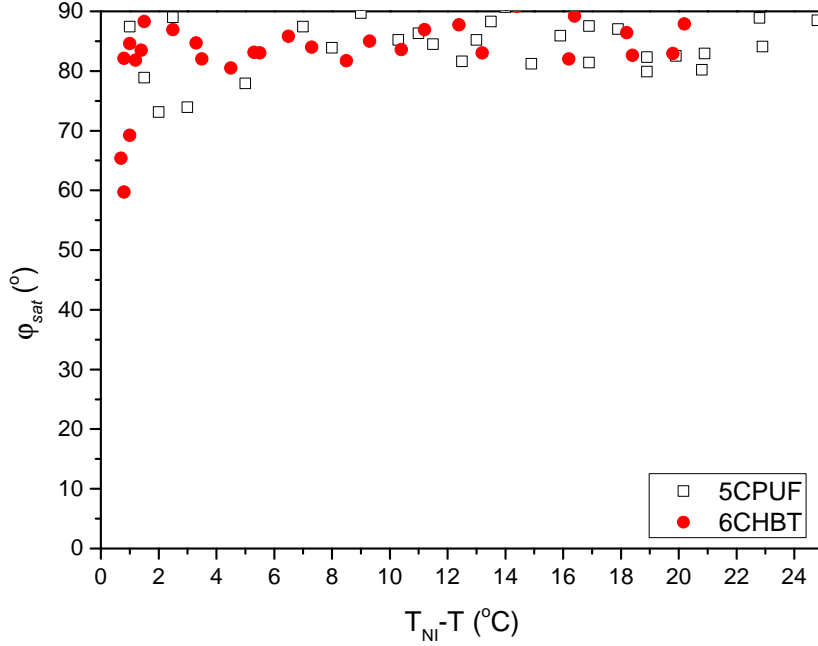


Figure 3.9: Temperature dependence of the saturated azimuthal photoalignment angle  $\varphi_{sat}$  measured for 5CPUF and 6CHBT.

becomes meaningless. Similarly, when the pump beam is switched off, the nematic phase reappears within seconds and the signal tends towards the initial value.

For the estimation of the zenithal photoalignment the temporal evolution of the transmitted light intensity has been monitored in the experimental setup as described in Section 2.4. Figure 3.11 (a) and (b) shows the time evolution of the transmitted light intensity measured at different temperatures  $T_{NI} - T$  for NLCs 5CPUF and 6CHBT, respectively. The pump beam has been switched on at  $t = 100$  s and off at  $t = 300$  s in all cases as indicated in Figure 3.11. For 5CPUF no oscillations in the transmitted light intensity is detected at any temperature when the pump beam is turned on/off, except very close to the clearing point – see at  $T_{NI} - T = 0.5$  °C in Figure 3.11(a). These oscillations, however, appear not because of a significant zenithal photoalignment, but because of the thermal effect of the pump beam: the pump beam heats the sample and drives it through a nematic-to-isotropic phase transition as illustrated in Figure 3.10. Similarly to 5CPUF, in samples with 6CHBT no oscillations in the transmitted light intensity of the



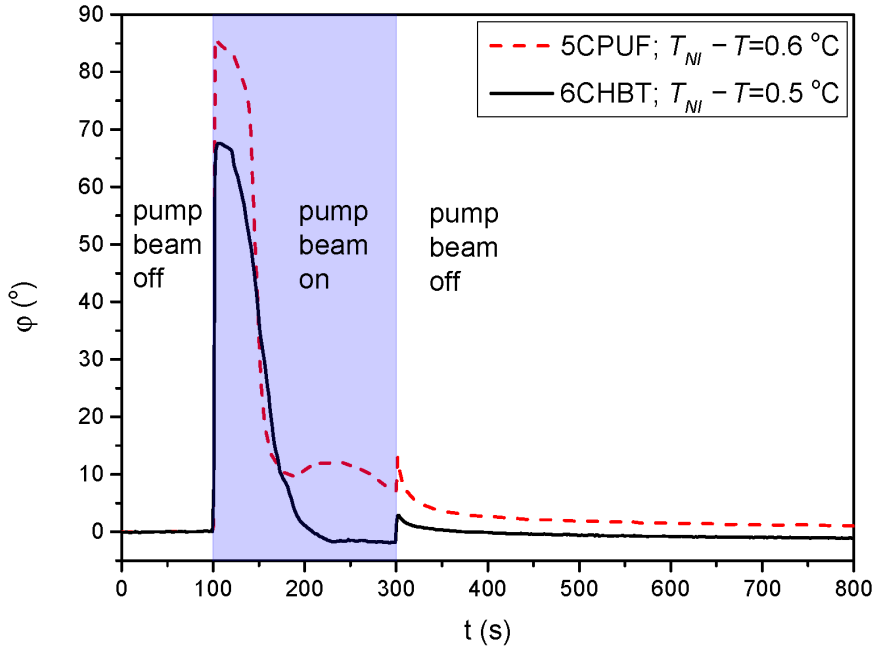
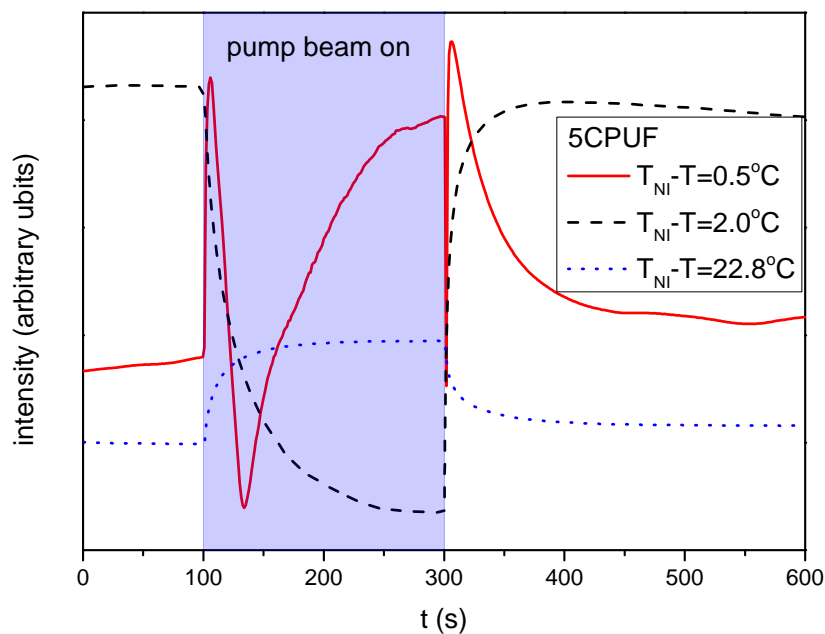


Figure 3.10: Temporal evolution of the azimuthal photoalignment angle  $\varphi$  measured for 5CPUF and 6CHBT at temperatures close to the phase transition temperature  $T_{NI}$ .

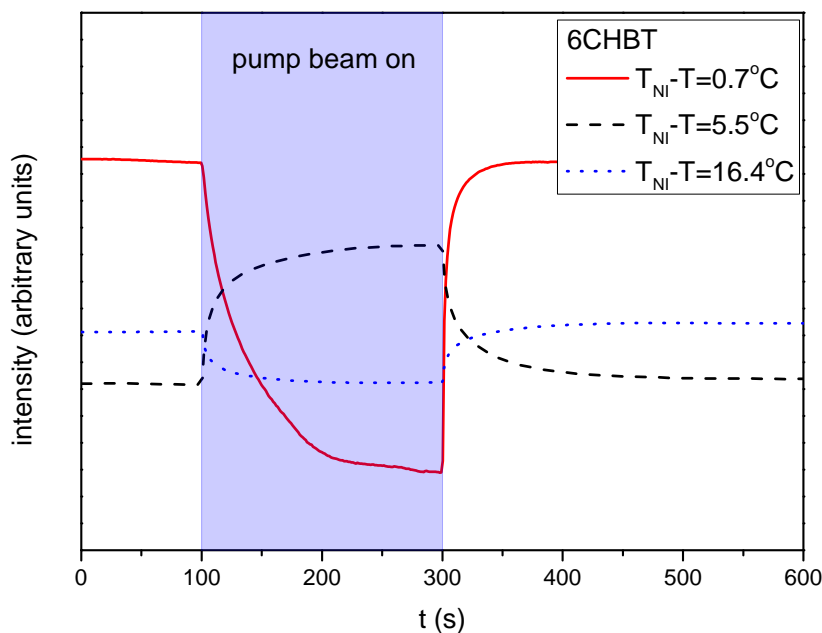
probe beam have been observed either – see Figure 3.11(b).

The back-relaxation of the azimuthal photoalignment has also been monitored for 6CHBT and 5CPUF. Figure 3.12(a) shows the time dependence of  $\varphi$  after the pump beam is switched off (at  $t = 0$  s) for 6CHBT and 5CPUF at nearly the same temperature  $T_{NI} - T$  as indicated in the legend. The relaxation in 5CPUF is somewhat faster than in 6CHBT. Considering the temperature dependence of the back-relaxation dynamics, the general rule for all NLCs is that it becomes faster with the increase of the temperature (i.e., with the decrease of  $T_{NI} - T$ ), as it has also been found for other NLCs previously (for PCH homologous series, E7, E63, and ZLI1695)[90, N1, N2]. Here, we illustrate such a temperature dependence for 5CPUF in 3.12(b).

All our expectations are now confirmed by the experimental results: a complete (or close to complete) azimuthal photoalignment has been found almost in the whole temperature range of the nematic phase for both 5CPUF and 6CHBT (except very close to  $T_{NI}$  —see Figure 3.9), and no considerable zenithal photoalignment is detected (Figure 3.11). At a given  $T_{NI} - T$  temperature, the back relaxation dynamics for 5CPUF

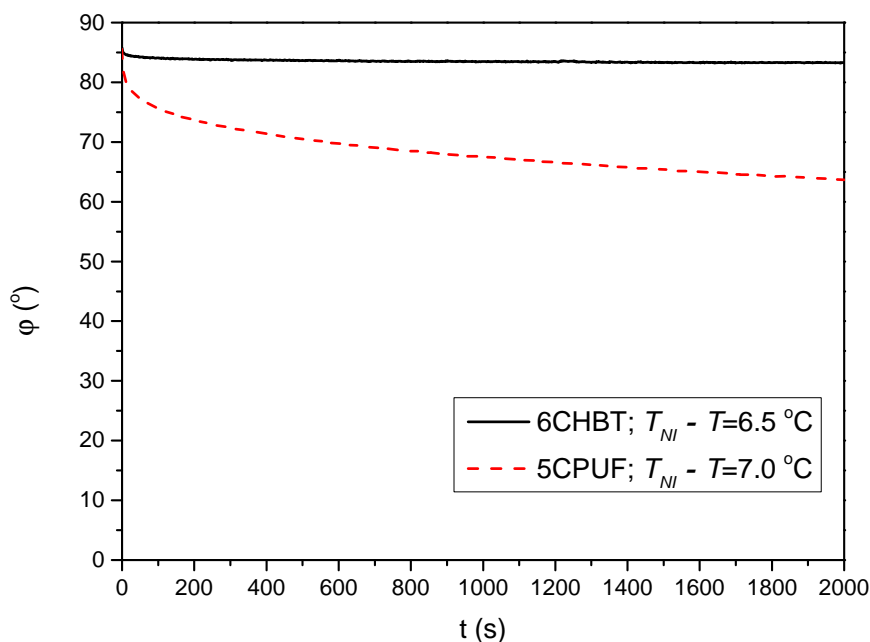


(a)

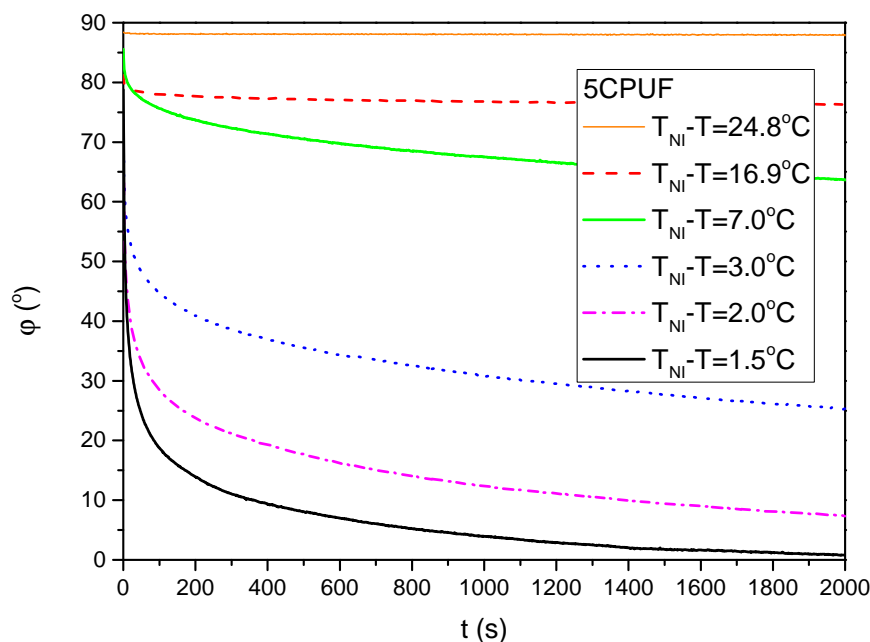


(b)

Figure 3.11: Temporal variation of the transmitted light intensity of the probe beam measured in cells with (a) 5CPUF, (b) 6CHBT, at different temperatures, in the setup for detection of zenithal photoreorientation (pump beam polarization direction perpendicular to  $\mathbf{n}$ , probe beam polarization direction encloses  $45^\circ$  with  $\mathbf{n}$ ).



(a)



(b)

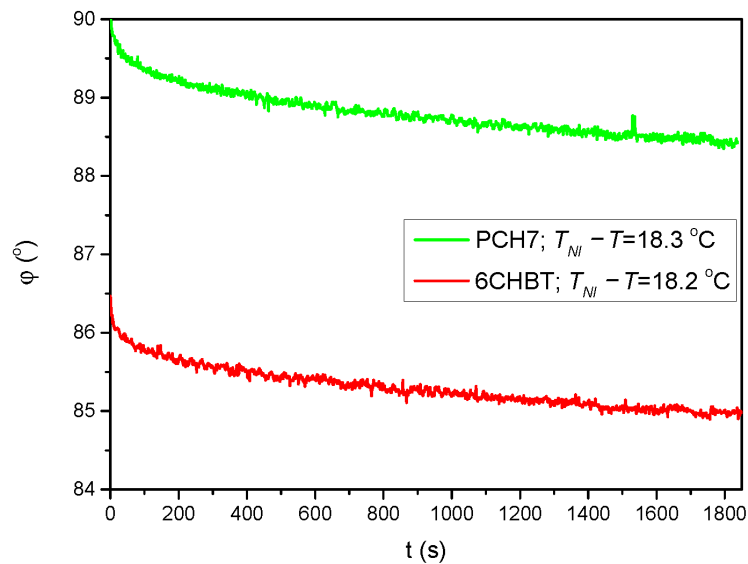
Figure 3.12: Back-relaxation of the azimuthal photoalignment angle,  $\varphi$  for 6CHBT and 5CPUF at relative temperatures  $T_{NI} - T$  indicated in the legend. (b) Temperature dependence of the back-relaxation dynamics for the 5CPUF NLC.

and 6CHBT has been found much slower than in cyanobiphenyl NLC compounds — *cf.* Figures 3.12 and 3.1(a). Moreover, the back-relaxation dynamics of 6CHBT resembles to those obtained for the PCH NLCs. This fact is illustrated in Figure 3.13(a), where the relaxation in 6CHBT is compared with that in PCH7 at about the same relative temperature  $T_{NI} - T \approx 18$  °C.

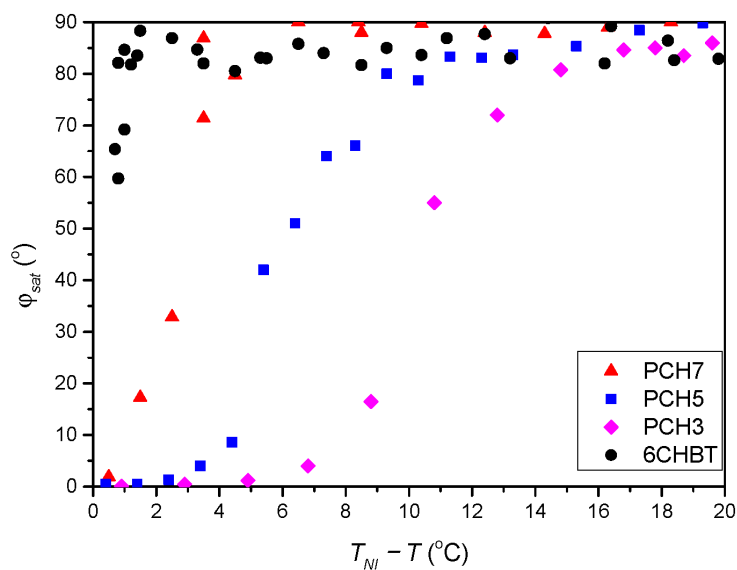
The assumption that the alkyl chain length plays a role in photoalignment has also been raised in our investigations. Focusing on the temperature dependence of the azimuthal photo-reorientation angle  $\varphi(\Delta T)$  for PCH homologous series in Figure 3.3, and on the data from Table 2.1, one can note that the phase transition temperature  $T_{NI}$  increases with the increase of the length of the chain, and the azimuthal photoalignment is maintained to temperatures closer to  $T_{NI}$  as the length of the alkyl chain is increased. Since 6CHBT has similar molecular structure, and shows similar photoalignment characteristics to the PCH homologous series, it is logical to make a comparison in this regard. Figure 3.13(b) compares the temperature dependence of the saturated azimuthal photoalignment angle for 6CHBT and PCH series. Obviously, 6CHBT maintains azimuthal photoalignment the closest to  $T_{NI}$ , despite having a shorter alkyl chain compared to PCH7. Note that on the absolute scale, 6CHBT has the lowest  $T_{NI}$  among these NLC—see Table 2.1. Therefore, the dependence of the photoalignment on the length of the alkyl chain is non-trivial, and still remains puzzling.

The non-trivial thickness dependence of the back-relaxation kinetics shown in Figure 3.6 (and that of the temperature range in which the sudden decrease of  $\varphi$  is detected for E7 [90]) indicates that these processes are much more influenced by some condition(s)/factor(s) other than the sample thickness  $d$ . Such condition/factor could be for example differences in the quality of the pDR1 layer for different cells (despite of the same preparation procedure), or the exact illumination history with the pump beam for each sample.

Finally, we provide the MESP created by MarvinSketch software for 5CPUF, 6CHBT and 8CB LC compounds (where 8CB is representative example of all cyanobiphenyl LCs), as well as some of the conformers of the pDR1 polymer [N2]. The charge distributions



(a)



(b)

Figure 3.13: (a) A comparison of the azimuthal photoalignment angle back-relaxation, in 6CHBT and PCH7 at  $T_{NI} - T \approx 18$  °C as shown in the legend. (b) The temperature dependence of the saturated azimuthal photoalignment angle,  $\varphi_{sat}$  for both PCH homologous series and 6CHBT.

### 3.4. DISCUSSION

---

of molecules are shown in three dimensions, using a color code where blue represents positive and red represents negative – see Figure 3.14(a).

As expected [111], the three fluorine atoms in the structure of 5CPUF change the MESP of the phenyl ring considerably compared to the cyano-group in 8CB. In contrast to that, the thiocyanate (SCN) group in 6CHBT does not change significantly the MESP of the phenyl ring compared to the cyano-group in 8CB. Therefore, in this respect, 6CHBT can be regarded very similar to the benzonitrile containing PCH LC homologous series.

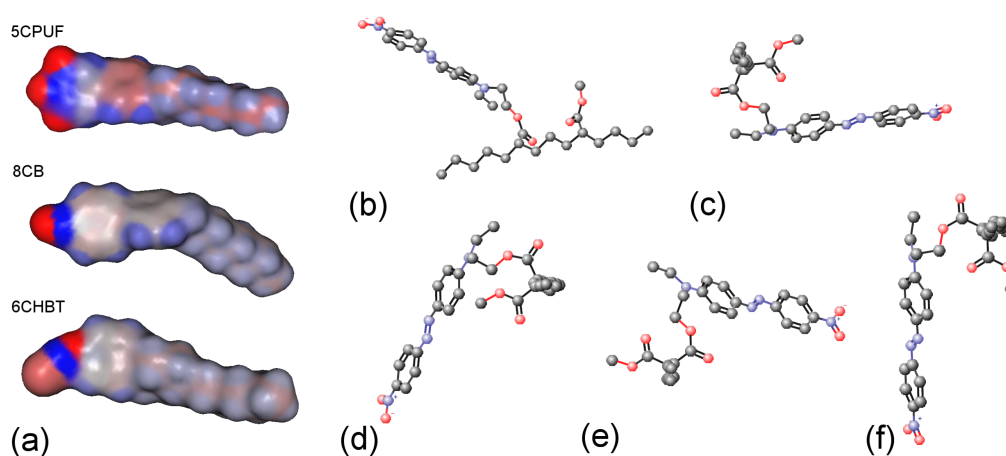


Figure 3.14: (a) Molecular electrostatic potentials (MESPs, blue is positive, red is negative) mapped for 5CPUF, 8CB and 6CHBT molecules; (b–f) some examples of various conformers of a pDR1 segment.

Possible conformations of the photosensitive polymer, pDR1, have been also investigated. For simplicity, only a segment shown in Figure 3.14(b) has been considered. Even for such an oversimplified polymer segment about 100 different conformations have been found, with most of them having energy difference in the order of  $RT = 0.593$  kcal/mol. We illustrate some of these conformers in Figures 3.14(b), (c), (d), (e), and (f), having energies of 127.74 kcal/mol, 126.62 kcal/mol, 125.96 kcal/mol, 134.14 kcal/mol, and 126.10 kcal/mol, respectively. For further simplification, in Figures. 3.14(c)-(f) we fixed the main-chain segment [visible in Figure 3.14(b)] perpendicular to the plain of the pictures.

One should note that the conformations of the pDR1 polymer shown in Figure 3.14(b–f) are oversimplified: they consider only a particular (one of the most simple) possible segment of the polymer chain, do not take into account the whole polymer chain, the

entanglements and the interactions between the chains, the actual phase of the polymer, etc. However, to our belief, even such an oversimplified picture can give some hints that bring us closer to understanding the photoalignment process at the pDR1–NLC interface. Namely, for the explanation of experimental results obtained in [90] (including the temperature induced anchoring transition), a different temperature dependence of the zenithal and azimuthal anchoring strengths at the pDR1–NLC interface has been proposed. The different temperature dependencies of the anchoring strengths have been associated with the flexibility of the spacer consisting of two methylene units connecting the PMMA main chain with the azobenzene moiety. The representation used in Figure 3.14(b-f) indicates that the trans-isomer of the azobenzene moiety has the ability to orient itself in any direction, from horizontal to vertical, with a minimal energy expense of a few RT. It seems more likely that the flexibility of the PMMA polymer main chain is responsible for the differing temperature dependence of the zenithal and azimuthal anchoring strengths, rather than the flexibility of the two methylene unit spacer [N2].

The above assumption is supported by our preliminary experiments at the interface of the derivatized methyl red (dMR) [112] monolayer and cyanobiphenyl NLCs, 5CB as well as mixture E7. The dMR monolayer has been prepared by chemisorption of its triethoxysilane unit on the activated glass substrate. The triethoxysilane unit is connected to the azobenzene containing methyl red via three methylene units, i.e., the spacer unit here is longer than in pDR1. Our preliminary measurements on these systems have shown a quite efficient azimuthal photoalignment of 5CB and E7 over the whole temperature range of the nematic phase, an absence of zenithal photoalignment, and a much slower back-relaxation than in systems with pDR1. All these observations indicate that the eventual flexibility of the methylene spacer does not play a role in the photoalignment, seen at the interface of cyanobiphenyl NLCs with pDR1.

We also note that we have carried out photoalignment measurements on contaminated or partially decomposed NLCs of PCH3, PCH5, and Mixture ZLI1132 (which primarily consists of PCH homologues: 25 wt% of PCH7, 36 wt% of PCH5, 24 wt% of PCH3 and 15 wt% of BCH5). The detection of contamination or partial decomposition was easily

### 3.4. DISCUSSION

---

observed, as it resulted in a significant reduction of the phase transition temperature  $T_{NI}$ , as well as in a considerable broadening of the temperature interval in which the nematic and isotropic phases coexist. We have found that, instead of the expected literature data:  $T_{NI} = 47$  °C,  $T_{NI} = 53.5$  °C, and  $T_{NI} = 71$  °C for PCH3, PCH5, and ZLI1132, respectively, the nematic-to-isotropic phase transition has occurred in the temperature range of  $37 - 41$  °C,  $40 - 45.5$  °C, and  $59 - 66$  °C. The azimuthal photoalignment angle was found to be small ( $\varphi < 10^\circ$ ) in every cell prepared with these NLCs, demonstrating the importance of the purity of NLCs interfacing the pDR1 polymer for photoalignment.





---

---

# CHAPTER 4

---

## ROLE OF THE LIQUID CRYSTALLINE PHASE IN PHOTOALIGNMENT

To determine experimentally how different LC phases influence the photoalignment, the cyanobiphenyl compound 8CB (see Table 2.1) possessing both smectic A and nematic phases has been chosen. Measurements on the azimuthal and zenithal photoalignment have been performed in the whole temperature range of both (smectic A and nematic) LC phases. The temporal evolution of the back-relaxation has also been monitored. In the nematic phase of 8CB, similar photoalignment characteristics are expected as in other NLCs with biphenyl rigid core (5CB, E63 and E7).

### 4.1 Azimuthal (in-plane) photoalignment

In Figure 4.1 we present the temperature dependence (relative to the nematic-to-isotropic phase transition temperature,  $T_{NI}$ ) of the saturated azimuthal photoalignment angle,  $\varphi_{sat}$  measured for 8CB. In the figure, the temperature ranges of the isotropic (I), nematic (N) and smectic A (SmA) phases are also indicated together with the nematic-to-smectic A phase transition temperature at  $T_{NI} - T = 8.5$  °C.

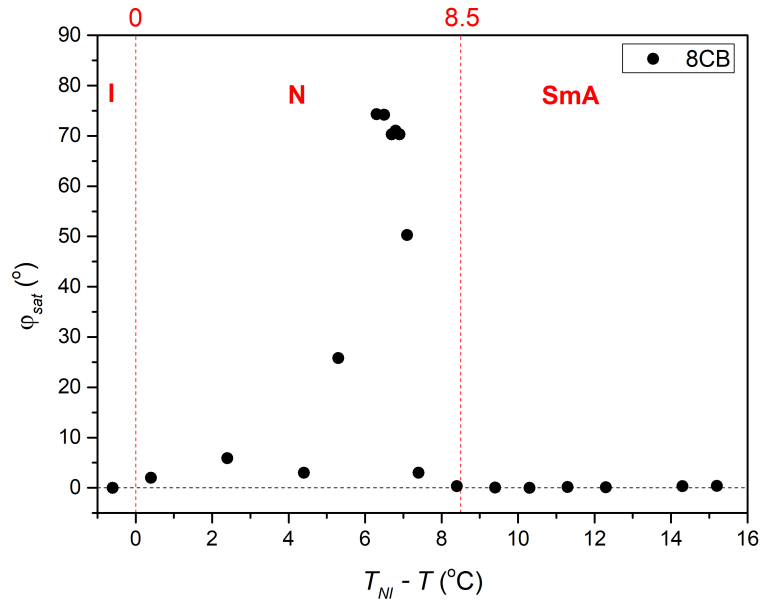


Figure 4.1: Temperature dependence of the saturated azimuthal photoalignment angle  $\varphi_{sat}$  measured for 8CB liquid crystals (I, N and SmA indicate the temperature range of isotropic, nematic and smectic A phase, respectively).

At low temperatures, in the smectic A (SmA) phase ( $T_{NI} - T > 8.5$  °C) no azimuthal photoalignment has been observed ( $\varphi_{sat} = 0$ ). In the nematic (N) phase, at temperatures close to the SmA phase ( $7.1$  °C  $< T_{NI} - T < 8.5$  °C) no significant azimuthal photoalignment has been detected ( $\varphi_{sat} < 5^\circ$ ) either. With the further increase of the temperature in a narrow range of  $5.3$  °C  $\leq T_{NI} - T \leq 7.1$  °C an incomplete azimuthal photoalignment has been measured ( $25^\circ < \varphi_{sat} < 75^\circ$ ).

In the high temperature range of the nematic phase  $0 < T_{NI} - T < 5.3$ °C a negligible azimuthal photoalignment has been found again ( $\varphi_{sat} < 6^\circ$ ), while the definition of  $\varphi_{sat}$  in the I phase ( $T_{NI} - T < 0$ ) becomes meaningless. After switching off the pump beam, the back-relaxation of 8CB, illustrated in Figure 4.2, has been found by orders of magnitude faster than in 5CPUF, 6CHBT, ZLI1695 and PCH homologous series [N1, N2].

## 4.2 Zenithal (out-of-plane) photoalignment

Figure 4.3 shows the temporal evolution of the transmitted light intensity obtained at various temperatures  $T_{NI} - T$ . The pump beam was switched on at  $t = 100$  s and switched

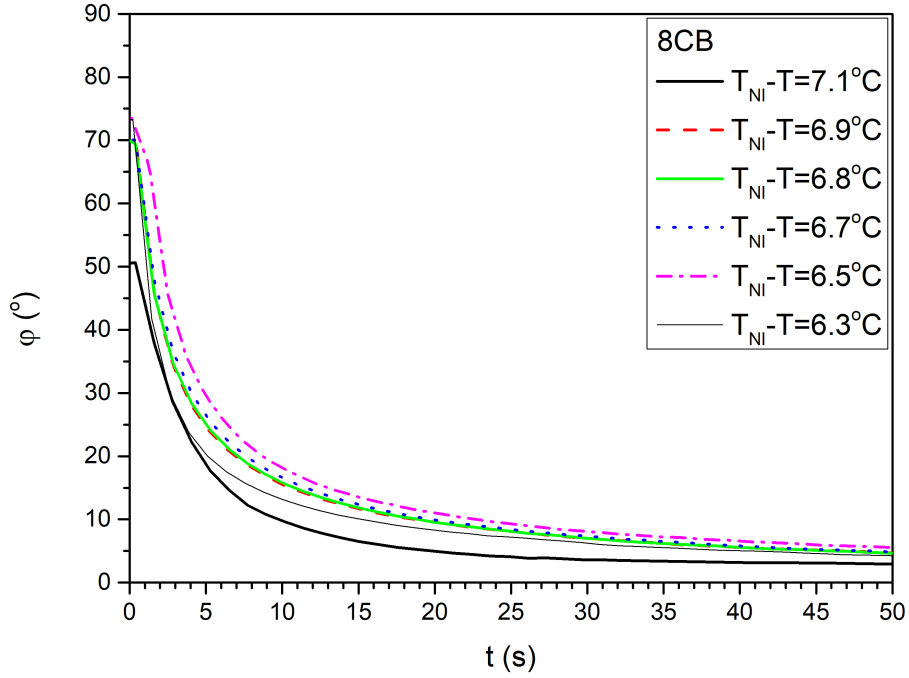


Figure 4.2: Back-relaxation of the azimuthal photo-reorientation angle  $\varphi$  (pump beam switched off at  $t = 0$  s) measured at different temperatures as indicated in the legend on a cell filled with 8CB.

off at  $t = 300$  s.

In the SmA phase, the transmitted intensity of the probe beam remains nearly unchanged upon the photo-excitation by the pump beam, as shown in Figure 4.3 at  $T_{NI} - T = 15.2$  °C. By increasing the temperature in the nematic phase in the temperature range of  $5.3$  °C  $\leq T_{NI} - T < 8.5$  °C), the change of transmitted light intensity becomes bigger when the pump beam is switched on (see Figure 4.3 at  $T_{NI} - T = 7.1$  °C), however, no temporal oscillations in the intensity were observed. At even higher temperatures of the nematic phase ( $T_{NI} - T < 5.3$  °C, where no significant azimuthal photoalignment has been observed), the transmitted light intensity of the probe beam started to oscillate upon switching on/off the pump beam, as illustrated in Figure 4.3 at  $T_{NI} - T = 1.9$  °C, indicating a significant zenithal photoalignment. One should note, that these oscillations were observed well below  $T_{NI}$ , and therefore, cannot be attributed to the nematic-to-isotropic phase transition induced by the thermal effect of the pump beam [N2].

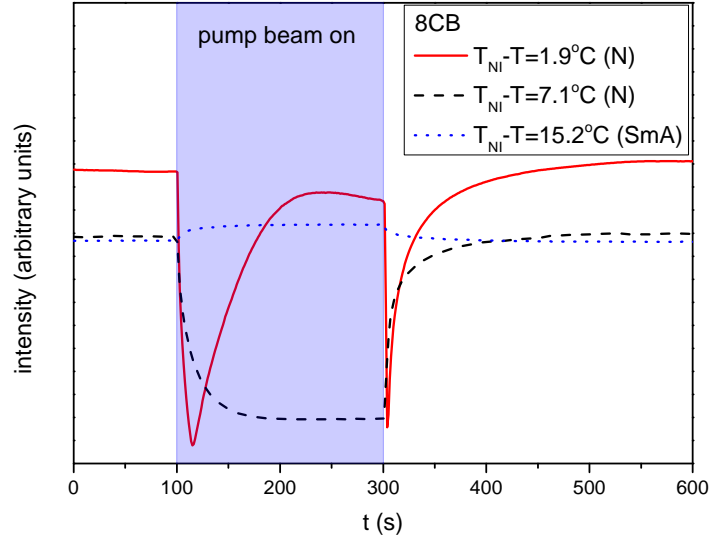


Figure 4.3: Temporal variation of the transmitted light intensity of the probe beam measured in cell with 8CB at different temperatures, in the setup for detection of zenithal photo-reorientation (pump beam polarization direction perpendicular to  $\mathbf{n}$ , probe beam polarization direction encloses  $45^\circ$  with  $\mathbf{n}$ ).

### 4.3 Discussion

Cyanobiphenyl LC 8CB in nematic phase is expected to have similar photoalignment characteristics to other cyanobiphenyl NLC compounds (5CB, E63 and E7). The results have verified these expectations. Namely, in the high temperature range of the nematic phase ( $0 < T_{NI} - T < 5.3 \text{ }^\circ\text{C}$ ), no considerable azimuthal photoalignment has been detected (see Figure 4.1), while oscillation in the amplitude of the transmitted light intensity indicates considerable zenithal photoalignment (see Figure 4.3 at  $T_{NI} - T = 1.9 \text{ }^\circ\text{C}$ ). With the decrease of the temperature, in the narrow range of  $5.3 \text{ }^\circ\text{C} \leq T_{NI} - T \leq 7.1 \text{ }^\circ\text{C}$  an incomplete azimuthal photoalignment (Figure 4.1), and no considerable zenithal photoalignment (see Figure 4.3 at  $T_{NI} - T = 7.1 \text{ }^\circ\text{C}$ ) has been found.

These results are in complete agreement with the results obtained on 5CB, E7 and E63 nematics [90, N1]. With further decrease of the temperature, in the nematic phase, but close to the nematic-to-smectic A phase transition ( $7.1 \text{ }^\circ\text{C} < T_{NI} - T < 8.5 \text{ }^\circ\text{C}$ ), as well as in the smectic A phase ( $T_{NI} - T > 8.5 \text{ }^\circ\text{C}$ ), both the azimuthal and the zenithal

photoalignment vanish. In the nematic phase it is presumably due to the smectic pretransitional fluctuations, which substantially increase the bend and twist elastic constants ( $K_{33}$  and  $K_{22}$ ) [113, 114, 115], that are the most important parameters for the azimuthal and zenithal photoalignment, respectively. In the smectic A phase, neither azimuthal, nor zenithal photoalignment is expected because the bend and twist deformations within this phase require changes in layer spacing with high energy cost [116].

Finally, one should note that 5CB and 8CB are compounds of the same homologous series, with 8CB having a longer alkyl chain, and that the temperature range of the nematic phase (from room temperature) is roughly the same for both compounds. For 5CB, no significant azimuthal photoalignment has been found down to  $T_{NI} - T \approx 10$  °C (room temperature). In contrast, for 8CB, a relatively significant (but incomplete) azimuthal reorientation was detected already at  $T_{NI} - T \approx 5.3$  °C, as shown in Figure 4.1. Therefore, the issue of whether the length of the alkyl chain plays a role in photoalignment, as mentioned earlier, and discussed for the PCH series, is once again raised. However, the absolute value of  $T_{NI}$  is higher for 8CB than for 5CB, similarly to the case for PCH compounds, where  $T_{NI}$  increases with the increase of the length of the alkyl chain. Therefore, the clarification of this question remains for future studies.



---

---

## CHAPTER 5

---

# ROLE OF THE POLYMER COMPOSITION IN PHOTOALIGNMENT

Results presented in Chapters 3 and 4 have shown that the mechanism and the efficiency of photalignment/photocontrol do not depend on the composition of the photosensitive polymer layer (often called as command surface) exclusively, but also on the liquid crystal material (and its phase) in contact with the command surface [90, N1, N2]. This Chapter highlights the role of the composition of the polymeric command layer in photoalignment. Namely, when the command surface is made of a polymer layer, two preparation methods are known in the literature: physical mixing of the polymer host with photochromic units, and chemical attachment of photochromic units to the polymer chain.

As for the polymer host, in the case of physical mixing with azobenzene derivatives, polyimide [65, 67, 117, 118, 119] and polyvinyl alcohol [120] was used. On the other hand, various azo-monomers were chemically attached to the modified main-chain of polyacrylates [121, 122], polymethacrylates [87, 88, 123, 124, 125, 126], polyamides [127], polyvinyl alcohols [63, 72, 128, 129], or polysiloxanes [130, 131].

The composition variety of the command surfaces in the above-mentioned photoalign-



ing systems largely prevents direct comparison of the benefits and disadvantages of the two fabrication methods (physical mixing/doping, and chemical binding). Therefore, for comparative investigations on these two systems, the use of the same polymer, same photochromic unit, and same liquid crystal compound is desirable. To the best of our knowledge, such a comparative investigation has not been reported yet, and one of the aims of our work presented in this Chapter is to fill this gap.

The second aim of our work presented in this Chapter regards the investigations on the photoinduced mass transfer at the polymer-air interface [102, 132]. Namely, when the layer of a polymer grafted with azobenzene derivative is illuminated with a sinusoidal intensity pattern (obtained from the interference of two coherent laser beams), a large scale modulation of the free surface is obtained [133, 134, 135], which is referred to as surface relief gratings (SRG). The amplitude of the surface modulations has been found of the order of 100 nm, and the periodicity of the grooves was matching the periodicity of the illuminating interference pattern. Similarly, when the surface of the azobenzene-containing polymer film is irradiated with a single Gaussian laser beam with a radius focused down to few  $\mu\text{m}$ , a crater is formed, due to the photoinduced mass transfer [136, 137]. Although, the mechanism with which the molecular trans-cis-trans cyclic photoisomerization converts to a macroscopic mass transfer is still under debate, the dependence of the created surface reliefs on the spatial modulation of the light intensity and on the light polarization is known [102].

In our work, we do not produce interference pattern resulting in SRG, nor we focus the Gaussian laser beam to create a crater with radius of the order of  $\mu\text{m}$ , but rather we expand the laser beam to obtain photoalignment over a considerably large area. However, the question, how the photoaligning illumination modifies the free surface of the polymer, and whether a photoinduced mass transfer is detectable under these conditions, is still relevant.

## 5.1 Photoalignment at different polymer layers

We compare photoaligning properties of polymer layers fabricated from the same constituents: polymethyl-methacrylate (PMMA) and azo-dye Disperse Red 1 (DR1), either chemically attached to the PMMA main-chain, or physically mixed with it—see Figure 2.3.

The choice of the LC mixture E7 for further measurements on photoalignment is based on our previous studies (Chapters 3 and 4). Namely, besides of the conveniently wide temperature range of the nematic liquid crystal phase (up to  $T_{NI} = 60^\circ\text{C}$ ), at the interface with the pDR1 polymer layer E7 showed the richest variety of photo-induced mechanisms (compared to other nematic LC compounds, [N1, N2]).

The pump-probe optical setup (described in Section 2.4) has been used here too. The only difference between the measurement method presented here and those reported in Chapters 3 and 4 is that for the determination of the azimuthal photoalignment angle, here, the polarization of the pump beam enclosed  $45^\circ$  with the initial director orientation  $\mathbf{n}$  (instead of being parallel with it). The reason for this change was to avoid accidental creation of a supertwist deformation in the LC cell [138]. Consequently, when switched on, the pump beam is expected to induce twist deformation in the LC cell with  $\varphi = 45^\circ$  at the photosensitive plate for the complete azimuthal photoalignment.

In Figure 5.1 results on the *azimuthal* photoalignment/photoreorientation are shown, measured on LC cells with a photosensitive polymer layer from pDR1, as well as from PMMA1+DR1 mixture (with 30 wt% DR1 content) at a temperature  $T_{NI} - T = 32^\circ\text{C}$ , i.e., close to the room temperature. As we mentioned above, the polarization of the pump beam encloses  $45^\circ$  with the initial director orientation  $\mathbf{n}$  at the reference plate.

Results on the azimuthal photoalignment in the LC cell with pDR1 are in agreement with the previous results [90, N1]: at low temperatures, upon light excitation, the azimuthal photoreorientation angle at the surface of pDR1 reaches a saturated value of  $\varphi_{sat} \approx 40^\circ$  relatively fast, i.e., almost a complete azimuthal photoalignment occurs via photo-induced twist deformation in the LC layer. When the photo-excitation is switched

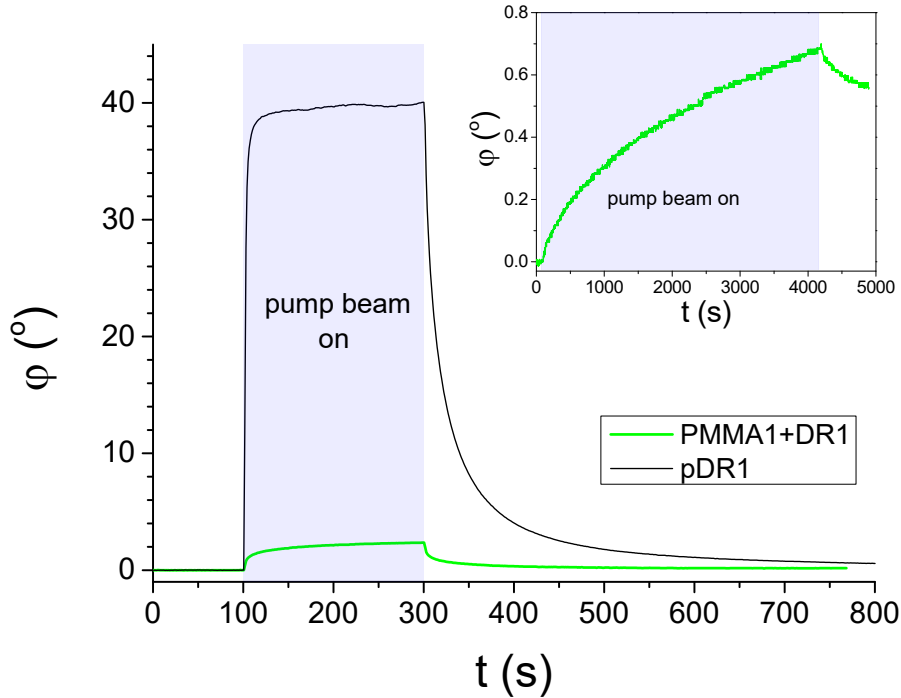


Figure 5.1: Azimuthal photo-reorientation angle  $\varphi$  in time, measured at temperature  $T_{NI} - T = 32$  °C in cells filled with E7 and having pDR1, or PMMA1+DR1 mixture (with 30 wt% DR1 content) layer as a photosensitive plate. The pump-beam was switched on at  $t = 100$  s, and switched off at  $t = 300$  s. The power of the pump beam was  $P = 10$  mW in case of the cell with pDR1, and  $P = 70$  mW for the cell with PMMA1+DR1. Inset: long time illumination measurement on another location of the cell with PMMA1+DR1 (pump-beam switched on at  $t = 100$  s, and switched off at  $t = 4200$  s).

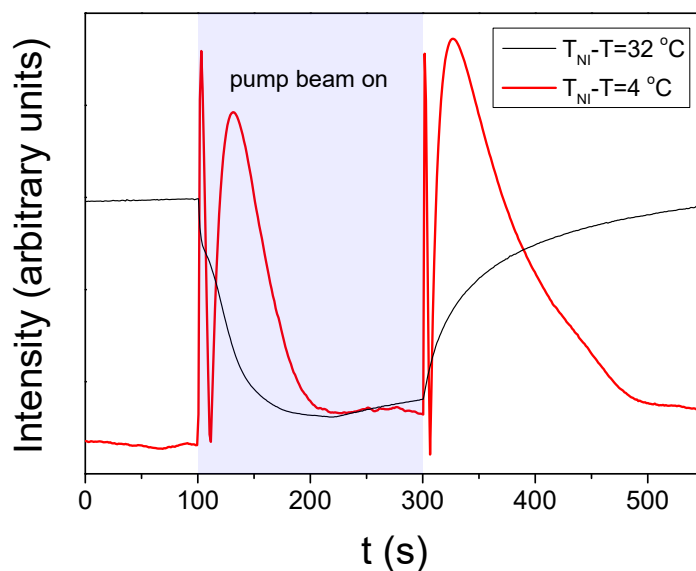
off, a relatively fast back-relaxation is observed – the system returns to the initial, planar orientation.

In contrast, in the LC cell with the polymer layer from the PMMA1+DR1 mixture, upon the light excitation (despite of the much higher light power), a much smaller change in the azimuthal photoalignment angle has been observed (typically up to  $\varphi \approx 3^\circ$ ), and the small photo-induced change does not seem to saturate even for long illumination times – see the inset of Figure 5.1. When the pump beam is switched off, the small photo-induced change in  $\varphi$  relaxes back slowly.

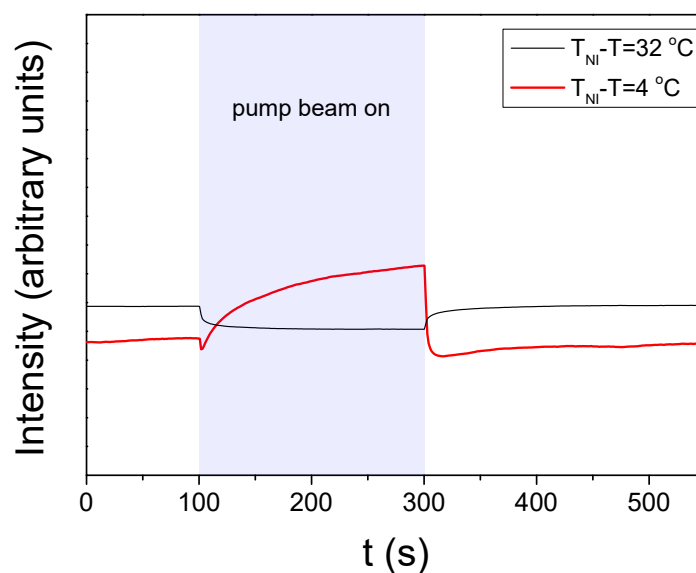
For the investigations on the *zenithal* photoalignment, the polarization of the probe beam has enclosed  $45^\circ$  with  $\mathbf{n}$  (to maximise the sensitivity), while the polarization of the pump beam has been set perpendicular to  $\mathbf{n}$ , which ensures the absence of the azimuthal

## 5.1. PHOTOALIGNMENT AT DIFFERENT POLYMER LAYERS

photoalignment and its influence on the results. The results on zenithal photoalignment are shown in Figure 5.2 for two (low and high) temperatures, and for both cells with pDR1 and PMMA1+DR1.



(a)



(b)

Figure 5.2: Temporal variation of the transmitted light intensity of the probe beam measured in E7 cells at two different temperatures in the setup for detection of zenithal photo-reorientation (pump beam polarization perpendicular to  $\mathbf{n}$ , probe beam polarization encloses  $45^\circ$  with  $\mathbf{n}$ ). The pump-beam of power  $P$  switched on at  $t = 100$  s, and switched off at  $t = 300$  s. **(a)** pDR1,  $P = 10$  mW; **(b)** PMMA1+DR1 mixture (with 30 wt% DR1 content),  $P = 70$  mW.

Again, results on the zenithal photoalignment in the LC cell with pDR1 [Figure 5.2(a)] are in agreement with the previous results [90]: at low temperatures, upon irradiation, only a slight change in the transmitted light intensity has been observed, indicating the absence of zenithal photoalignment; at high temperatures, however, oscillations in the transmitted light intensity, both when pump beam is switched on and off, clearly indicate a significant zenithal photoalignment.

In contrast, in the LC cell with the polymer layer from the PMMA1+DR1 mixture, upon the light excitation (despite of the much higher light power), only a slight change in the transmitted light intensity of the probe beam has been observed in the whole temperature range (from room temperature, up to  $T_{NI}$ ) – see Figure 5.2(b). This slight change at all temperatures, may originate either from a small misalignment of the director at the two bounding surfaces, or from a small misalignment of the polarization direction of the pump beam and  $\mathbf{n}$ , or eventually, from a slight zenithal photoalignment as it was discussed in Reference [90].

We note here, that in the photoalignment measurements presented above, only the results on the mixture of PMMA1 [with the smallest  $\langle n \rangle$  – see Figure 2.3(b)] with 30 wt% DR1 are shown. Other polymer layers have also been prepared from the mixtures of PMMA1, PMMA2, or PMMA3 with DR1 in different concentrations (with DR1 content ranging from 6.2 wt% to 42 wt%). Photoalignment measurements on LC cells with these substrates has led to essentially same results as those presented in Figures 5.1 and 5.2(b). Therefore, it seems that the photoaligning properties of polymer layers composed of the PMMA and DR1 mixture do not depend substantially on the degree of polymerisation, nor on the concentration of the photochromic material.

## 5.2 Photoinduced mass transfer

Experimental results, discussed in Chapter 3 have shown that at the pDR1 surface, the relatively fast back-relaxation of the azimuthal photoalignment angle  $\varphi$  when the exciting illumination is switched off (as shown in Figure 5.1), happens only when the pDR1 surface

## 5.2. PHOTOINDUCED MASS TRANSFER

---

interfaces LC material having biphenyl in its rigid core [N1, N2]. When pDR1 is in contact with LCs not having biphenyl in the molecular structure, there is no back-relaxation, or it is extremely slow. Therefore, it is reasonable to expect, that the pDR1 surface in contact with the air will not relax back on the time scales of hours after the exciting illumination. This assumption is a prerequisite for the AFM measurements presented in this Section considering the time scales ( $\sim$  hour) of those measurements.

Glass substrates with pDR1 and with PMMA1+DR1 mixture (having 35 wt% DR1 content) have been prepared identically as those for photoalignment measurements. AFM scans were performed at certain location prior and after the illumination with polarised light having intensity of the order of  $100 \text{ mW/cm}^2$  (at  $\lambda = 405 \text{ nm}$ ).

AFM scans on the pDR1 substrate are shown in Figure 5.3 prior (a), and after (b) the illumination. Obviously, the polarized light illumination has induced changes in the surface relief of pDR1 polymer. The "grooves" (presumably originating from the spin-coating procedure) visible on the surface prior the illumination [Figure 5.3(a)] have faded out upon the illumination [Figure 5.3(b)], indicating a significant photoinduced mass transfer.

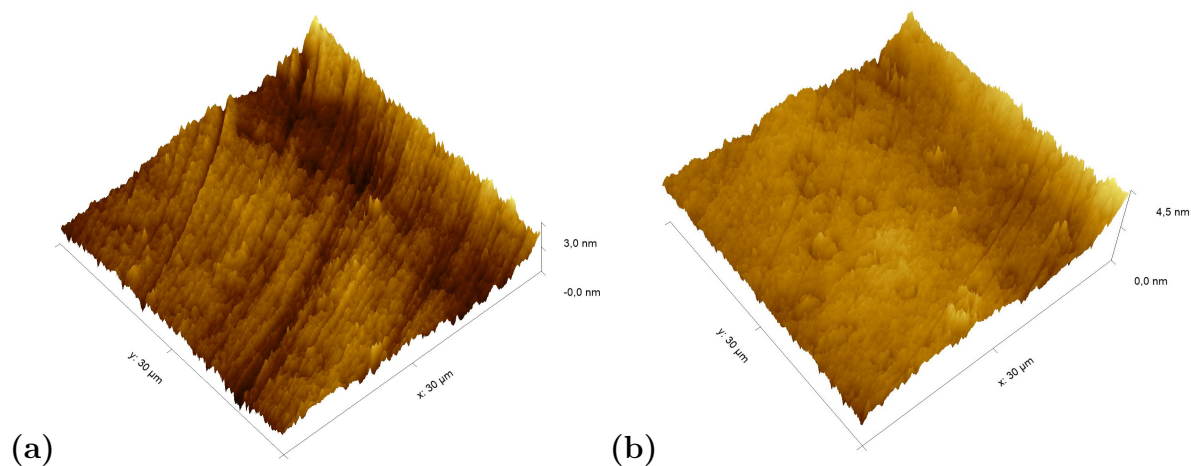


Figure 5.3: Atomic force microscope images on pDR1 polymer layer prior (a), and after (b) the illumination with polarized light.

For a more quantitative determination of the influence of the illumination it is critical to compare the same area of the substrate before and after the irradiation of known polarization direction. For that purpose, the polarization direction of the illumination

was set vertical (along the y direction) in Figure 5.4, and reference locations have been selected which can be undoubtedly identify both prior and after the irradiation. Those locations are marked with black circles in Figures 5.4(a) and (b). One can see some photoinduced changes immediately from the AFM scans. First, changes in the surface relief: horizontal grooves (along x-axis) present prior the illumination (again, presumably caused by the spin-coating) [Figures 5.4(a) and (c)], disappear after the illumination [Figures 5.4(b) and (d)]. The relative positions of the reference locations have slightly changed [*cf.* the positions of the locations marked with black circles in Figures 5.4(a) and (b)].

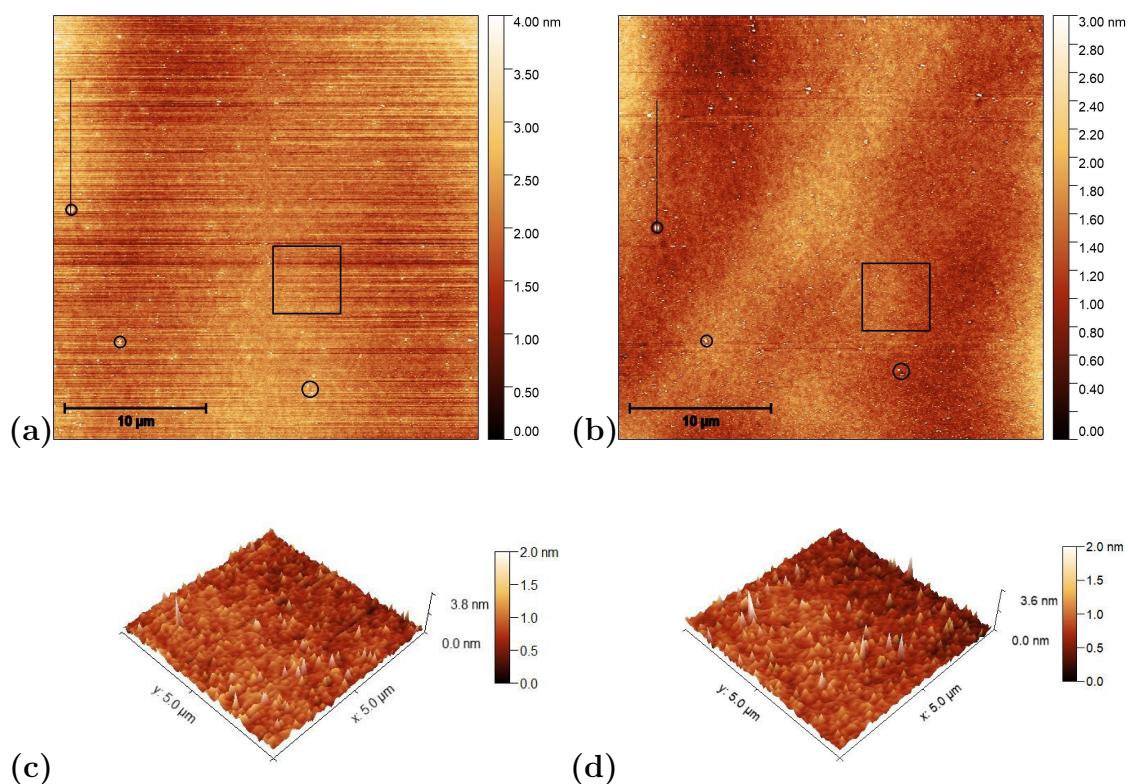


Figure 5.4: AFM images taken on the pDR1 surface prior [(a) and (c)], and after [(b) and (d)] the laser illumination. Encircled spots in (a) and (b) serve as reference locations to identify the same area for AFM scanning prior and after the illumination, while the squares denote the area that are presented in (c) and (d) in three dimensions. The vertical lines in (a) and (c) denote the locations from which the one dimensional profiles shown in Fig. 5.7(a) are taken.

A closer look at the enlarged images shown in Figure 5.5 proves that even within the original reference location (black circle) the two white spots change their relative



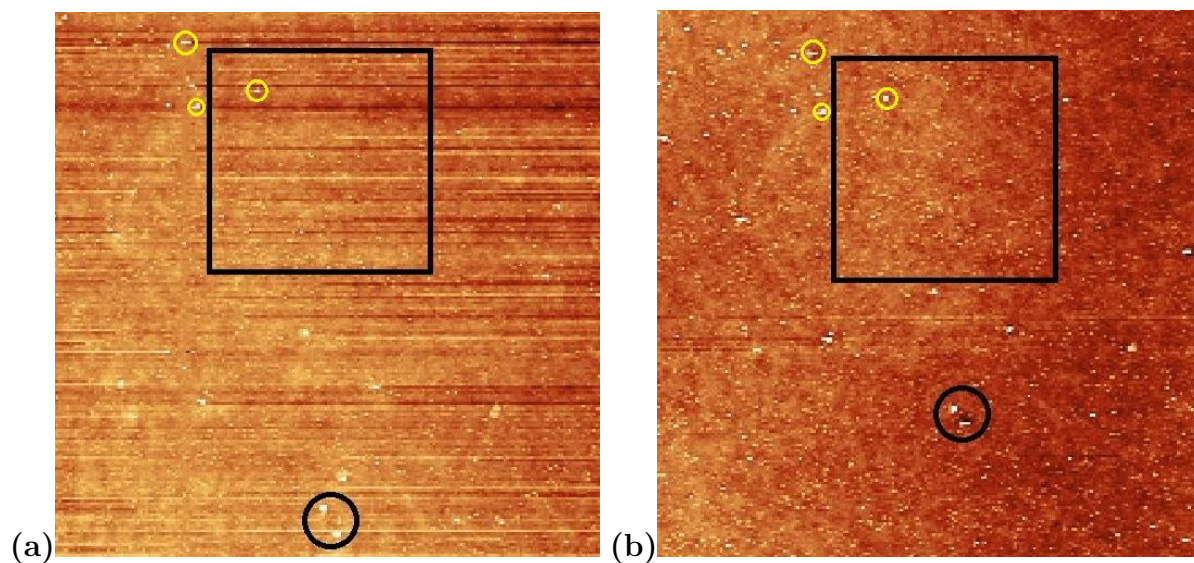


Figure 5.5: Enlarged images of the neighborhood of squares shown in Figures 5.4(a) and (b) with the new reference locations encircled with yellow; (a) prior the laser illumination; (b) after the illumination.

positions upon the irradiation. These are strong indications of the photoinduced mass transfer, and therefore, the selection of the area for the three-dimensional representation, shown in Figures 5.4(c) and (d), was based on new reference locations that do not change their relative positions upon illumination [indicated by yellow circles in Figures 5.5(a) and (b)].

AFM scans on the PMMA1+DR1 substrate are shown in Figure 5.6 before [(a) and (c)], and after [(b) and (d)] the illumination. Again, the polarization direction of the illumination was set vertical (along the  $y$  direction). Here, no obvious photoinduced change is detectable. A more detailed information about the photoinduced changes can be obtained from one dimensional profiles presented in Figure 5.7, taken along the lines shown in Figures 5.4 and 5.6, before and after the laser illumination. One dimensional profiles taken on the pDR1 substrate along the line indicated in Figures 5.4(a) and (b) are shown in Figure 5.7(a). As a starting point ( $y = 0$ ) for the profiles, one of the reference points – the high peak encircled in Figures 5.4(a) and (b) has been used. Obviously, the illumination smoothens the  $z(y)$  profile: the roughness of  $z(y) \approx \pm 0.5$  nm evidently becomes smaller after the illumination. In the same time, the smoothing causes a significant lateral photoinduced mass transfer too: for example, the high peak at  $y =$



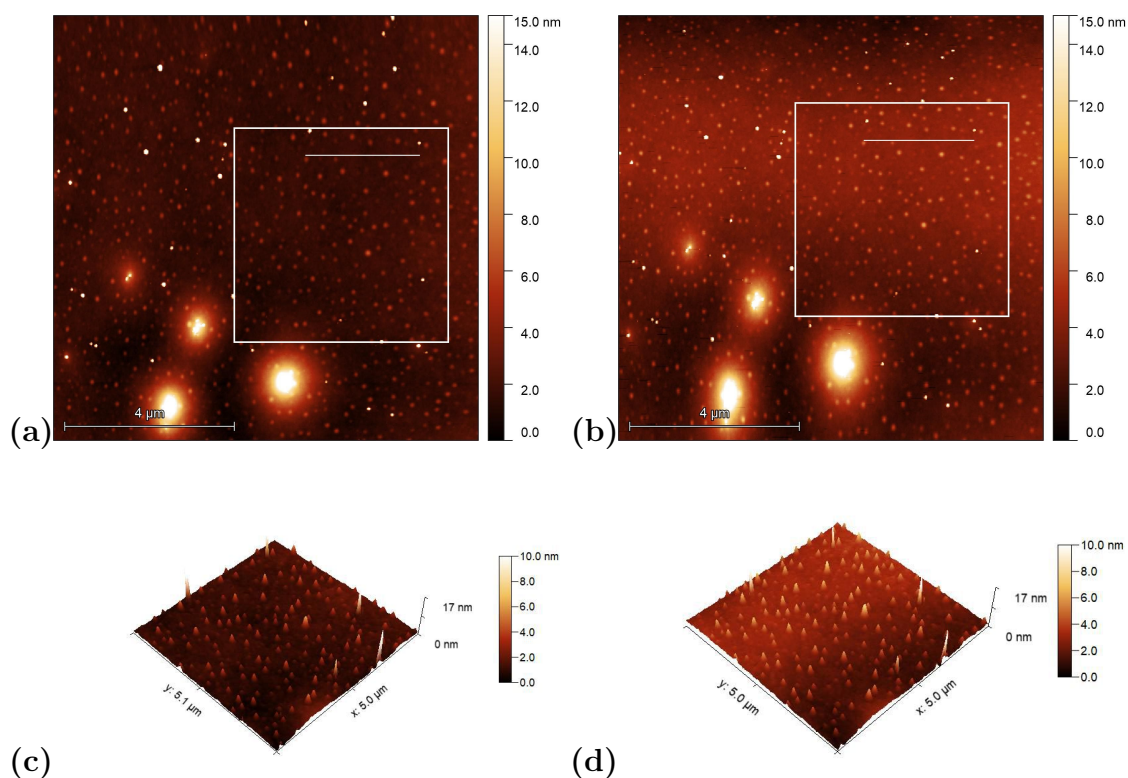


Figure 5.6: AFM images taken on the surface of PMMA1+DR1 mixture (with 35 wt% DR1 content) prior [(a) and (c)], and after [(b) and (d)] the laser illumination. The squares in (a) and (b) denote the area that are presented in (c) and (d) in three dimensions, while the horizontal lines in squares denote the locations from which the one dimensional profiles shown in Fig. 5.7(b) are taken.

$3.2 \mu\text{m}$  prior the illumination has moved to the position  $y = 3.7 \mu\text{m}$  after the illumination. One dimensional profiles taken on the PMMA1+DR1 substrate along the line indicated in Figures. 5.6(a) and (b) are shown in Figure 5.7(b). Here, the changes in the profile after the illumination are minimal, and are very close to the resolution of the AFM. The peaks and valleys undergo only slight changes upon illumination, and can be well identified individually before and after the illumination. Note that the last double peak at  $x \approx 2.4 \mu\text{m}$  shifts laterally by about 40 nm upon illumination, which is more than an order of magnitude smaller shift than that observed on pDR1 substrate, indicating a very small light induced mass transfer compared to that in pDR1.

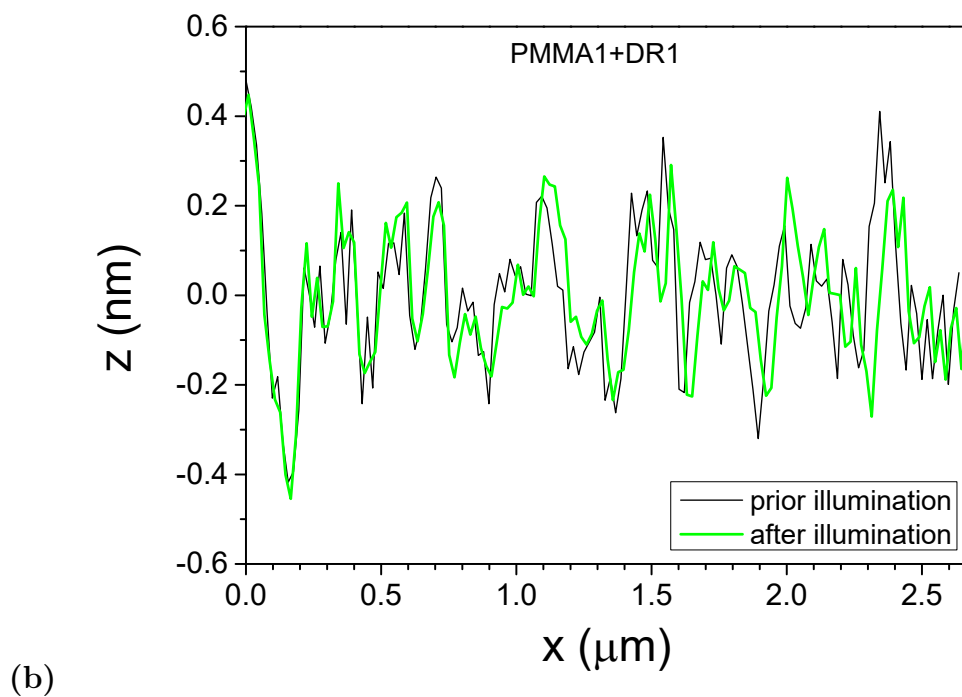
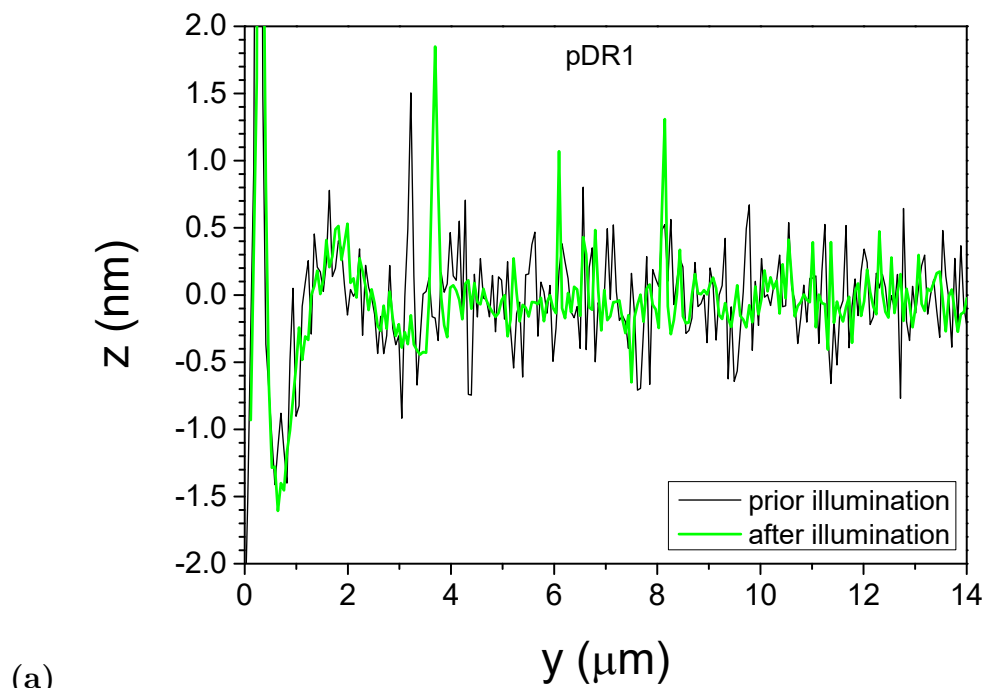


Figure 5.7: One dimensional profiles along the lines shown in Figures 5.4 and 5.6, taken before and after the laser illumination; (a) pDR1; (b) PMMA1+DR1.

### 5.3 Discussion

Photoalignment measurements on LC cells with a pDR1 substrate and with E7 nematic LC mixture have confirmed our previous results [90, N1] concerning both the azimuthal and the zenithal photoalignment. In contrast to that, measurements on LC cells with various PMMA+DR1 substrates, filled with E7 have resulted in a very small, but measurable azimuthal photoalignment angles, while the zenithal photoalignment has been found negligible, if exists at all.

It is worth to compare the results of azimuthal photoalignment obtained here on PMMA+DR1 substrates, with previous studies on a different system [130, 139]. In Refs. [130, 139], the command surface was prepared from the mixture of polyimide (PI) and azo dye Disperse Orange 3 (DO3). More precisely, the substrates were coated with a saturated solution of DO3 in polyamic acid solution, and the imidization was completed thermally. Under similar illumination conditions, a much larger azimuthal photoalignment angle was found in cells with PI+DO3 substrate ( $\varphi \geq 15^\circ$ ) than with PMMA+DR1 command surface ( $\varphi \leq 3^\circ$ ). We have also prepared substrates from PMMA+DO3 mixtures and we have detected very similar photoalignment performance as with PMMA+DR1 (typically,  $\varphi \leq 3^\circ$ ). Therefore, one can assume that the poor photoalignment efficiency originates from the PMMA matrix.

For the very weak photo-response measured in the LC cells with PMMA+DR1 substrates one can anticipate two possible reasons: **(i.)** the orientation of the DR1 molecules, and **(ii.)** the rigidity of the PMMA matrix.

Reason **(i.)** comes from both theoretical considerations and experimental data, evidencing that rod-like molecules often have a tendency to orient perpendicular to the free (air contacting) surface of the film [140]. Such an orientation of the azo-benzene derivatives is unfavorable for photoalignment when the light irradiation is performed (as in our case) with normal incidence to the film (substrate) plane, because this orientation results in poor light absorption. Assumption **(i.)** can be, however, tested by a slantwise illumination [123]. Namely, when illuminated with non-polarized light, the *trans* azo-benzene

### 5.3. DISCUSSION

---

derivatives tend to reorient with their long axis in the direction parallel with the light propagation direction. Following the work of Ref. [123] we have tried to influence the initial orientation of DR1 molecules in the substrate made of PMMA1+DR1 mixture. In order to do that, after the preparation of the substrate from PMMA1+DR1 mixture, the polymer layer has been illuminated slantwise from a non-polarised  $\lambda = (457 \pm 7)$  nm light source with illumination dose of  $7.5 \text{ J/cm}^2$  and with light propagation direction which encloses  $30^\circ$  with the polymer film plane. The LC cell was than assembled, and prior as well as during filling the cell with E7, it was again illuminated with the same non-polarised light source in the same geometry with a dose of  $7.5 \text{ J/cm}^2$ . Such procedure is supposed to reorient long axis of DR1 molecules so that they enclose  $30^\circ$  with the polymer film plane, making the photoalignment experiments much more efficient. Photoalignment measurements on this LC cell, however, have led to results very similar to those shown in Figures 5.1 and 5.2(b).

Therefore, we assume that reason (ii.), i.e., the rigidity of the PMMA matrix in the glassy state stays behind the poor photoalignment performance of the polymer layers made from PMMA+DR1 mixtures. Presumably, the rigid matrix hinders the cooperative motion (induced by the *trans-cis* isomerization of the DR1 molecules) necessary for an efficient photoalignment. In contrast to that, we have shown previously for a polymer segment of pDR1 that the *trans*-isomer of the azo-benzene moiety can take any direction at an energy expense of few  $RT$ , more likely due to the flexibility of the main chain than to the flexibility of the short spacer that connects the azo-dye with the polymer chain [N2].

Results obtained from AFM scans on polymer reliefs in contact with the air are in line with the photoalignment measurements. The pDR1 surface evidently becomes smoother after the illumination, and the photoinduced changes in surface relief are accompanied with a significant photoinduced mass transfer. In contrast, the relief of PMMA1+DR1 surface does not change noticeably upon the illumination, and the photoinduced mass transfer has been found very close to the resolution of the AFM.



---

---

# CHAPTER 6

---

## SUMMARY

We have performed series of experimental studies on the photoalignment at NLC–pDR1 polymer interface. While employing the same preparation procedure of the photosensitive pDR1 polymer layer, we have systematically varied the rigid core of NLCs from biphenyl, through phenylcyclohexane to bicyclohexane. Substantial differences in the photoalignment process have been found depending on the molecular structure of NLCs. In NLCs with biphenyl rigid core azimuthal photoalignment was detected only in the lower temperature range of the nematic phase. In the higher temperature range of the nematic phase zenithal photoalignment has occurred, and additionally, at temperatures close to  $T_{NI}$  a temperature induced orientational transition (from planar towards the homeotropic) has been also found.

In contrast, in NLCs with phenylcyclohexane or bicyclohexane rigid core, no zenithal photoalignment has been detected, and the azimuthal photoalignment has been maintained over almost the whole temperature range of the nematic phase. In these NLCs  $\varphi$  decreases only at temperatures close to  $T_{NI}$ , where temperature induced orientational transition is anticipated.

We interpreted the experimental results with offset stacked aromatic  $\pi - \pi$  interactions between the biphenyl rigid core of the NLCs and the trans isomer of the azobenzene moiety in the pDR1 polymer. Such interactions are absent in the case of NLCs with bicyclohexane, or phenylcyclohexane rigid core, and therefore, do not influence the photoalignment process.

To test the validity of this interpretation, a NLC has been employed that contains a biphenyl rigid core, but one of the phenyl rings is modified with three fluorine atoms at positions (3, 4, 5), which effectively invert the MESP of the ring [111]. We have shown that replacement of the polar cyano group with fluorine atoms in NLC having biphenyl in the rigid core modifies the MESP of the phenyl rings to an extent that prevents the offset stacked  $\pi - \pi$  aromatic interaction between the biphenyl part of NLC and the trans isomer of the azobenzene moiety in the interfacing polymer. The absence of this interaction changes the characteristics of the photoalignment: instead of having both azimuthal and zenithal photoalignments in different temperature ranges (like in cyano-biphenyl NLCs), only the azimuthal photoalignment has occurred (like in phenylcyclohexane and bicyclohexane NLC compounds).

Analysis of the possible conformations on the simplest segment of pDR1 have shown that the trans-isomer of the azobenzene moiety can take almost any direction (from horizontal to vertical) at an energy expense of few  $RT$ , and therefore, rather the flexibility of the PMMA polymer main chain is responsible for the different temperature dependencies of the zenithal and azimuthal anchoring strengths at the pDR1–NLC interface, than the flexibility of the two methylene units spacer (as it has been proposed earlier [N1]).

Cyano-biphenyl compound 8CB has been chosen to determine the influence of the LC phase on photoalignment. Namely, this compound, besides the nematic phase, possess smectic A (SmA) phase too—see Table 2.1. In the nematic phase, the compound exhibited similar photoalignment characteristics as other cyano-biphenyl nematics, i.e., zenithal photoalignment occurred in the high temperature range of the N phase, and azimuthal photoalignment in the lower temperature range. With further decrease of the temperature, just above the nematic-to-smectic A phase transition temperature (still in the N

---

phase), however, both the azimuthal and the zenithal photoalignment vanished. This is attributed to the smectic pretransitional fluctuations, which suppress the photoalignment (both azimuthal and zenithal) in the nematic phase, due to the large increase of the bend and twist elastic constants, that are the most important parameters for the azimuthal and zenithal photoalignment, respectively. In the smectic A phase no azimuthal, nor zenithal photoalignment has been observed, since the bend and twist deformations would involve changes in the layer spacing that request very high energies [N2].

Photoaligning properties of polymer layers fabricated from the same constituents have been compared: the azo-dye Disperse Red 1 (DR1) was either chemically attached to the PMMA main-chain (pDR1), or physically mixed with it (PMMA+DR1). Photoalignment has been found to be far more efficient when PMMA is functionalized with DR1 compared to the case of physical mixing the constituents. This finding is supported by atomic force microscope (AFM) scans, monitoring the light-induced changes at the polymer–air interface, and revealing a photoinduced mass transfer, especially in the case of functionalized PMMA [N3].





---

---

# APPENDIX A

---

## PHOTOALIGNMENT IN FERROELECTRIC NEMATIC PHASE

In Chapter 1, I have shown that the nematic phase has inversion symmetry ( $\mathbf{n} \equiv -\mathbf{n}$ ), therefore, nematic is known as an apolar phase. When the inversion symmetry is broken, the phase becomes polar (ferroelectric).

A century ago [141], Born predicted that the ferroelectric phase should exist when the dipole-dipole interaction between NLC molecules is large enough to overcome the thermal fluctuations.

Recently, two research groups [142, 143] independently reported two substances, RM734 and DIO, which are known now to have a new polar phase besides the conventional apolar nematic phase. The new phase is the so-called ferroelectric nematic ( $N_F$ ). Ferroelectric nematic is a three-dimensional liquid with macroscopic electric polarization. Every molecule dipole is restricted to be almost parallel to its molecular long axis, resulting in a strong orientational coupling which makes the polarization ( $\mathbf{P}$ ) locally parallel to the director  $\mathbf{n}$ . This feature allows for responding to small electric fields (thousand times smaller than the field required to reorient conventional nematics), which

makes the ferroelectric nematic phase promising in electro-optics technology [144], while the polarization direction can be efficiently controlled by photo-aligned [145].

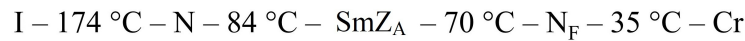
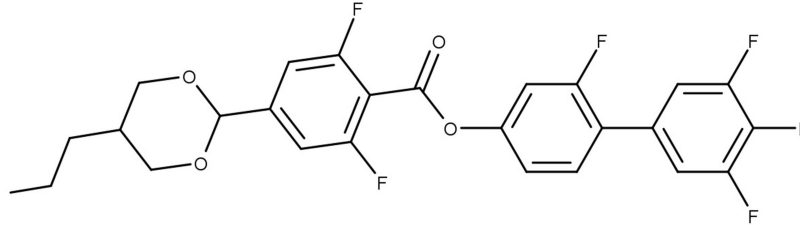


Figure A.1: Molecular structure and phase transition temperatures of DIO liquid crystal compound. Cr, N<sub>F</sub>, SmZ<sub>A</sub>, N and I stand for crystal, ferroelectric nematic, smectic Z<sub>A</sub>, nematic and isotropic phase, respectively [146].

DIO LC has two nematic phases: at low temperatures exhibits a ferroelectric nematic phase, and at high temperatures exhibits a nematic phase; while an intermediate phase has been identified very recently [147] to be antiferroelectric smectic Z<sub>A</sub> (SmZ<sub>A</sub>) and lies between the nematic and ferroelectric nematic phase—see Figure A.1 for the molecular structure and the phase transition temperatures.

LC cells filled with DIO have been prepared as described in Section 2.2. Figure A.2 illustrates the temporal evolution of the photoinduced twist angle,  $\varphi$ , measured at  $T = 96$  °C in the nematic phase. According the graph, DIO, far above the nematic to smectic Z<sub>A</sub> phase transition temperature, has azimuthal photoalignment characteristics similar to those observed in cyanobiphenyl nematic LCs (nearly complete azimuthal photoalignment angle, and relatively fast back-relaxation after switching off the pump beam).

However, in the ferroelectric nematic phase the photoalignment became far more complicated and quite unpredictable. Figure A.3 illustrates the temporal evolution of the photoinduced twist angle  $\varphi$ , measured at  $T = 55$  °C in the ferroelectric nematic phase at two different spots of the same cell. At one spot (indicated with red), the pump beam was switched on at  $t = 100$  s and switched off at  $t = 300$  s, while at the other spot (indicated with blue), the pump beam was switched on at  $t = 100$  s and switched off at  $t = 400$  s. As one can see, during the photoexcitation, the azimuthal photoalignment angle

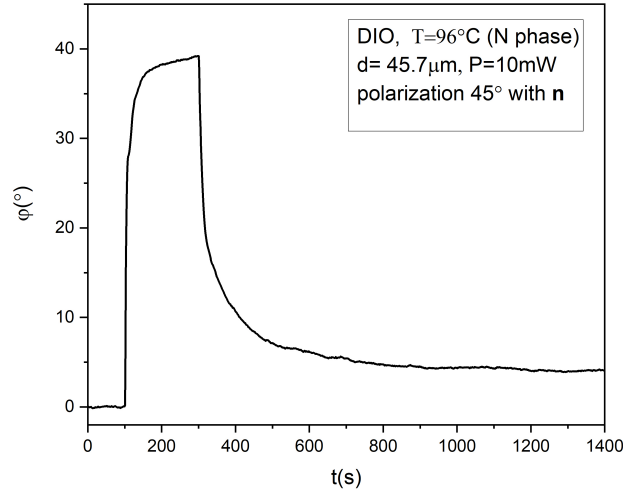


Figure A.2: Azimuthal photo-reorientation angle  $\varphi$  in time, measured at  $T = 96 \text{ }^\circ\text{C}$  in cell filled with DIO. The polarization of the pump beam encloses  $45^\circ$  with the director  $\mathbf{n}$ . The pump-beam was switched on at  $t = 100 \text{ s}$ , and switched off at  $t = 300 \text{ s}$ .

changes non-monotonously, in a quite unpredictable way, in some cases significantly going beyond the expected value of  $\varphi = 45^\circ$ . Moreover, after switching off the pump beam, the system does not seem to relax at all.

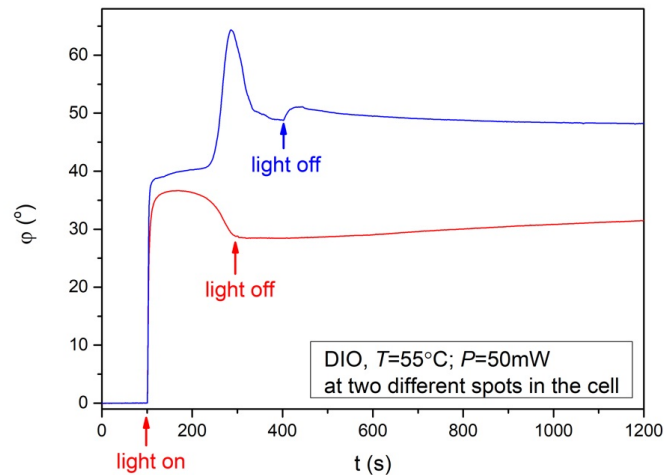


Figure A.3: Azimuthal photo-reorientation angle  $\varphi$  in time, measured in the ferroelectric nematic phase. The polarization of the pump beam encloses  $45^\circ$  with the director  $\mathbf{n}$ . The pump-beam was switched on at  $t = 100 \text{ s}$ , and switched off at  $t = 300 \text{ s}$  (red), and at  $t = 400 \text{ s}$  (blue).

Results of another experiment are plotted in Figure A.4. The experiment has started

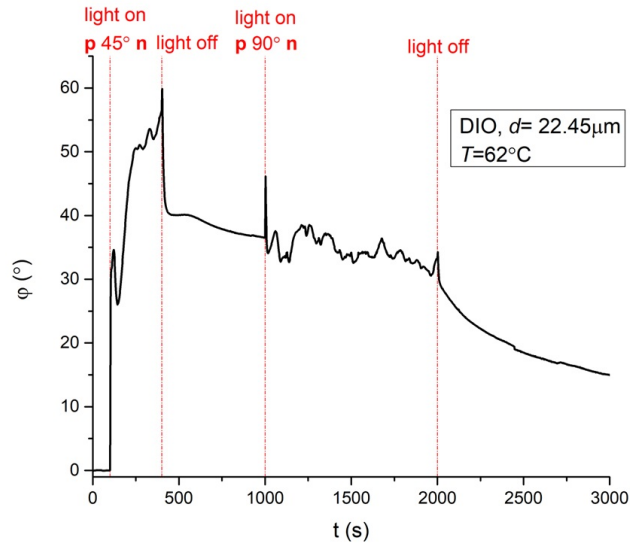


Figure A.4: Azimuthal photo-reorientation angle  $\varphi$  in time, measured in the ferroelectric nematic phase. The polarization of the pump beam encloses  $45^\circ$  with the director  $\mathbf{n}$ . The pump-beam was switched on at  $t = 100$  s, and switched off at  $t = 400$  s. Then, the polarization of the pump beam set to be perpendicular with  $\mathbf{n}$ , the pump-beam was switched on at  $t = 1000$  s, and switched off at  $t = 2000$  s.

with switching on the pump beam with polarization direction enclosing  $45^\circ$  with  $\mathbf{n}$  at  $t = 100$  s. Again, the azimuthal photoalignment angle has increased in a non-monotonous way well above the expected value of  $\varphi = 45^\circ$  till the pump beam has been switched off at  $t = 400$  s. Since after switching off the pump beam,  $\varphi$  did not relax back towards the initial value of  $\varphi = 0$ , in an attempt to make the back-relaxation faster, the polarization of the pump beam has been changed to be perpendicular to the initial  $\mathbf{n}$  and has been switched on at  $t = 1000$  s. Surprisingly, instead of a fast back relaxation towards  $\varphi = 0$ ,  $\varphi$  started to unpredictably fluctuate around the value of  $35^\circ$ , and after switching off the restoring pump beam at  $t = 2000$  s, a smooth, very slow back-relaxation took place.

Figure A.5 summarizes the temperature dependence of the azimuthal photoalignment angle,  $\varphi$ , measured for DIO LC, relative to the isotropic-nematic phase transition temperature,  $T_{NI}$ . In the figure, the temperature ranges of the nematic (N), smectic  $Z_A$  (Sm  $Z_A$ ), and ferroelectric nematic ( $N_F$ ) phases are also indicated together with the ferroelectric nematic-to-smectic  $Z_A$ , and smectic  $Z_A$ -to-nematic phase transitions at  $T_{NI} - T = 104^\circ\text{C}$  and  $90^\circ\text{C}$ , respectively.

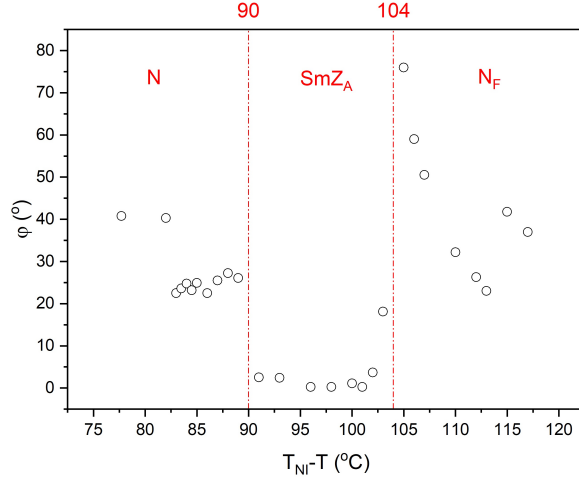


Figure A.5: Temperature dependence of the saturated azimuthal photoalignment angle  $\varphi_{sat}$  measured for DIO liquid crystal. (N, SmZ<sub>A</sub> and N<sub>F</sub> indicate the temperature range of nematic, smectic Z<sub>A</sub> and ferroelectric nematic phase, respectively).

In the higher temperature range of the nematic phase, an almost complete azimuthal photoalignment angle ( $\varphi = 42^\circ$ ) has been measured. In the lower temperature range of the nematic phase, close to  $N - \text{SmZ}_A$  phase transition temperature, a decrease of the azimuthal photoalignment angle has occurred ( $\varphi \approx 25^\circ$ ). This decrease may be related to the pretransitional smectic fluctuations (similarly to that above the nematic-to-smectic A phase transition temperature discussed in Chapter 4 for 8CB liquid crystal), but additional measurements are needed to confirm that. In the temperature range of the SmZ<sub>A</sub> ( $90^\circ\text{C} < T_{NI} - T < 104^\circ\text{C}$ )  $\varphi$  became negligibly small, presumably due to the layered structure of the SmZ<sub>A</sub> phase and for the same reasons as discussed for the smectic A phase of 8CB in Chapter 4. In the temperature range of the ferroelectric N<sub>F</sub> phase, the values of  $\varphi$  scatter in an unpredictable way as explained for Figures A.3 and A.4. Therefore, this part of the Figure A.5 should be considered as informative only.

Finally, one should mention that after finishing the measurement series shown in Figure A.5, the phase transition temperatures of the sample has been checked again. Both the N-to-SmZ<sub>A</sub> and the SmZ<sub>A</sub>-to-N<sub>F</sub> phase transition temperatures have been found lower by few  $^\circ\text{C}$  than initially. The decrease of the phase transition temperatures is a clear sign of temporal degradation of DIO, presumably caused by keeping it at elevated

temperatures for a long time (more than a week). This observation has two consequences. First, temperatures plotted in Figure A.5 should be considered by taking into account the temporal decrease of the phase transition temperatures. Second, the eventual degradation of DIO may influence the efficiency of the photoalignment, as we have discussed it in the last paragraph of Section 3.4.

To understand the unexpected and unpredictable fluctuations of  $\varphi$  in time detected in the  $N_F$  phase and illustrated in Figures A.3 and A.4, the optical setup introduced in Chapter 2, Figure 2.7 has been employed. The setup allows for direct optical observation via POM while the sample is excited by the pump beam.

While the textures of the  $N$  and  $\text{SmZ}_A$  phase have been found uniform, this is not true for the  $N_F$  phase—see Figure A.6(a). Two different domains have been detected separated by domain walls. The texture has been described in details very recently [148].

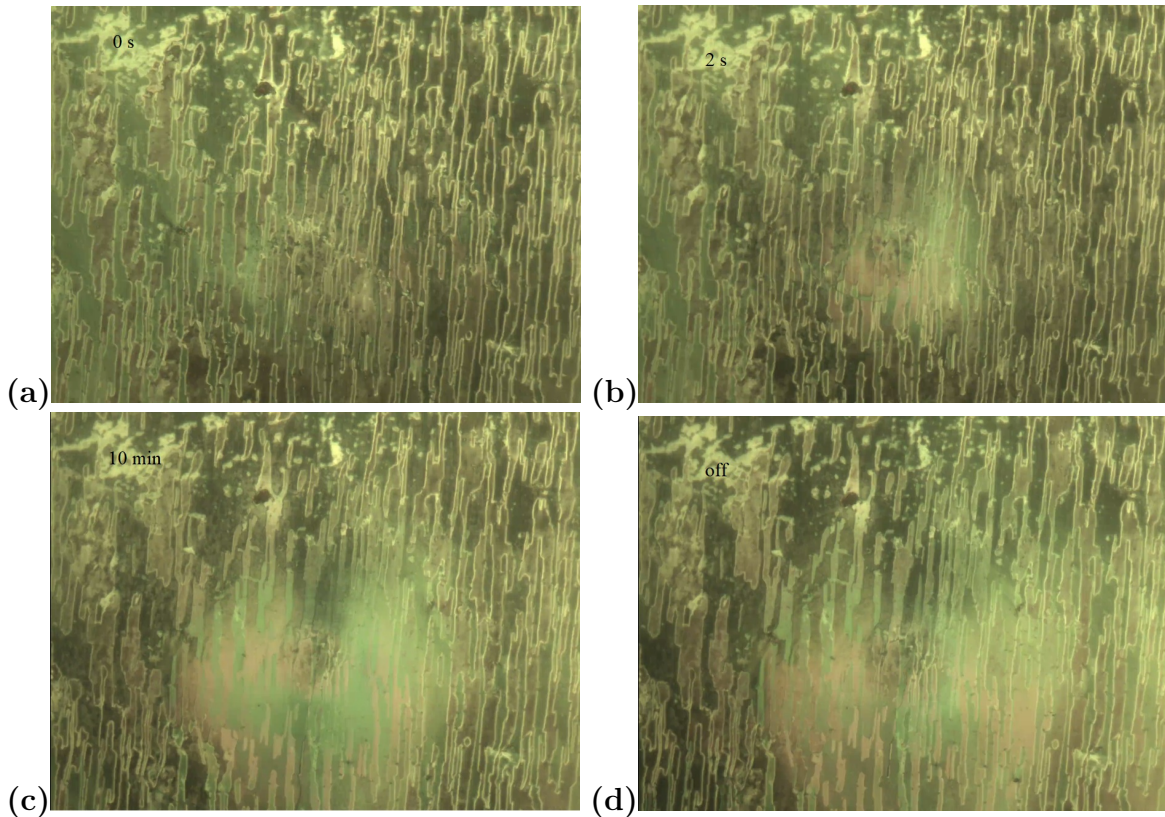


Figure A.6: POM images taken for a cell filled with DIO LC prior the illumination (a), 2 seconds of illumination (b), 10 minutes of illumination (c) and 2 minutes after illumination with laser (d).

---

In the two domains the electric polarization directions are parallel with the rubbing direction on the reference plate, but they point to the opposite direction. The two domains are separated by  $\pi$ -walls (disclination lines), which represent defects in the director field. When the sample is irradiated by the pump beam [Figures A.6(b) and (c)], during the photoalignment, the  $\pi$ -walls move in a quite unpredictable way and cause the observed fluctuations in the measured value of  $\varphi$ . The motion of the  $\pi$ -walls eventually may not stop after switching off the pump beam either [Figure A.6(d)] during the back-relaxation process.

Obviously,  $\pi$ -walls make the azimuthal photoalignment angle measurements meaningless in the  $N_F$  phase, and for precise photoalignment measurements one needs a large area of  $N_F$  monodomain, in which the electric polarization,  $\mathbf{P}$ , points in the same direction. This is in principle achievable by fabrication of extremely thin ( $d < 3\mu\text{m}$ ) LC cells [148]. To make so thin LC cells with uniform thickness and with lateral sizes of  $\sim$  cm in default of a clean room is a technological challenge, but we will make significant efforts to attain it in the forthcoming months.



---

## BIBLIOGRAPHY

- [1] F. Reinitzer, “Beiträge zur kenntniss des cholesterins,” *Monatshefte für Chemie und verwandte Teile anderer Wissenschaften*, vol. 9, pp. 421–441, 1888. [Online]. Available: <https://doi.org/10.1007/BF01516710>
- [2] D. Dunmur and T. Sluckin, *Soap, science, and flat-screen TVs: a history of liquid crystals*. Oxford University Press, 2014.
- [3] F. Reinitzer, “Contributions to the knowledge of cholesterol (translation from the German of the original paper published in monatshefte für chemie 1888, 9, 421-441),” *Liquid Crystals*, vol. 5, no. 1, pp. 7–18, 1989. [Online]. Available: <https://doi.org/10.1080/02678298908026349>
- [4] O. Lehmann, “Über fließende krystalle,” *Zeitschrift für Physikalische Chemie*, vol. 4, pp. 462–472, 1889. [Online]. Available: <https://doi.org/10.1515/zpch-1889-0434>
- [5] G. A. DiLisi, *An Introduction to Liquid Crystals*, J. J. DeLuca, Ed. Ohio, USA: Morgan & Claypool Publishers, 2019. [Online]. Available: <https://dx.doi.org/10.1088/2053-2571/ab2a6f>

- [6] D. Vorländer, “Chemie der kristallinen flüssigkeiten,” *Zeitschrift für Kristallographie - Crystalline Materials*, vol. 79, no. 1-6, pp. 61–89, 1931. [Online]. Available: <https://doi.org/10.1524/zkri.1931.79.1.61>
- [7] G. Friedel, “Les états mésomorphes de la matière,” *Annales de Physique*, vol. 9, no. 18, pp. 273–474, 1922. [Online]. Available: <https://doi.org/10.1051/anphys/192209180273>
- [8] S. Chandrasekhar, *Liquid Crystals*, 2nd ed. Cambridge: Cambridge University Press, 1992. [Online]. Available: <https://doi.org/10.1017/CBO9780511622496>
- [9] V. Fréedericksz and A. Repiewa, “Theoretisches und experimentelles zur frage nach der natur der anisotropen flüssigkeiten,” *Zeitschrift für Physik*, vol. 42, no. 7, pp. 532–546, 1927. [Online]. Available: <https://doi.org/10.1007/BF01397711>
- [10] C. W. Oseen, “The theory of liquid crystals,” *Trans. Faraday Soc.*, vol. 29, pp. 883–899, 1933. [Online]. Available: <http://dx.doi.org/10.1039/TF9332900883>
- [11] F. C. Frank, “I. liquid crystals. On the theory of liquid crystals,” *Discussions of the Faraday Society*, vol. 25, pp. 19–28, 1958. [Online]. Available: <http://dx.doi.org/10.1039/DF9582500019>
- [12] W. Maier and A. Saupe, “Eine einfache molekulare theorie des nematischen kristallinflüssigen zustandes,” *Zeitschrift für Naturforschung A*, vol. 13, no. 7, pp. 564–566, 1958. [Online]. Available: <https://doi.org/10.1515/zna-1958-0716>
- [13] M. Schadt and W. Helfrich, “Voltage-dependent optical activity of a twisted nematic liquid crystal,” *Applied Physics Letters*, vol. 18, no. 4, pp. 127–128, 1971. [Online]. Available: <https://doi.org/10.1063/1.1653593>
- [14] K. Weiss, C. Wöll, E. Böhm, B. Fiebranz, G. Forstmann, B. Peng, V. Scheumann, and D. Johannsmann, “Molecular orientation at rubbed polyimide surfaces determined with x-ray absorption spectroscopy: Relevance for liquid crystal

- alignment,” *Macromolecules*, vol. 31, pp. 1930–1936, 1998. [Online]. Available: <https://doi.org/10.1021/ma971075z>
- [15] B. Jerome, “Surface effects and anchoring in liquid crystals,” *Reports on Progress in Physics*, vol. 54, no. 3, pp. 391–451, 1991. [Online]. Available: <https://dx.doi.org/10.1088/0034-4885/54/3/002>
- [16] R. Stannarius, “More than display fillings,” *Nature Materials*, vol. 8, p. 617–618, 2009. [Online]. Available: <https://doi.org/10.1038/nmat2503>
- [17] J. P. Lagerwall and G. Scalia, “A new era for liquid crystal research: Applications of liquid crystals in soft matter nano-, bio- and microtechnology,” *Current Applied Physics*, vol. 12, no. 6, pp. 1387–1412, 2012. [Online]. Available: <https://doi.org/10.1016/j.cap.2012.03.019>
- [18] T. Ube and T. Ikeda, “A historical overview of photomechanical effects in materials, composites, and systems,” in *Photomechanical Materials, Composites, and Systems: Wireless Transduction of Light into Work*, T. J. White, Ed. Hoboken, USA: John Wiley & Sons, Ltd, 2017, ch. 1, pp. 1–35. [Online]. Available: <https://doi.org/10.1002/9781119123279.ch1>
- [19] A. Jákli and A. Saupe, *One- and Two-Dimensional Fluids: Properties of Smectic, Lamellar and Columnar Liquid Crystals*, 1st ed. Boca Raton: CRC Press, 2006. [Online]. Available: <https://doi.org/10.1201/9781420012200>
- [20] P. J. Wojtowicz, “Lyotropic liquid crystals and biological membranes: The crucial role of water,” in *Introduction to Liquid Crystals*, E. B. Priestley, P. J. Wojtowicz, and P. Sheng, Eds. Boston, MA: Springer US, 1975, pp. 333–350. [Online]. Available: [https://doi.org/10.1007/978-1-4684-2175-0\\_18](https://doi.org/10.1007/978-1-4684-2175-0_18)
- [21] A. M. Figueiredo Neto and S. R. A. Salinas, *The Physics of Lyotropic Liquid Crystals: Phase Transitions and Structural Properties*. Oxford University Press, 2005. [Online]. Available: <https://doi.org/10.1093/acprof:oso/9780198525509.001.0001>

## BIBLIOGRAPHY

---

- [22] S. L. Kakani and A. Kakani, *Material science*. New Delhi: New Age International Publishers, 2004.
- [23] D. Janietz, “Liquid crystals at interfaces,” in *Handbook of Surfaces and Interfaces of Materials*, H. S. Nalwa, Ed. Burlington: Academic Press, 2001, pp. 423–446. [Online]. Available: <https://doi.org/10.1016/B978-012513910-6/50014-1>
- [24] M. J. Hardie, “Self-assembled cages with cyclotrimeratrylene-type host molecules,” *Israel Journal of Chemistry*, vol. 51, no. 7, pp. 807–816, 2011. [Online]. Available: <https://doi.org/10.1002/ijch.201100060>
- [25] P. K. Challa, O. Curtiss, J. C. Williams, R. Twieg, J. Toth, S. McGill, A. Jákli, J. T. Gleeson, and S. N. Sprunt, “Light scattering from liquid crystal director fluctuations in steady magnetic fields up to 25 tesla,” *Physical Review E*, vol. 86, p. 011708, 2012. [Online]. Available: <https://link.aps.org/doi/10.1103/PhysRevE.86.011708>
- [26] P. J. Collings and M. Hird, *Introduction to Liquid Crystals: Chemistry and Physics*, 1st ed. London: CRC Press, 1997. [Online]. Available: <https://doi.org/10.1201/9781315272801>
- [27] I. W. Stewart, *The Static and Dynamic Continuum Theory of Liquid Crystals*, 1st ed. Boca Raton: CRC Press, 2004. [Online]. Available: <https://doi.org/10.1201/9781315272580>
- [28] P. Oswald and P. Pieranski, *Nematic and Cholesteric Liquid Crystals: Concepts and Physical Properties Illustrated by Experiments*, 1st ed. Boca Raton: CRC Press, 2005. [Online]. Available: <https://doi.org/10.1201/9780203023013>
- [29] R. A. Reddy and C. Tschierske, “Bent-core liquid crystals: polar order, superstructural chirality and spontaneous desymmetrisation in soft matter systems,” *Journal of Materials Chemistry*, vol. 16, pp. 907–961, 2006. [Online]. Available: <http://dx.doi.org/10.1039/B504400F>

## BIBLIOGRAPHY

---

- [30] A. Jákli, O. D. Lavrentovich, and J. V. Selinger, “Physics of liquid crystals of bent-shaped molecules,” *Reviews of Modern Physics*, vol. 90, p. 045004, Nov 2018. [Online]. Available: <https://link.aps.org/doi/10.1103/RevModPhys.90.045004>
- [31] M. Mitov, “Liquid-crystal science from 1888 to 1922: Building a revolution,” *ChemPhysChem*, vol. 15, no. 7, pp. 1245–1250, 2014. [Online]. Available: <https://doi.org/10.1002/cphc.201301064>
- [32] D. Demus and L. Richter, *Textures of liquid crystals*, 1st ed. Weinheim: Verlag Chemie, 1978. [Online]. Available: <https://doi.org/10.1002/bbpc.19800841227>
- [33] P. G. d. Gennes and J. Prost, *The Physics of Liquid Crystals*, 2nd ed. Oxford University Press, 1995.
- [34] V. Chigrinov, A. Kudreyko, and Q. Guo, “Patterned photoalignment in thin films: physics and applications,” *Crystals*, vol. 11, no. 2, p. 84, 2021. [Online]. Available: <https://doi.org/10.3390/cryst11020084>
- [35] A. Kudreyko, V. Chigrinov, G. Hegde, and D. Chausov, “Photoaligned liquid crystalline structures for photonic applications,” *Crystals*, vol. 13, no. 6, p. 965, 2023. [Online]. Available: <https://www.doi.org/10.3390/cryst13060965>
- [36] O. Yaroshchuk and Y. Reznikov, “Photoalignment of liquid crystals: basics and current trends,” *Journal of Materials Chemistry*, vol. 22, pp. 286–300, 2012. [Online]. Available: <http://dx.doi.org/10.1039/C1JM13485J>
- [37] V. G. Chigrinov, V. M. Kozenkov, and H.-S. Kwok, “Photoalignment of liquid crystalline materials: physics and applications,” in *Wiley-SID Series in Display Technology*, A. C. Lowe, Ed. Chichester, England: John Wiley & Sons, Ltd, 2008. [Online]. Available: <https://onlinelibrary.wiley.com/doi/abs/10.1002/9780470751800>

## BIBLIOGRAPHY

---

- [38] D. Andrienko, “Introduction to liquid crystals,” *Journal of Molecular Liquids*, vol. 267, pp. 520–541, 2018. [Online]. Available: <https://doi.org/10.1016/j.molliq.2018.01.175>
- [39] D. Demus, J. Goodby, G. Gray, H. Spiess, and V. Vill, *Handbook of Liquid Crystals*. Weinheim: John Wiley & Sons, Ltd., 1998.
- [40] V. G. Chigrinov, *Liquid crystal devices: physics and applications*. Artech House Publisher, 1999.
- [41] J. L. Ericksen, “Conservation Laws for Liquid Crystals,” *Transactions of The Society of Rheology*, vol. 5, no. 1, pp. 23–34, 1961. [Online]. Available: <https://doi.org/10.1122/1.548883>
- [42] F. M. Leslie, “Some constitutive equations for anisotropic fluids,” *The Quarterly Journal of Mechanics and Applied Mathematics*, vol. 19, no. 3, pp. 357–370, 1966. [Online]. Available: <https://doi.org/10.1093/qjmam/19.3.357>
- [43] F. M. Leslie, “Some constitutive equations for liquid crystals,” *Archive for Rational Mechanics and Analysis*, vol. 28, pp. 265–283, 1968. [Online]. Available: <https://doi.org/10.1007/BF00251810>
- [44] O. Parodi, “Stress tensor for a nematic liquid crystal,” *Journal de Physique*, vol. 31, no. 7, pp. 581–584, 1970. [Online]. Available: <https://doi.org/10.1051/jphys:01970003107058100>
- [45] L. M. Blinov, *Structure and Properties of Liquid Crystals*. Springer Netherlands, 2011. [Online]. Available: <https://doi.org/10.1007%2F978-90-481-8829-1>
- [46] M. Miesowicz, “The three coefficients of viscosity of anisotropic liquids,” *Nature*, vol. 158, no. 4001, p. 27, 1946. [Online]. Available: <https://doi.org/10.1038/158027b0>
- [47] B. Broughton, “Surface alignment of liquid crystals,” in *Handbook of Liquid Crystals*, J. W. Goodby, P. J. Collings, T. Kato, H. Gleeson, C. Tschierske, V. Vill,

## BIBLIOGRAPHY

---

- and P. Raynes, Eds. Weinheim, Germany: Wiley-VCH, 2014, vol. 2, pp. 309–330. [Online]. Available: <https://doi.org/10.1002/9783527671403.hlc030>
- [48] C. Mauguin, “Sur les cristaux liquides de M. Lehmann,” *Bulletin de Minéralogie*, vol. 34, no. 3, pp. 71–117, 1911. [Online]. Available: <https://doi.org/10.3406/bulmi.1911.3472>
- [49] T. Matsunobe, N. Nagai, R. Kamoto, Y. Nakagawa, and H. Ishida, “FT-IR study of the molecular orientation of rubbed polyimide alignment films,” *Journal of Photopolymer Science and Technology*, vol. 8, no. 2, pp. 263–268, 1995. [Online]. Available: <https://doi.org/10.2494/photopolymer.8.263>
- [50] N. A. J. M. van Aerle, M. Barmentlo, and R. W. J. Hollering, “Effect of rubbing on the molecular orientation within polyimide orienting layers of liquid-crystal displays,” *Journal of Applied Physics*, vol. 74, no. 5, pp. 3111–3120, 09 1993. [Online]. Available: <https://doi.org/10.1063/1.354577>
- [51] K.-H. Kim and J.-K. Song, “Technical evolution of liquid crystal displays,” *NPG Asia Materials*, vol. 1, pp. 29–36, 2009. [Online]. Available: <https://doi.org/10.1038/asiamat.2009.3>
- [52] J. van Haaren, “Out of the groove,” *Nature*, vol. 392, pp. 331–333, 1998. [Online]. Available: <https://doi.org/10.1038/32771>
- [53] H. Yoshida, “Vertically aligned nematic (van) lcd technology,” in *Handbook of Visual Display Technology*, J. Chen, W. Cranton, and M. Fihn, Eds. Berlin, Heidelberg: Springer Berlin Heidelberg, 2012, pp. 1485–1505. [Online]. Available: [https://doi.org/10.1007/978-3-540-79567-4\\_91](https://doi.org/10.1007/978-3-540-79567-4_91)
- [54] Y. B. Kim, H. Olin, S. Y. Park, J. W. Choi, L. Komitov, M. Matuszczyk, and S. T. Lagerwall, “Rubbed polyimide films studied by scanning force microscopy,” *Applied Physics Letters*, vol. 66, no. 17, pp. 2218–2219, 1995. [Online]. Available: <https://doi.org/10.1063/1.113172>

- [55] A. J. Pidduck, G. P. Bryan-Brown, S. Haslam, R. Bannister, I. Kitley, T. J. McMaster, and L. Boogaard, “Atomic force microscopy studies of rubbed polyimide surfaces used for liquid crystal alignment,” *Journal of Vacuum Science & Technology A*, vol. 14, no. 3, pp. 1723–1728, 1996. [Online]. Available: <https://doi.org/10.1116/1.580327>
- [56] D. W. Berreman, “Solid surface shape and the alignment of an adjacent nematic liquid crystal,” *Physical Review Letters*, vol. 28, pp. 1683–1686, 1972. [Online]. Available: <https://link.aps.org/doi/10.1103/PhysRevLett.28.1683>
- [57] J. M. Geary, J. W. Goodby, A. R. Kmetz, and J. S. Patel, “The mechanism of polymer alignment of liquid-crystal materials,” *Journal of Applied Physics*, vol. 62, no. 10, pp. 4100–4108, 1987. [Online]. Available: <https://doi.org/10.1063/1.339124>
- [58] X. Wei, X. Zhuang, S.-C. Hong, T. Goto, and Y. R. Shen, “Sum-frequency vibrational spectroscopic study of a rubbed polymer surface,” *Physical Review Letters*, vol. 82, pp. 4256–4259, 1999. [Online]. Available: <https://link.aps.org/doi/10.1103/PhysRevLett.82.4256>
- [59] B. Bahadur, “Liquid crystal displays,” *Molecular Crystals and Liquid Crystals*, vol. 109, no. 1, pp. 3–93, 1984. [Online]. Available: <https://doi.org/10.1080/00268948408080827>
- [60] H. Aoyama, Y. Yamazaki, N. Matsuura, H. Mada, and S. Kobayashi, “Alignment of liquid crystals on the stretched polymer films,” *Molecular Crystals and Liquid Crystals*, vol. 72, no. 4, pp. 127–132, 1981. [Online]. Available: <https://doi.org/10.1080/01406568108084048>
- [61] J. van Haaren, “Wiping out dirty displays,” *Nature*, vol. 411, p. 29–30, 2001. [Online]. Available: <https://doi.org/10.1038/35075178>
- [62] K. Ichimura, T. Seki, Y. Kawanishi, Y. Suzuki, M. Sakuragi, and T. Tamaki, “Photocontrol of liquid crystal alignment by command surfaces,” in *Photo-reactive ma-*



## BIBLIOGRAPHY

---

- terials for ultrahigh density optical memory*, M. Irie, Ed. Elsevier, Amsterdam, 1994, p. 55.
- [63] Y. Kawanishi, T. Seki, T. Tamaki, K. Ichimura, M. Ikeda, and K. Aoki, “Reversible alignment change of nematic liquid crystals by photochromic polymer films,” *Polymers for Advanced Technologies*, vol. 1, no. 5-6, pp. 311–318, 1990. [Online]. Available: <https://doi.org/10.1002/pat.1990.220010505>
- [64] M. Schadt, K. Schmitt, V. Kozinkov, and V. Chigrinov, “Surface-induced parallel alignment of liquid crystals by linearly polymerized photopolymers,” *Japanese Journal of Applied Physics*, vol. 31, p. 2155, 1992. [Online]. Available: <https://dx.doi.org/10.1143/JJAP.31.2155>
- [65] W. M. Gibbons, P. J. Shannon, S.-T. Sun, and B. J. Swetlin, “Surface-mediated alignment of nematic liquid crystals with polarized laser light,” *Nature*, vol. 351, no. 6321, pp. 49–50, 1991. [Online]. Available: <https://doi.org/10.1038/351049a0>
- [66] A. Dyadyusha, T. Y. Marusii, V. Y. Reshetnyak, Y. A. Reznikov, and A. Khizhnyak, “Orientational effect due to a change in the anisotropy of the interaction between a liquid crystal and a bounding surface,” *JETP Letters*, vol. 56, no. 1, pp. 18–21, 1992. [Online]. Available: [http://jetpletters.ru/ps/1281/article\\_19369.pdf](http://jetpletters.ru/ps/1281/article_19369.pdf)
- [67] W. Gibbons, T. Kosa, P. Palffy-Muhoray, P. Shannon, and S. Sun, “Continuous grey-scale image storage using optically aligned nematic liquid crystals,” *Nature*, vol. 377, pp. 43–46, 1995. [Online]. Available: <https://doi.org/10.1038/377043a0>
- [68] K. Ichimura, Y. Suzuki, T. Seki, A. Hosoki, and K. Aoki, “Reversible change in alignment mode of nematic liquid crystals regulated photochemically by command surfaces modified with an azobenzene monolayer,” *Langmuir*, vol. 4, no. 5, pp. 1214–1216, 1988. [Online]. Available: <https://doi.org/10.1021/la00083a030>
- [69] K. Ichimura, Y. Hayashi, H. Akiyama, T. Ikeda, and N. Ishizuki, “Photo-optical liquid crystal cells driven by molecular rotors,” *Applied Physics Letters*, vol. 63, no. 4, pp. 449–451, 1993. [Online]. Available: <https://doi.org/10.1063/1.110020>

## BIBLIOGRAPHY

---

- [70] K. Aoki, Y. Kawanishi, T. Seki, M. Sakuragi, T. Tamaki, and K. Ichimura, “Reversible alignment change of liquid crystals induced by photochromic molecular films: Properties of azobenzene chromophores covalently attached to silica surfaces,” *Liquid Crystals*, vol. 19, no. 1, pp. 119–125, 1995. [Online]. Available: <https://doi.org/10.1080/02678299508036728>
- [71] H. Knobloch, H. Orendi, M. Büchel, T. Seki, S. Ito, and W. Knoll, “Command surface controlled liquid crystalline waveguide structures as optical information storage,” *Journal of Applied Physics*, vol. 76, no. 12, pp. 8212–8214, 12 1994. [Online]. Available: <https://doi.org/10.1063/1.357883>
- [72] K. Ichimura, Y. Suzuki, T. Seki, Y. Kawanishi, T. Tamaki, and K. Aoki, “Reversible alignment change of liquid crystals induced by photochromic molecular films,” *Japanese Journal of Applied Physics*, vol. 28, no. S3, pp. 289–292, 1989. [Online]. Available: <https://dx.doi.org/10.7567/JJAPS.28S3.289>
- [73] Y. Kawanishi, T. Tamaki, M. Sakuragi, T. Seki, Y. Suzuki, and K. Ichimura, “Photochemical induction and modulation of nematic homogeneous alignment by the polarization photochromism of surface azobenzenes,” *Langmuir*, vol. 8, no. 11, pp. 2601–2604, 1992. [Online]. Available: <https://doi.org/10.1021/la00047a006>
- [74] T. Fischer, L. Läsker, J. Stumpe, and S. Kostromin, “Photoinduced optical anisotropy in films of photochromic liquid crystalline polymers,” *Journal of Photochemistry and Photobiology A: Chemistry*, vol. 80, no. 1, pp. 453–459, 1994. [Online]. Available: [https://doi.org/10.1016/1010-6030\(94\)01056-0](https://doi.org/10.1016/1010-6030(94)01056-0)
- [75] M. Schadt, H. Seiberle, A. Schuster, and S. M. K. S. M. Kelly, “Photo-induced alignment and patterning of hybrid liquid crystalline polymer films on single substrates,” *Japanese Journal of Applied Physics*, vol. 34, no. 6B, pp. L764–L767, 1995. [Online]. Available: <https://dx.doi.org/10.1143/JJAP.34.L764>

- [76] M. Schadt, H. Seiberle, and A. Schuster, “Optical patterning of multi-domain liquid-crystal displays with wide viewing angles,” *Nature*, vol. 381, no. 6579, pp. 212–215, 1996. [Online]. Available: <https://doi.org/10.1038/381212a0>
- [77] K. Ichimura, “Photoregulation of liquid crystal alignment by photochromic molecules and polymeric thin films,” in *Polymers as Electrooptical and Photooptical Active Media. Macromolecular Systems — Materials Approach*, V. P. Shibaev, Ed. Berlin, Heidelberg: Springer, 1996, pp. 138–172. [Online]. Available: [https://doi.org/10.1007/978-3-642-79861-0\\_4](https://doi.org/10.1007/978-3-642-79861-0_4)
- [78] V. Chigrinov, H. S. Kwok, H. Takada, and H. Takatsu, “Photo-aligning by azo-dyes: Physics and applications,” *Liquid Crystals Today*, vol. 14, no. 4, pp. 1–15, 2005. [Online]. Available: <https://doi.org/10.1080/14645180600617908>
- [79] G. Babakhanova and O. D. Lavrentovich, “The techniques of surface alignment of liquid crystals,” in *Modern Problems of the Physics of Liquid Systems. Selected Reviews from the 8th International Conference “Physics of Liquid Matter: Modern Problems”*, L. A. Bulavin and L. Xu, Eds., vol. 223. Kyiv, Ukraine: Springer, 2018, pp. 165–197. [Online]. Available: [https://doi.org/10.1007/978-3-030-21755-6\\_7](https://doi.org/10.1007/978-3-030-21755-6_7)
- [80] H. M. D. Bandara and S. C. Burdette, “Photoisomerization in different classes of azobenzene,” *Chemical Society Reviews*, vol. 41, pp. 1809–1825, 2012. [Online]. Available: <http://dx.doi.org/10.1039/C1CS15179G>
- [81] J. F. Rabek, *Photochemistry and photophysics*. Boca Raton, FL: CRC Press, 1990, ch. 4.
- [82] M. Aguilar and J. San Román, “Introduction to smart polymers and their applications,” in *Smart Polymers and their Applications*, M. R. Aguilar and J. San Román, Eds. Cambridge, UK: Woodhead Publishing, 2014, ch. 1, pp. 1–11. [Online]. Available: <https://doi.org/10.1533/9780857097026.1>
- [83] K.-S. Lee, Ed., “Polymers for photonics applications II. Nonlinear optical, photorefractive and two-photon absorption polymers,” in *Advances in Polymer*

- Science*. Berlin, Heidelberg: Springer, 2003, vol. 161. [Online]. Available: <https://doi.org/10.1007/3-540-45642-2>
- [84] D. Yan, Z. Wang, and Z. Zhang, “Stimuli-responsive crystalline smart materials: From rational design and fabrication to applications,” *Accounts of Chemical Research*, vol. 55, 7, p. 1047–1058, 2022. [Online]. Available: <https://doi.org/10.1021/acs.accounts.2c00027>
- [85] K. Ichimura, “Photoalignment of liquid-crystal systems,” *Chemical Reviews*, vol. 100, no. 5, pp. 1847–1874, 2000. [Online]. Available: <https://doi.org/10.1021/cr980079e>
- [86] J. Michl and E. Thulstrup, *Spectroscopy with polarized light: solute alignment by photoselection in liquid crystals, polymers and membranes*. United States: VCH Publishers, 1995.
- [87] K. Ichimura, H. Akiyama, N. Ishizuki, and Y. Kawanishi, “Azimuthal orientation of liquid crystals photo-controlled by an azobenzene pendent polymer,” *Die Makromolekulare Chemie, Rapid Communications*, vol. 14, no. 12, pp. 813–817, 1993. [Online]. Available: <https://doi.org/10.1002/marc.1993.030141213>
- [88] H. Akiyama, K. Kudo, and K. Ichimura, “Novel polymethacrylates with laterally attached azobenzene groups displaying photoinduced optical anisotropy,” *Macromolecular Rapid Communications*, vol. 16, pp. 35–41, 1995. [Online]. Available: <https://doi.org/10.1002/marc.1995.030160107>
- [89] P. Palffy-Muhoray, T. Kosa, and Weinan E, “Brownian motors in the photoalignment of liquid crystals,” *Applied Physics A*, vol. 75, pp. 293–300, 2002. [Online]. Available: <https://doi.org/10.1007/s003390201321>
- [90] T. Tóth-Katona and I. Jánossy, “Photoalignment at the nematic liquid crystal-polymer interface: experimental evidence of three-dimensional reorientation,” *Journal of Molecular Liquids*, vol. 285, pp. 323–329, 2019. [Online]. Available: <https://doi.org/10.1016/j.molliq.2019.04.074>

- [91] C. B. Walsh and E. I. Franses, “Ultrathin PMMA films spin-coated from toluene solutions,” *Thin Solid Films*, vol. 429, no. 1-2, pp. 71–76, 2003. [Online]. Available: [https://doi.org/10.1016/S0040-6090\(03\)00031-2](https://doi.org/10.1016/S0040-6090(03)00031-2)
- [92] E. V. Thompson, “Dependence of the glass transition temperature of poly(methyl methacrylate) on tacticity and molecular weight,” *Journal of Polymer Science Part A-2: Polymer Physics*, vol. 4, no. 2, pp. 199–208, 1966. [Online]. Available: <https://onlinelibrary.wiley.com/doi/abs/10.1002/pol.1966.160040204>
- [93] K. Ute, N. Miyatake, and K. Hatada, “Glass transition temperature and melting temperature of uniform isotactic and syndiotactic poly (methyl methacrylate)s from 13mer to 50mer,” *Polymer*, vol. 36, no. 7, pp. 1415–1419, 1995. [Online]. Available: [https://doi.org/10.1016/0032-3861\(95\)95919-R](https://doi.org/10.1016/0032-3861(95)95919-R)
- [94] H. A. Haque, M. Hara, S. Nagano, and T. Seki, “Photoinduced in-plane motions of azobenzene mesogens affected by the flexibility of underlying amorphous chains,” *Macromolecules*, vol. 46, no. 20, pp. 8275–8283, 2013. [Online]. Available: <https://doi.org/10.1021/ma401536r>
- [95] “DSC measurement has been performed at Alphamicron Inc., Kent OH, USA.”
- [96] A. M. Parshin, V. A. Gunyakov, V. Y. Zyryanov, and V. F. Shabanov, “Electric and magnetic field-assisted orientational transitions in the ensembles of domains in a nematic liquid crystal on the polymer surface,” *International Journal of Molecular Sciences*, vol. 15, no. 10, pp. 17 838–17 851, 2014. [Online]. Available: <https://doi.org/10.3390/ijms151017838>
- [97] N. Hartshorne and A. Stuart, *Crystals and the Polarising Microscope*, 4th ed. London: Edward Arnold LTD, 1970.
- [98] I. Dierking, *Textures of Liquid Crystals*. Weinheim: WILEY-VCH Verlag, 2003. [Online]. Available: <https://onlinelibrary.wiley.com/doi/book/10.1002/3527602054>

## BIBLIOGRAPHY

---

- [99] “Gwyddion – free SPM data analysis software,” (accessed: 22 august 2023). [Online]. Available: <http://gwyddion.net>
- [100] A. O. Solak, S. Ranganathan, T. Itoh, and R. L. McCreery, “A mechanism for conductance switching in carbon-based molecular electronic junctions,” *Electrochemical and Solid-State Letters*, vol. 5, no. 8, p. E43–E46, 2002. [Online]. Available: <https://doi.org/10.1149/1.1490716>
- [101] R. Eelkema and B. L. Feringa, “Amplification of chirality in liquid crystals,” *Organic & Biomolecular Chemistry*, vol. 4, no. 20, pp. 3729–3745, 2006. [Online]. Available: <http://dx.doi.org/10.1039/B608749C>
- [102] S. L. Oscurato, M. Salvatore, P. Maddalena, and A. Ambrosio, “From nanoscopic to macroscopic photo-driven motion in azobenzene-containing materials,” *Nanophotonics*, vol. 7, no. 8, pp. 1387–1422, 2018. [Online]. Available: <https://doi.org/10.1515/nanoph-2018-0040>
- [103] C. A. Hunter, K. R. Lawson, J. Perkins, and C. J. Urch, “Aromatic interactions,” *Journal of the Chemical Society, Perkin Transactions 2*, no. 5, pp. 651–669, 2001. [Online]. Available: <https://doi.org/10.1039/b008495f>
- [104] C. A. Hunter and J. K. M. Sanders, “The nature of  $\pi - \pi$  interactions,” *Journal of the American Chemical Society*, vol. 112, no. 14, pp. 5525–5534, 1990. [Online]. Available: <https://doi.org/10.1021/ja00170a016>
- [105] M. L. Waters, “Aromatic interactions in model systems,” *Current Opinion in Chemical Biology*, vol. 6, no. 6, pp. 736–741, 2002. [Online]. Available: [https://doi.org/10.1016/S1367-5931\(02\)00359-9](https://doi.org/10.1016/S1367-5931(02)00359-9)
- [106] R. P. Matthews, T. Welton, and P. A. Hunt, “Competitive pi interactions and hydrogen bonding within imidazolium ionic liquids,” *Physical Chemistry Chemical Physics*, vol. 16, pp. 3238–3253, 2014. [Online]. Available: <http://dx.doi.org/10.1039/C3CP54672A>

## BIBLIOGRAPHY

---

- [107] A. Chana, M. A. Concejero, M. De Frutos, M. J. González, and B. Herradón, “Computational studies on biphenyl derivatives. analysis of the conformational mobility, molecular electrostatic potential, and dipole moment of chlorinated biphenyl: Searching for the rationalization of the selective toxicity of polychlorinated biphenyls (pcbs),” *Chemical Research in Toxicology*, vol. 15, no. 12, p. 1514 – 1526, 2002. [Online]. Available: <https://doi.org/10.1021/tx025596d>
- [108] R. J. Mandle, E. J. Davis, C.-C. A. Voll, D. J. Lewis, S. J. Cowling, and J. W. Goodby, “Self-organisation through size-exclusion in soft materials,” *Journal of Materials Chemistry C*, vol. 3, no. 10, pp. 2380–2388, 2015. [Online]. Available: <http://dx.doi.org/10.1039/C4TC02991G>
- [109] C. Cojocar, A. Airinei, and N. Fifere, “Molecular structure and modeling studies of azobenzene derivatives containing maleimide groups,” *SpringerPlus*, vol. 2, p. 586, 2013. [Online]. Available: <https://doi.org/10.1186/2193-1801-2-586>
- [110] B. U. Emenike, S. N. Bey, B. C. Bigelow, and S. V. S. Chakravartula, “Quantitative model for rationalizing solvent effect in noncovalent CH–aryl interactions,” *Chemical Science*, vol. 7, pp. 1401–1407, 2016. [Online]. Available: <http://dx.doi.org/10.1039/C5SC03550C>
- [111] K. Shimizu, C. E. Bernardes, and J. N. Canongia Lopes, “The complex structure of ionic liquids at an atomistic level: From ”red-and-greens” to charge templates,” *Pure and Applied Chemistry*, vol. 86, no. 2, p. 119 – 133, 2014. [Online]. Available: <http://dx.doi.org/10.1515/pac-2014-5021>
- [112] I. Jánossy, K. Fodor-Csorba, A. Vajda, L. Palomares, and T. Tóth-Katona, “Light-induced instabilities in photo-oriented liquid crystal cells,” *Molecular Crystals and Liquid Crystals*, vol. 594, no. 1, pp. 92–99, 2014. [Online]. Available: <https://doi.org/10.1080/15421406.2014.917496>
- [113] L. Cheung, R. B. Meyer, and H. Gruler, “Measurements of nematic elastic constants near a second order nematic-smectic-*a* phase change,”

- Physical Review Letters*, vol. 31, pp. 349–352, 1973. [Online]. Available: <https://link.aps.org/doi/10.1103/PhysRevLett.31.349>
- [114] M. Delaye, R. Ribotta, and G. Durand, “Rayleigh scattering at a second-order nematic to smectic-*a* phase transition,” *Physical Review Letters*, vol. 31, pp. 443–445, 1973. [Online]. Available: <https://link.aps.org/doi/10.1103/PhysRevLett.31.443>
- [115] H. Coles and M. Sefton, “Pretransitional behaviour of the splay and twist elastic and viscotic constants for the nematic to smectic a phase transition in octyl cyanobiphenyl (8CB),” *Molecular Crystals and Liquid Crystals Letters*, vol. 4, no. 5, pp. 123–130, 1987. [Online]. Available: <https://www.tandfonline.com/doi/abs/10.1080/01406566.1987.10766888>
- [116] D. Dunmur and K. Toriyama, “Elastic properties,” in *Handbook of Liquid Crystals*, D. Demus, J. W. Goodby, G. W. Gray, H.-W. Spiess, and V. Vill, Eds. Weinheim: Wiley-VCH, 1998, vol. 1, ch. 7, pp. 253–280.
- [117] P. Shannon, W. Gibbons, and S.-T. Sun, “Patterned optical properties in photopolymerized surface-aligned liquid-crystal films,” *Nature*, vol. 368, no. 6471, pp. 532–533, 1994. [Online]. Available: <https://doi.org/10.1038/368532a0>
- [118] I. Jánossy, A. Jákli, G. G. Nair, K. K. Raina, and T. Kósa, “Optical control of the alignment of a liquid crystal in the smectic a phase,” *Molecular Crystals and Liquid Crystals*, vol. 329, pp. 507–516, 1999. [Online]. Available: <https://doi.org/10.1080/10587259908025975>
- [119] I. Jánossy, A. Vajda, T. Paksi, and T. Kósa, “Photoinduced surface alignment: The role of liquid-crystalline order,” *Molecular Crystals and Liquid Crystals*, vol. 359, pp. 157–166, 2001. [Online]. Available: <https://doi.org/10.1080/10587250108035577>
- [120] Y. Iimura, J. ichi Kusano, S. Kobayashi, Y. Aoyagi, and T. Sugano, “Alignment control of a liquid crystal on a photosensitive polyvinylalcohol film,” *Japanese*



- Journal of Applied Physics*, vol. 32, part 2, no. 1A/B, pp. L93–L96, 1993. [Online]. Available: <https://dx.doi.org/10.1143/JJAP.32.L93>
- [121] A. Ryabchun, A. Y. Bobrovsky, and V. Shibaev, “Photoinduced reorientation processes in thin films of photochromic LC polymers on substrates with a photocontrollable command surface,” *Polymer Science Series A*, vol. 52, no. 8, pp. 812–823, 2010. [Online]. Available: <https://doi.org/10.1134/S0965545X10080079>
- [122] A. Bobrovsky, A. Ryabchun, and V. Shibaev, “Liquid crystals photoalignment by films of side-chain azobenzene-containing polymers with different molecular structure,” *Journal of Photochemistry and Photobiology A: Chemistry*, vol. 218, pp. 137–142, 2011. [Online]. Available: <https://doi.org/10.1016/j.jphotochem.2010.12.013>
- [123] K. Ichimura, S. Morino, and H. Akiyama, “Three-dimensional orientational control of molecules by slantwise photoirradiation,” *Applied Physics Letters*, vol. 73, no. 7, pp. 921–923, 08 1998. [Online]. Available: <https://doi.org/10.1063/1.122038>
- [124] C. Ruslim and K. Ichimura, “Comparative studies on isomerization behavior and photocontrol of nematic liquid crystals using polymethacrylates with 3,3'- and 4,4'-dihexyloxyazobenzenes in side chains,” *Macromolecules*, vol. 32, no. 13, pp. 4254–4263, 1999. [Online]. Available: <https://doi.org/10.1021/ma990102d>
- [125] C. Ruslim and K. Ichimura, “Photocontrolled alignment of chiral nematic liquid crystals,” *Advanced Materials*, vol. 13, no. 9, pp. 641–644, 2001. [Online]. Available: [https://doi.org/10.1002/1521-4095\(200105\)13:9<641::AID-ADMA641>3.0.CO;2-B](https://doi.org/10.1002/1521-4095(200105)13:9<641::AID-ADMA641>3.0.CO;2-B)
- [126] P. Palffy-Muhoray, T. Kosa, and E. Weinan, “Dynamics of a light driven molecular motor,” *Molecular Crystals and Liquid Crystals*, vol. 375, no. 1, pp. 577–591, 2002. [Online]. Available: <https://doi.org/10.1080/10587250210584>
- [127] A. Ryabchun, A. Bobrovsky, S.-H. Chun, and V. Shibaev, “A novel generation of photoactive comb-shaped polyamides for the photoalignment of liquid crystals,”

## BIBLIOGRAPHY

---

- Journal of Polymer Science Part A: Polymer Chemistry*, vol. 51, no. 19, pp. 4031–4041, 2013. [Online]. Available: <https://doi.org/10.1002/pola.26831>
- [128] Y. Kawanishi, T. Tamaki, T. Seki, M. Sakuragi, Y. Suzuki, K. Ichimura, and K. Aoki, “Multifarious liquid crystalline textures formed on a photochromic azobenzene polymer film,” *Langmuir*, vol. 7, no. 7, pp. 1314–1315, 1991. [Online]. Available: <https://doi.org/10.1021/la00055a003>
- [129] H. Akiyama, M. Momose, K. Ichimura, and S. Yamamura, “Surface-selective modification of poly(vinyl alcohol) films with azobenzenes for in-plane alignment photocontrol of nematic liquid crystals,” *Macromolecules*, vol. 28, pp. 288–293, 1995. [Online]. Available: <https://doi.org/10.1021/ma00105a040>
- [130] Y. Tang, D. Liu, P. Xie, and R. Zhang, “Photo-driven liquid crystal cell using azobenzene-grafted ladderlike polysiloxane as command layer,” *Macromolecular Rapid Communications*, vol. 17, no. 11, pp. 759–766, 1996. [Online]. Available: <https://doi.org/10.1002/marc.1996.030171102>
- [131] Y. Tang, P. Xie, D. Liu, R. Zhang, Z. Zhang, and N. Yao, “Performance-improved photo-driven liquid crystal cell using azobenzene-grafted ladderlike polysiloxane as command layer,” *Macromolecular Chemistry and Physics*, vol. 198, no. 6, pp. 1855–1863, 1997. [Online]. Available: <https://doi.org/10.1002/macp.1997.021980614>
- [132] V. P. Shibaev and A. Y. Bobrovsky, “Liquid crystalline polymers: development trends and photocontrollable materials,” *Russian Chemical Reviews*, vol. 86, no. 11, p. 1024, 2017. [Online]. Available: <https://dx.doi.org/10.1070/RCR4747>
- [133] P. Rochon, E. Batalla, and A. Natansohn, “Optically induced surface gratings on azoaromatic polymer films,” *Applied Physics Letters*, vol. 66, no. 2, pp. 136–138, 1995. [Online]. Available: <https://doi.org/10.1063/1.113541>
- [134] D. Y. Kim, S. K. Tripathy, L. Li, and J. Kumar, “Laser-induced holographic surface relief gratings on nonlinear optical polymer films,” *Applied Physics Letters*, vol. 66, no. 10, pp. 1166–1168, 1995. [Online]. Available: <https://doi.org/10.1063/1.113845>

- [135] D. Y. Kim, L. Li, X. L. Jiang, V. Shivshankar, J. Kumar, and S. K. Tripathy, “Polarized laser induced holographic surface relief gratings on polymer films,” *Macromolecules*, vol. 28, no. 26, pp. 8835–8839, 1995. [Online]. Available: <https://doi.org/10.1021/ma00130a017>
- [136] S. Bian, L. Li, J. Kumar, D. Y. Kim, J. Williams, and S. K. Tripathy, “Single laser beam-induced surface deformation on azobenzene polymer films,” *Applied Physics Letters*, vol. 73, no. 13, pp. 1817–1819, 1998. [Online]. Available: <https://doi.org/10.1063/1.122292>
- [137] S. Bian, W. Liu, J. Williams, L. Samuelson, J. Kumar, and S. Tripathy, “Photoinduced surface relief grating on amorphous poly(4-phenylazophenol) films,” *Chemistry of Materials*, vol. 12, no. 6, pp. 1585–1590, 2000. [Online]. Available: <https://doi.org/10.1021/cm000071x>
- [138] I. Jánossy, T. Tóth-Katona, T. Kósa, and L. Sukhomlinova, “Super-twist generation and instabilities in photosensitive liquid crystal cells,” *Journal of Molecular Liquids*, vol. 267, pp. 177–181, 2018. [Online]. Available: <https://doi.org/10.1016/j.molliq.2017.12.071>
- [139] I. Jánossy and T. Tóth-Katona, “Photo-orientation of liquid crystals on azo dye-containing polymers,” *Polymers*, vol. 14, no. 1, p. 159, 2022. [Online]. Available: <https://doi.org/10.3390/polym14010159>
- [140] T. Seki, “New strategies and implications for the photoalignment of liquid crystalline polymers,” *Polymer Journal*, vol. 46, no. 11, pp. 751–768, 2014. [Online]. Available: <https://doi.org/10.1038/pj.2014.68>
- [141] M. Born, “Ueber anisotrope flüssigkeiten: Versuch einer theorie der flüssigen kristalle und des elektrischen kerr-effekts in flüssigkeiten,” *Sitzungsberichte der Königlich Preussischen Akademie der Wissenschaften*, vol. 30, pp. 614–650, 1916.
- [142] R. J. Mandle, S. J. Cowling, and J. W. Goodby, “A nematic to nematic transformation exhibited by a rod-like liquid crystal,” *Physical Chemistry*

- Chemical Physics*, vol. 19, pp. 11 429–11 435, 2017. [Online]. Available: <http://dx.doi.org/10.1039/C7CP00456G>
- [143] H. Nishikawa, K. Shiroshita, H. Higuchi, Y. Okumura, Y. Haseba, S.-i. Yamamoto, K. Sago, and H. Kikuchi, “A fluid liquid-crystal material with highly polar order,” *Advanced Materials*, vol. 29, no. 43, p. 1702354, 2017. [Online]. Available: <https://doi.org/10.1002/adma.201702354>
- [144] X. Chen, E. Korblova, M. A. Glaser, J. E. MacLennan, D. M. Walba, and N. A. Clark, “Polar in-plane surface orientation of a ferroelectric nematic liquid crystal: Polar monodomains and twisted state electro-optics,” *Proceedings of the National Academy of Sciences*, vol. 118, no. 22, p. e2104092118, 2021. [Online]. Available: <https://www.pnas.org/doi/abs/10.1073/pnas.2104092118>
- [145] N. Sebastián, M. Lovšin, B. Berteloot, N. Osterman, A. Petelin, R. J. Mandle, S. Aya, M. Huang, I. Drevenšek-Olenik, K. Neyts *et al.*, “Polarization patterning in ferroelectric nematic liquids via flexoelectric coupling,” *Nature Communications*, vol. 14, no. 1, p. 3029, 2023. [Online]. Available: <https://doi.org/10.1038/s41467-023-38749-2>
- [146] R. J. Mandle, “A new order of liquids: polar order in nematic liquid crystals,” *Soft Matter*, vol. 18, pp. 5014–5020, 2022. [Online]. Available: <http://dx.doi.org/10.1039/D2SM00543C>
- [147] X. Chen, V. Martinez, E. Korblova, G. Freychet, M. Zhernenkov, M. A. Glaser, C. Wang, C. Zhu, L. Radzihovsky, J. E. MacLennan, D. M. Walba, and N. A. Clark, “The smectic  $Z_A$  phase: Antiferroelectric smectic order as a prelude to the ferroelectric nematic,” *Proceedings of the National Academy of Sciences*, vol. 120, no. 8, p. e2217150120, 2023. [Online]. Available: <https://www.pnas.org/doi/abs/10.1073/pnas.2217150120>
- [148] B. Basnet, M. Rajabi, H. Wang, P. Kumari, K. Thapa, S. Paul, M. O. Lavrentovich, and O. D. Lavrentovich, “Soliton walls paired by polar surface interactions in a

## BIBLIOGRAPHY

---

ferroelectric nematic liquid crystal,” *Nature Communications*, vol. 13, no. 1, p. 3932, 2022. [Online]. Available: <https://doi.org/10.1038/s41467-022-31593-w>



---

# LIST OF PUBLICATIONS

## Publications related to theses points

- [N1] A.R.K. Nassrah, I. Jánossy and T. Tóth-Katona, “Photoalignment at the Nematic Liquid Crystal-Polymer Interface: The Importance of the Liquid Crystalline Molecular Structure.” *J. Mol. Liq.*, **312**, 113309/1-7 (2020).  
<https://doi.org/10.1016/j.molliq.2020.113309>. Q1, IF.: 6.165
- [N2] A.R.K. Nassrah, I. Jánossy, V. Kenderesi, T. Tóth-Katona, “Polymer-Nematic Liquid Crystal Interface: On the Role of the Liquid Crystalline Molecular Structure and the Phase Sequence in Photoalignment.” *Polymers* **13**, 193/1-13 (2021).  
<https://doi.org/10.3390/polym13020193>. Q1, IF.: 4.967
- [N3] A.R.K. Nassrah, M. Batkova, N. Tomašovičová, T. Tóth-Katona, ”Photoaligning Polymeric Command Surfaces: Bind, or Mix?.” *Polymers* **15**, 4271/1-12 (2023).  
<https://doi.org/10.3390/polym15214271>. Q1, IF.: 5

## Conference presentations related to theses points

- [N4] A.R.K. Nassrah, I. Jánossy and T. Tóth-Katona, “Photoalignment at the nematic liquid crystal-polymer interface: the importance of the liquid crystalline molecular

structure”. 18th International Conference on Thin Films & 18th Joint Vacuum Conference (ICTF-JVC2020). November 22-26, 2020, Budapest, Hungary. (poster presentation, [book of abstracts](#), pp. 157-158).

[N5] A.R.K. Nassrah and T. Tóth-Katona, “Nematics interfacing photosensitive substrates”. Oral presentation at Doctoral Student Conference ([DOFFI-2021](#)). September 16-18, 2021, Balatonvilágos, Hungary.

[N6] A.R.K. Nassrah and T. Tóth-Katona, “Nematics interfacing photosensitive substrates: experiments on photoalignment”. 28th International Liquid Crystal Conference ([ILCC2022](#)). July 24-29, 2022, Lisbon, Portugal. (poster presentation, [book of abstracts](#), pp. 79, PC.100).

## Awards

- Stipendium Hungaricum scholarship Programme (2019-2023).
- IUVESTA-Elsevier Student Award for the participation on the 18th International Conference on Thin Films & 18th Joint Vacuum Conference (ICTF-JVC2020).
- Erasmus+ scholarship for short-term doctoral mobility (15-28th June, 2023).
- The Stipendium Hungaricum Dissertation Scholarship (01.09.2023 - 30.04.2024).



---

# THESES

1. In order to clarify the role of the molecular structure of the nematic liquid crystal (NLC) in photoalignment, I have systematically varied the rigid core of the NLC from biphenyl, through phenylcyclohexane, to bicyclohexane. I found substantial differences in the photoalignment process depending on the molecular structure of NLCs. In NLCs with biphenyl rigid core, I have confirmed the previous results regarding the existence of both azimuthal and zenithal photoalignment, their temperature dependence, as well as the relatively fast back-relaxation of the system to the initial orientation when the photo-excitation is switched off.

In contrast, in NLCs with phenylcyclohexane, or bicyclohexane rigid core only azimuthal photoalignment has occurred, and the back-relaxation of the director was extremely slow upon switching off the irradiation. No zenithal photoalignment has been detected at any temperature in these systems.

The different temperature dependence of the azimuthal and zenithal anchoring strengths can not solely explain the observed differences in photoalignment phenomena. Therefore, in addition to it, the possibility of the offset stacked aromatic  $\pi$ - $\pi$  interaction has been proposed between the NLC biphenyl rigid core, and the azobenzene moiety in the polymer layer. [N1]

2. To validate the role of the aromatic  $\pi$ - $\pi$  interaction between the NLC biphenyl rigid core, and the interfacing azobenzene moiety in the polymer layer, I have chosen for further studies a NLC compound containing biphenyl in the rigid core, with one of the phenyl rings being modified with three fluorine atoms, which invert the molecular electrostatic surface potential (MESP) of the ring. This modification, in principle, prevents the offset stacked  $\pi$ - $\pi$  aromatic interaction between the biphenyl part of NLC and the azobenzene moiety of the interfacing polymer. Therefore, instead of both azimuthal and zenithal photoalignment, only an azimuthal photoalignment was expected for this particular NLC compound. The experimental results have confirmed this expectation, thus, indirectly verifying the role of the aromatic  $\pi$ - $\pi$  interaction in photoalignment. [N2]
  
3. To clarify how the type of the LC phase influences photoalignment, I have chosen a LC compound with biphenyl rigid core, having both nematic (N) and smectic A (SmA) phase. In the N phase, the compound possessed similar photoalignment characteristics as the other nematics with biphenyl rigid core, i.e., zenithal photoalignment occurred in the high temperature range of the N phase, and azimuthal photoalignment in the lower temperature range. With further decrease of the temperature, just above the nematic-to-smectic A phase transition temperature (still in the N phase), however, both the azimuthal and the zenithal photoalignment vanish. This is attributed to the smectic pretransitional fluctuations, which suppress the photoalignment (both the azimuthal and the zenithal) in the nematic phase, due to the large increase of the bend and twist elastic constants, that are the most important parameters for the azimuthal and zenithal photoalignment, respectively. In the smectic A phase no azimuthal, nor zenithal photoalignment has observed, since the bend and twist deformations would involve changes in the layer spacing that request very high energies. [N2]

4. I have compared photoaligning properties of polymer layers fabricated from the same constituents: polymethyl-methacrylate (PMMA) and azo-dye Disperse Red 1 (DR1), either chemically attached to the PMMA main-chain, or physically mixed with it. The efficiency of the photoalignment decreases drastically in case of the physical mixture compared to that detected in case of polymer functionalized with DR1. Only a slight azimuthal photoalignment and no zenithal photoalignment has been obtained for the polymer layer prepared by physical mixing. The poor photoalignment performance of the polymer layers prepared from mixtures has been attributed to the rigidity of the PMMA matrix. [N3]
  
5. I have revealed photoinduced changes on the free polymer surface in contact with the air by atomic force microscopy (AFM). The polymer functionalized with DR1 became smoother after the illumination, and the photoinduced changes in surface relief were accompanied with a significant photoinduced mass transfer. In contrast, the polymer layer surface obtained by physical mixing did not change noticeably upon the illumination. [N3]